University of Cape Town
Faculty of Science
Department of Molecular and Cell Biology

Limbs gone batty: The role of the anterior-posterior patterning signal, *Sonic Hedgehog*, in the development of the unique bat limb.

Dorit Hockman

Supervisors: Prof. Nicola Illing (MCB) and Prof. David Jacobs (Zoology)

Research report

Submitted in fulfillment of the requirements for the degree of Master of Science (Molecular Biology)

December 2007

"Twinkle, twinkle, little bat!
How I wonder what you're at!
Up above the world you fly,
Like a teatray in the sky."

-The Mad Hatter

Lewis Carroll's *Alice's Adventures in Wonderland*.

Table of Contents

List of Figures and Tables

Abbreviations

AER	Apical ectodermal ridge
BMP/*Bmp*	Bone morphogenic protein
BCIP	5-bromo-4-chloro-3-indolyl phosphate
BLAST	Basic local alignment search tool
BSA	Bovine serum albumin
CHAPS	[3-[(3-Cholamidopropyl)dimethylammonio]-1-propanesulfonate
CRL	Crown-rump length
DEPC	Diethyl pyrocarbonate
DIG	Digoxigenin
DTT	1,4-Dithiothreitol
E...	Embryonic day
EDTA	Ethylenediaminetetraacetic acid
...E	Early
EEM	Extra embryonic membranes
Fgf	Fibroblast growth factor
Ihh	Indian hedgehog
IPTG	Isopropyl-beta-D-thiogalactopyranoside
...L	Late
PBS	Phosphate buffered saline
PCR	Polymerase chain reaction
PFA	Paraformaldehyde
PTC1/ *Ptc1*	Patched1
RACE	Rapid amplification of cDNA ends
SHH/*Shh*	Sonic hedgehog
SMO	Smoothened
SSC	Standard saline citrate
...VE	Very early
X-Gal	5-bromo-4-chloro-3-indolyl- beta-D-galactopyranoside
ZPA	Zone of polarizing activity
ZRS	ZPA regulatory sequence

Acknowledgements

I would like to thank my supervisors Nicci Illing and David Jacobs for their guidance and support at every stage of this research project. I am incredibly grateful to Mandy Mason, who was integral in setting up this study, and Robyn Verrinder and Maryalice Walker for their indispensable assistance in the field. I am very appreciative of Richard Behringer, Chris Cretekos, John Rasweiler and Scott Weatherbee who trained me in the essential field and lab techniques needed for this study during my time in Trinidad and Texas. Thanks must also go out to Richard Behringer and Chris Cretekos for their donation of *Carollia perspicillata* embryos and *Shh* RNA probe template. I am very grateful to Brigid Hogan for her advice and for the generous donation of dissection equipment. A big thank you to Petra Muller of the UCT Zoology department for the use of the photomicroscope and to lab 425 for their advice and general assistance in the lab. Finally, I am indebted to my family and friends for their support and lending an ear to my endless stories about bat wings.

Abstract

The unique skeletal structure of the bat forelimb and hindlimb provides a new and exciting model for the field of evolutionary developmental biology, which seeks to reveal the molecular mechanisms behind vertebrate limb diversity. The digits of the bat forelimb, excluding the thumb, are considerably elongated and webbed. The hindlimb digits are free of webbing and are of uniform length, lacking the asymmetrical patterning of the forelimb. In this study, gene expression analysis has revealed that changes in the spatial and temporal expression patterns of the anterior-posterior patterning signal, *Sonic hedgehog* (*Shh*), and its downstream target, *Patched 1* (*Ptc1*), have contributed to the development of the unique bat limb.

The embryonic development of *Miniopterus natalensis* (Miniopteridae) is described for the first time and the expression patterns of *Shh* and *Ptc1* in the developing limbs of this species are compared to those in *Carollia perspicillata* (Phyllostomidae) and the mouse. Early in bat limb development (stage 14), *Shh* expression in the ZPA appears to be anteriorly expanded when compared to the mouse. This observation is in line with the reported expansion of *Fgf8* expression in the AER (Cretekos *et al.* 2007) and reveals that an enhancement of the *Shh-Fgf* positive feedback loop may be responsible for the initial posterior expansion of the bat forelimb. Later in development (stage 16) *Shh* and *Ptc1* acquire a novel domain of expression within the interdigital tissue of both the bat forelimb and hindlimb. These expression patterns parallel the reported up-regulation of *Fgf8, Gremlin* and *Bmp2* in the interdigital tissue of *C. perspicillata* (Weatherbee *et al.* 2006) and support the hypothesis that the *Shh-Fgf* positive feedback loop is re-initiated in the interdigital tissue of the bat limbs. The cell survival and proliferation signals provided by the *Shh-Fgf* signalling loop most likely contribute to the lengthening of the posterior forelimb digits, the survival of the tissue between the forelimb digits and the extension of digits 1 and 5 of the hindlimb to the same length of the remaining digits. The novel *Shh* and *Ptc1* expression patterns were observed in both *M. natalensis* and *C. perspicillata*, supporting the monophyly of the chiropteran sub-order, Verspertilioniformes.

Chapter 1

Hypotheses for the molecular mechanisms of bat limb development

---

1.1. Introduction

The order Chiroptera, to which the bats belong, is the second most diverse mammalian order after the Rodentia, representing up to a 1000 recognised species (Simmons 2001). This incredible diversity can be attributed to the innovations of powered flight and echolocation that have allowed bats to invade a niche that no other mammal has entered: the night sky. The bat's wings, formed by the skeletal modification of its forelimbs, are a biological mystery and the questions of why and how wings and powered flight would evolve in the bat ancestor remain topics of debate.

Ecological hypotheses have been developed to answer the question of why powered flight evolved in a mammal. These hypotheses are based on the selection pressures faced by the putative bat ancestor (reviewed in Speakman 2001). Until recently, the question of how bat wings may have evolved was tackled from a purely morphological perspective, describing skeletal growth during development (Adams 1992a; Adams 1992b). Current research in the field of evolutionary developmental biology is extending this question to a molecular level by searching for changes in the genetic composition and regulation of limb development pathways that may allow a mammalian forelimb to develop into a wing (Cretekos *et al.* 2001; Chen *et al.* 2005; Sears *et al.* 2006; Weatherbee *et al.* 2006).

1.2. The unique bat limb

The unique skeletal structure of bat forelimb consists of a small first digit (thumb), considerably elongated second to fifth digits (index finger to pinky) and an elongated zeugopod (forearm) (Fig. 1.1). A membrane persists between the digits and between

the forelimb, body and hindlimb allowing the forelimb to be used as a wing (Neuweiler 2000) (Fig. 1.1). The elongation of the second to fifth digits is not due to the presence of extra phalanges, as in the elongated digits of the dolphin flipper (Richardson & Oelschläger 2002). Rather, in the bat forelimb the third digit is the only digit with the typical mammalian pattern of three phalanges, while the fourth and fifth digits have only two and the second has a single phalanx (Chen *et al.* 2005). The extension of the digits is due rather to the considerable lengthening of the metacarpals and the phalanges (Neuweiler 2000) (Fig. 1.1).

In addition to these unique features of the forelimb, the bat hindlimb is different from the typical mammalian hindlimb. Unlike the forelimb, the digits of the hindlimb are not elongated, however, the patterning along the anterior-posterior axis (thumb to pinkie) is not as distinct as in the forelimb (Fig. 1.1). Due to the elongation of the first phalanx of the thumb, the digits of the hindlimb may all be nearly equal in length (Vaughan 1970). In some species, such as *Carollia perspicillata*, the digits of the foot are identical in length (Chen *et al.* 2005), thus lacking any anterior-posterior patterning. It is possible that this digit structure facilitates the strong grip that bats require to perch upside down (Vaughan 1970).

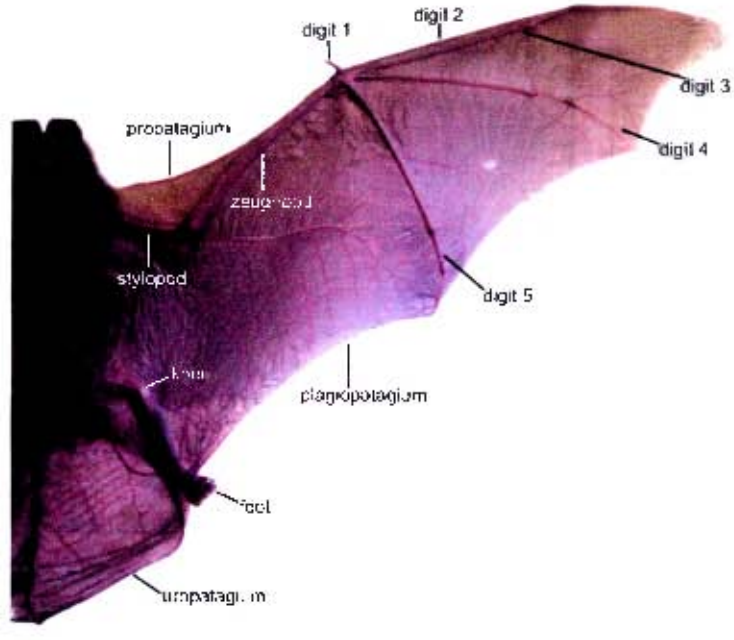

Fig. 1.1 Anatomy of the bat forelimb and hindlimb. Dorsal view of an adult *Miniopterus natalensis* with forelimb and hindlimb skeletal elements and wing membranes indicated. Digits 2 to 5 of the forelimb and the zeugopod elements are considerably elongated relative to digit 1, the stylopod and the hindlimb. The digits of the hindlimb are equal in length (Photograph courtesy of C. Schoeman).

1.3. Ecological hypotheses for bat wing development

Ecological hypotheses seek to explain why the evolution of this unique limb structure would have been a selective advantage in a putative bat ancestor. Most models for the evolution of wings describe the bat ancestor as an arboreal, nocturnal insectivore (reviewed in Speakman 2001). One such model known as the 'reach-hunting' hypothesis proposes that the bat ancestor possessed a primitive echolocation system and would use its forelimbs to reach out for prey as it flew past in the dark (Speakman 2001). Elongated, webbed forelimb digits that served as an advantage when clinging to trees gained an extra use in netting prey and were eventually adapted for gliding and finally for powered flight (Speakman 2001).

A second similar hypothesis suggests that the bat ancestor's webbed forelimbs were first used for gliding rather than as a means to capture insects (Smith 1977 in Speakman 2001). Speakman (2001) suggests that this second hypothesis would be more likely to occur if the bat ancestor was a diurnal frugivorous animal that used gliding as an efficient means of transport from tree to tree. This animal may have begun supplementing its diet with insects encountered while gliding and would have been forced into the nocturnal realm by the predation forces of birds (Speakman 2001).

Evidence for the above ecological hypotheses is lacking. The earliest known bat fossils, dating from the early Eocene (49-53 million years ago), provide little support for the state of a pre-bat ancestor, as these fossils possess fully formed wings (Speakman 2001). Thus, the order of events leading to the evolution of wings in the bat is unknown.

1.4. The morphological development of the bat limb

Despite this gap in the fossil record of bat evolution, it is possible to answer the question of how the unique bat limbs may have evolved by studying the progression of limb development in the bat embryo and comparing the developmental patterns to those in other vertebrates. The ontogeny of the bat limb provides insights into the

modifications in skeletal growth rate and patterning that must have occurred in the limbs of the bat ancestor. Skeletogenesis studies (*Myotis myotis*: Spillman 1925; *Vespertilio murinus*: Schumacher 1932; *Myotis myotis*: Joller 1977 in Adams 2000; *Myotis lucifugus*: Adams 1992a; Adams 1992b; *C. perspicillata*: Sears *et al.* 2006), morphological observations of embryonic development (*Syconycteris australis*: Lawrence 1991; *Rousettus amplexicaudatus*: Giannini *et al.* 2006; *Pipistrellus abramus*: Tokita 2006) and a timed embryonic staging system (*C. perspicillata*: Cretekos *et al.* 2005) have characterised the growth patterns of the limbs in the bat embryo that underlie the development of the unique structure of the wing and hindlimb.

During the early stages of limb development (stages 12 to 14) the bat forelimb buds are very similar to those of equivalently staged mouse embryos (Cretekos *et al* 2005). By stage 15, however, the shape and size of the bat forelimb bud is distinct due a posterior-distal expansion of the hand-plate (Chen *et al.* 2005; Giannini *et al.* 2006; Tokita 2006). In addition, the digital rays of both the hand- and foot-plates are evident during these early stages in the bat, while only appearing later in other mammals (Lawrence 1991; Tokita 2006). By stage 20 of development the zeugopod (radius and ulna) and autopod (carpals and digits) are noticeably longer than the stylopod (humerus) in the developing bat forelimb (Cretekos *et al.* 2005). This increase in length corresponds to an increase in size of the hypertrophic zone, the most mature area of the developing bone, in the growing metacarpals (Sears *et al.* 2006). The size of this mature zone relative to the length of the metacarpals is twice as large in the bat when compared to an equivalently staged mouse limb (Sears *et al.* 2006). In addition, the cartilage cells in the growth plates of the developing metacarpals show increased proliferation in the bat forelimb when compared to the bat hindlimb and the mouse forelimb (Sears *et al.* 2006). Thus, it appears that the bat forelimb increases in length through the increase in the number of cartilage cells relative to the hindlimb, and the subsequent accelerated maturation of these cells when compared to forelimb growth in other mammals. The result is acceleration in the growth rate of the forelimb digits relative to the rest of the body when compared to other mammals (Adams 1992b).

The thumb and the hindlimb digits do not experience this extreme extension. As in most mammals, the forelimb bud appears before that of the hindlimb in the bat

(Cretekos *et al.* 2005; Tokita 2006). However, while the hindlimb usually catches up to the forelimb in size in other mammals, the hindlimb and the forelimb of *C. perspicillata* never reach an equivalent relative size, due to the posterior extension of the forelimb (Cretekos *et al.* 2005). The only digit of the forelimb that remains synchronised in development with the hindlimb digits is the thumb. By stage 19 of development the thumb and all the digits of the hindlimb are the same size and possess distinct claw primordia at their tips (Cretekos *et al.* 2005; Tokita 2006), indicating an equivalent stage of differentiation. The thumb and hindlimb digits continue to resemble each other in size and differentiation throughout development, as the posterior digits of the forelimb elongate. These observations and the lack of any anterior-posterior patterning in the *C. perspicillata* hindlimb suggest that the molecular mechanisms that lead to the asymmetrical patterning and the extension of the posterior digits of the forelimb are absent in the developing thumb and hindlimb.

1.5. The molecular mechanisms of limb development

An exploration of the genetics behind limb development in bats is the next step in explaining how the unique morphological features of the bat limb evolved. A review of the established genetic models for limb development in model organisms, such as the mouse and the chicken, will facilitate the identification of candidate genes that may play a role in the evolution of bat limbs. Limb development and patterning (reviewed in: Mariani & Martin 2003; Tickle 2003; Sanz-Ezquerro & Tickle 2003) occurs along three axes: dorsal-ventral (top of hand to palm), proximal-distal (shoulder to fingers) and anterior-posterior (thumb to pinkie: digit one to digit five). An analysis of the genes involved in the early patterning mechanisms along the last of these axes in bats may reveal the factors that are responsible for initiating the process of elongation of the posterior digits two to five of the bat forelimb, while leaving the thumb short. It is also needed to explain the unusual absence of anterior-posterior patterning in the hindlimb in some bat species.

1.5.1. Sonic Hedgehog and the patterning of the anterior-posterior axis

Patterning along the anterior-posterior axis is mediated by the zone of polarizing activity (ZPA), a group of cells located in the posterior of the distal limb bud. When tissue from this region is grafted into the anterior limb bud, hands develop with additional digits in a mirror image pattern along the anterior-posterior axis (Saunders & Gasseling 1968 in Tickle 2003). It has been proposed that the ZPA mediates anterior-posterior patterning by releasing a morphogen that forms a concentration gradient, with its strongest concentration in the ZPA and it lowest concentration near the developing thumb. Different concentrations of this morphogen would specify differing cell fates along the anterior-posterior axis (Wolpert 1969).

Sonic hedgehog (SHH refers to the protein, *Shh* refers to the gene/mRNA transcripts) has been implicated as the signalling molecule involved in this morphogenic gradient. *Shh* expression is first evident at embryonic day (E) 9.75 of mouse development in the posterior cells of the forelimb, corresponding to the position of the ZPA (Echelard *et al.* 1993). As the fore- and hindlimb buds extend posteriorly (E10.5), *Shh* is expressed strongly in the posterior distal mesenchyme (Echelard *et al.* 1993). This expression pattern is down regulated in the E11.5 embryo and is absent by E12.5 in the mouse (Echelard *et al.* 1993).

Although *Shh* RNA is localized to the ZPA, SHH target genes are expressed throughout the posterior limb bud (Marigo *et al.* 1996a). The SHH protein is detected over most of the posterior half of the distal limb bud, over a distance of up to 30 cell diameters (Lewis *et al.* 2001), indicating its ability to act as morphogen. When *Shh* is expressed ectopically in the anterior of the limb bud of a chick embryo as well as in the posterior, the resultant limb develops with additional digits in a mirror-image sequence along the anterior-posterior axis (Riddle *et al.* 1993). This phenomenon indicates that ectopic *Shh* leads to the formation of a ZPA in the anterior of the limb bud (Riddle *et al.* 1993). The effect of the ectopic *Shh* on the chick limb bud is dose-dependent: high concentrations lead to extra digits with posterior identity (digits 4 and 3), while low concentrations lead to extra anterior digits (digit 2; Yang *et al.* 1997).

Recent studies have questioned the hypothesis that a spatial concentration gradient of SHH, and thus a spatial gradient of expression of SHH target genes, is sufficient for anterior-posterior patterning of the limb bud (reviewed in Zeller 2004 and McGlinn & Tabin 2006). Harfe *et al.* (2004) propose that a combined temporal and spatial gradient of SHH signalling mediates anterior-posterior patterning. Using fate-mapping techniques, Harfe *et al.* (2004) reveal that the cells of the ZPA that had once expressed *Shh* undergo proliferation and contribute to the entire structure of digit 4 and 5, and the posterior half of digit 3. Those cells that contribute to digit 3 cease to express *Shh* earlier in development than those contributing to digit 4 or 5 (Harfe *et al.* 2004). Thus a temporal gradient in autocrine SHH signalling (SHH producing cells signalling to themselves) specifies the identity of digits 3 to 5, with digit 5 being exposed to SHH for the longest period (Harfe *et al.* 2004). The cells that form digit 1 and 2 are not composed of *Shh* expressing cells and rely on differential concentrations of paracrine SHH (protein produced by neighbouring cells) to specify their identities (No SHH: digit 1, low SHH: digit 2; Harfe *et al.* 2004).

This temporal model for SHH patterning was confirmed by Scherz *et al.* (2007) who showed that when SHH signalling was inhibited by cyclopamine (an inhibitor of SHH signal transduction) early in development, thus shortening the period of SHH signalling, only the most anterior digits were specified. Exposure to cyclopamine later in development, and thus an increase in the time of uninterrupted SHH signalling, restored the presence of digits with posterior identities (Scherz *et al.* 2007).

Ahn & Joyner (2004), however, show that although the SHH protein is present for the longest period in the posterior limb bud, the cells is this area stop activating the SHH target gene, *Gli1*, before *Shh* expression is down regulated. Thus a linear temporal gradient in SHH presence does not lead to a parallel gradient of SHH target gene expression (Ahn & Joyner 2004). These insights show that anterior-posterior patterning of the limb bud is likely regulated by three factors: SHH concentration gradients, temporal gradients in autocrine signalling and thresholds of responsiveness of cells to SHH (Fig. 1.2).

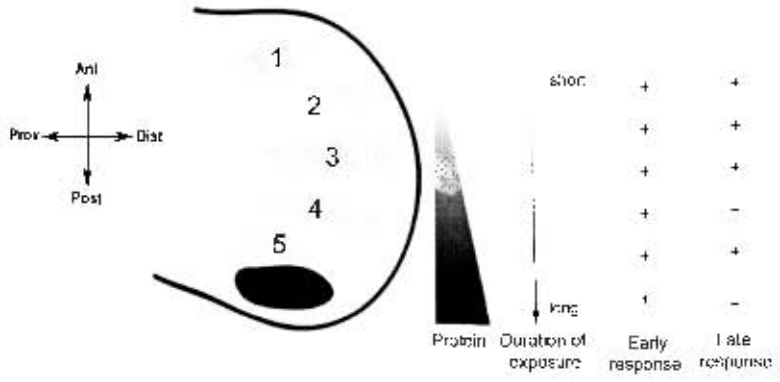

Fig. 1.2 Factors affecting SHH anterior-posterior patterning activity in the developing limb-bud. *Shh* gene expression is located in the zone of polarizing activity (black ellipse), in the posterior limb-bud. The SHH protein diffuses across the anterior-posterior axis of the limb-bud, with its highest concentration near the developing digit 5. The protein does not diffuse as far as digit one. This spatial gradient is combined with a temporal gradient, in which the cells of the most posterior digit five are exposed to autocrine SHH signalling for the longest period of time, while the cells of digit three receive autocrine signalling for the shortest period of time. Cells of digit two only ever receive low levels of paracrine SHH signalling. The most posterior cells of the developing limb-bud stop responding to the SHH signal before the more anterior cells despite being exposed to the highest concentration of signal for the longest time. + indicates SHH responding cells; - indicates non-responding cells.

1.5.2. Activation and maintenance of the Sonic Hedgehog signal

A *cis* regulatory region for *Shh* limb-specific expression has been identified approximately 1 megabase (10^6 bases) away from the *Shh* gene, within the locus of the *Lmbr1* gene (Sharpe *et al.* 1999; Lettice *et al.* 2002). Disruptions in different areas of this locus lead to both gain-of-function phenotypes (such as ectopic *Shh* expression in the anterior limb-bud) and complete loss-of-function phenotypes (loss of *Shh* expression in the limb) suggesting that this regulatory region may contain both repressor and enhancer elements (reviewed in Hill 2007 and Zeller & Zuniga 2007). It is possible that this regulatory region coordinates interactions between transcription activators and the *Shh* locus, ensuring the production of *Shh* mRNA in the posteriorly restricted domain of the ZPA.

dHAND, a basic helix-loop-helix transcription factor, may be responsible for activating *Shh* in the ZPA (reviewed in Panman & Zeller 2003). Initial *dHand* expression precedes that of *Shh* and becomes restricted to the posterior of the early

limb bud (E9.5) (Charité *et al.* 2000). In the absence of *dHand*, *Shh* expression is not activated in the limb bud, while ectopic *dHand* expression in the anterior of the limb bud leads to corresponding ectopic *Shh* activation and mirror image duplication of the posterior digits (Charité *et al.* 2000; Fernandez-Teran *et al.* 2000).

Once *Shh* has been activated, this signal is maintained in the ZPA by a positive feedback loop between *Shh* and fibroblast growth factors (*Fgf's*) produced by the most distal cells of the limb bud known as the apical ectodermal ridge (AER) (Laufer *et al.* 1994; Fig. 1.3). *Shh* maintains *Fgf* expression indirectly by activating *Gremlin*, a bone morphogenic protein (*Bmp*) inhibitor, in the cells anterior to the ZPA (Zuniga *et al.* 1999). *Gremlin* in turn inhibits the action of *Bmp's* in the AER, allowing the expression of *Fgf's*, which would otherwise be down-regulated by *Bmp's* (Zuniga *et al.* 1999). The *Fgf's* in the AER then signal to the ZPA, maintaining *Shh* expression (*Fgf4*: Niswander *et al.* 1994; *Fgf8*: Vogel *et al.* 1996) and cell proliferation in the limb bud (Lewandoski *et al.* 2000).

Interestingly, it is likely that *Shh* activates *Gremlin* through *Bmp2* activation (Nissim *et al.* 2006) (Fig. 1.3). The *Bmps* in the developing mesenchyme self-regulate their negative influence on *Fgf* expression in the AER by upregulating an antagonist, allowing the limb bud to grow to the required size for digit condensation to occur.

The *Shh-Fgf* feedback loop is further self-regulated by the proliferating cells of the ZPA (Scherz *et al.* 2004). The *Shh* producing cells of the ZPA and their daughter cells are not able to activate *Gremlin* (Scherz *et al.* 2004; Nissim *et al.* 2006). As these cells multiply they form a barrier between the *Shh* producing cells and the target *Gremlin* producing mesenchyme cells (Scherz *et al.* 2004). In the absence of the *Shh* signal, these cells stop producing *Gremlin*, breaking the *Shh-Fgf* feedback loop (Scherz *et al.* 2004). The termination of this signal relay is essential in controlling limb size. If the *Fgf* (Sanz-Ezquerro & Tickle 2003; Lu *et al.* 2006) or *Gremlin* (Scherz *et al.* 2004) signal is not terminated the hand/foot plate will continue to expand, leading to the development of longer digit primordia (Scherz *et al.* 2004), extra phalanges (Sans-Ezquerro & Tickle 2003) or extra digits (Lu *et al.* 2006).

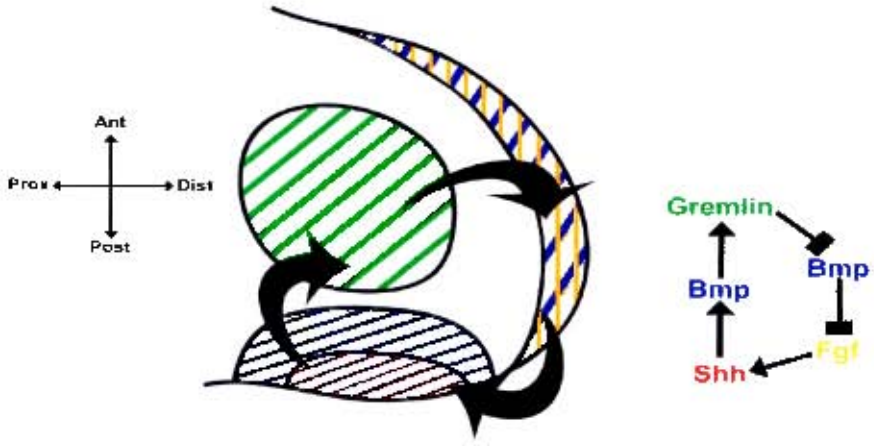

Fig. 1.3 The *Shh-Fgf* positive feedback loop. *Shh* (red) in the ZPA activates *Bmp2* (blue) in the ZPA and surrounding cells. *Bmp2* then activates *Gremlin* (green) in the mesenchyme of the limb bud. *Gremlin* acts to antagonise *Bmp* action in the AER. *Bmp's* usually suppress *Fgf* (orange) expression in the AER, thus the presence of *Gremlin* promotes *Fgf* expression in the AER. *Fgf's* then activate *Shh* expression in the ZPA, completing the positive feedback loop. The large arrows indicate the direction of action of the *Shh-Fgf* positive feedback loop within the developing limb bud.

1.5.3. Building the Sonic Hedgehog protein

Transcriptional activation and translation lead to the creation of a SHH protein precursor. The active SHH protein is created through a process of autoproteolytic cleavage, in which the protein cleaves itself in half using the chemical attributes of conserved amino acids located in the carboxy-terminal region (Lee *et al.* 1994). This leads to the addition of a cholesterol tail to the end of the resulting amino-terminal fragment (Porter *et al.* 1996) followed by the addition of palmitoyl (Pepinsky *et al.* 1998).

Alterations in the auto-processing and subsequent lipid modification of SHH alter the diffusibility and efficiency of the final protein (Lee *et al.* 1994; Pepinsky *et al.* 1998). Lewis *et al.* (2001) propose that inhibition of the cholesterol modification of SHH disrupts SHH diffusion leading to an absence of long-range SHH signalling in the mouse limb bud. In the absence of the cholesterol tail only the most posterior digits four and five form, along with the most anterior digit one (Lewis *et al.* 2001). This phenotype suggests that while SHH short-range signalling is occurring in the extreme posterior portion of the limb bud, the long-range signal needed to activate the intermediate digits is absent (Lewis *et al.* 2001). Li *et al.* (2006), however, propose

that the cholesterol tail serves to limit the range of SHH to the posterior limb bud rather than facilitate its movement. They show they when the cholesterol is absent the SHH protein is able to diffuse further towards the anterior of the limb bud, ectopically activating SHH target genes (Li *et al.* 2006). These conflicting results reveal the complicated nature of SHH signalling and point out the need for further research to understand the chemical mechanisms behind this patterning pathway.

1.5.4. Transduction of the Sonic Hedgehog signal

The SHH signalling cascade within target cells is initiated by SHH binding to the cell-membrane receptor Patched (PTC1) (Marigo *et al.* 1996b; Stone *et al.* 1996). In the conventional model for SHH signalling (Fig. 1.4) unbound PTC1 inhibits the cell-membrane protein Smoothened (SMO) through direct interaction in a receptor complex (Stone *et al.* 1996; Murone *et al.* 1999) (Fig. 1.4A). SHH binding inactivates PTC1 and allows the SHH signal to be transduced into the cell through a conformational change in SMO (Stone *et al.* 1996) (Fig. 1.4B).

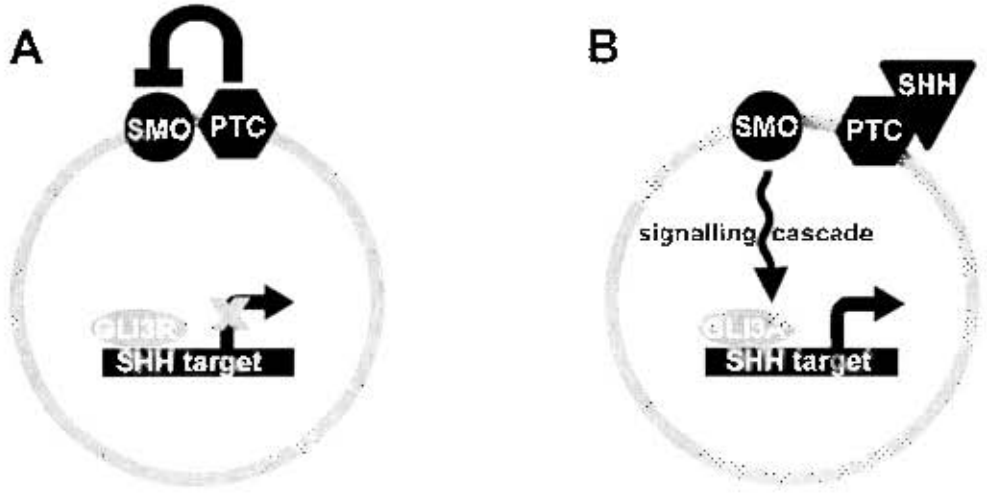

Fig. 1.4 The conventional model of SHH signalling. A) In the absence of SHH, SMO and PTC1 form a receptor complex in which PTC1 inhibits SMO. As a result, the transcription of SHH target genes is inhibited by the repressor form (R) of GLI3. B) Upon SHH binding to PTC1, SMO is released from PTC1 inhibition and initiates a signalling cascade that leads to the promotion of the activator form (A) of GLI3 and subsequent activation of SHH target genes.

Recently, Rohatgi *et al.* (2007) revealed an alternative mechanism of SHH signalling by monitoring the movements of PTC1 and SMO in the primary cilia (cell surface projections involved in detecting signals) of mammalian cells. They showed that in the absence of SHH, PTC1 is present at the base of the cilia and along their shafts, while SMO is absent from these structures. SHH binding leads to the loss of PTC1 from the cilia while SMO presence increases. These results suggest that PTC1 inhibits the SHH pathway by excluding SMO from the primary cilia, and that SHH binding to PTC1 leads to the activation of SMO through the removal of PTC1 from these structures (Rohatgi *et al.* 2007).

SHH signal transduction within the cells of the developing limb occurs through the regulation of the state of the transcription factor GLI3, which in the absence of SHH acts as a repressor of SHH target genes (Ingham & McMahon 2001) (Fig. 1.4A). The presence of elevated levels of SHH signalling ensures that GLI3 takes the form of an activator of SHH targets rather than a repressor (Aza-Blanc *et al.* 1997) (Fig. 1.4B). The gradient of SHH across the limb bud results in opposing gradients of GLI3 repressor and activator forms, with the repressor at its highest in the anterior where SHH is completely absent, and the activator highest in the posterior where the SHH signal is the strongest (Wang *et al.* 2000).

In the absence of functional SHH, only the repressor form of GLI3 is present (Litingtung *et al.* 2002). As a result a single unidentifiable cartilage element forms in the hand, while the foot consists of a single digit, identifiable as the first digit (Kraus *et al.* 2001; Chiang *et al.* 2001; Litingtung *et al.* 2002). A lack of functional GLI3 results in the development of a polydactylous limb (over five digits), with digits that are indistinguishable from one another in identity (Litingtung *et al.* 2002). A similar result occurs when both SHH and GLI3 are absent (Litingtung *et al.* 2002). These phenotypes indicate that the balance between GLI3 repressor and activator forms, mediated by SHH, is essential for the creation of a pentadactylous limb (five digits) with anterior-posterior asymmetry.

The suite of SHH targets activated by GLI3 genes include the SHH receptor gene, *Ptc1* (Marigo *et al.* 1996a). In the mouse *Ptc1* expression overlaps that of *Shh* as both are restricted to the posterior limb bud, however, *Ptc1* extends further towards the

anterior than the ZPA restricted *Shh* expression pattern (Goodrich *et al.* 1996). *Ptc1* gene expression, therefore, provides a measure of the extent of SHH protein diffusion across the limb-bud, indicating which cells are activating SHH targets (Marigo *et al.* 1996a). PTC1 has been proposed to function not only as a receptor for SHH, but also as a regulator of SHH movement. In developing *Drosophila* wings (Chen & Struhl 1996) and the developing mouse limb (Lewis *et al.* 2001), high levels of PTC1 are able to impede the movement of SHH across the A-P axis. By upregulating *Ptc1,* SHH limits its own range of action.

The *Shh* pathway has also been implicated in the regulation of the *5' Hoxd* genes, a set of important anterior-posterior patterning genes, in a feedback loop mechanism (Zakany *et al.* 2004). The expression pattern of the 5' *Hoxd* genes in the developing hand or foot has been divided into two phases (Nelson *et al.* 1996). In the first phase *Hoxd9* through to *Hoxd13* are sequentially activated in the proximal-distal limb bud in a nested concentric pattern, with *Hoxd13* expression confined to the most posterior position. In the second phase *Hoxd13* is expressed in a wider expression pattern, extending to the anterior of the limb bud. Zakany *et al.* (2004) suggest that activation of a first phase of 5' *Hoxd* genes in a collinear pattern, leads to the activation of *dHand* and subsequently *Shh* in the ZPA. A feedback loop between *Shh* and the 5' *Hoxd* genes mediates the second phase of the 5' *Hoxd* gene expression pattern, possibly though an enhancer element known as the global control region located upstream of the *Hoxd* cluster (Spitz *et al.* 2003).

1.6. Hypotheses for the role of Sonic Hedgehog and early anterior-posterior patterning in bat limb development

Carroll *et al.* (2005) suggest that alterations in the spatial and temporal regulation of key limb patterning genes has allowed the diversification of limb morphology among the vertebrates. This hypothesis is supported by recent studies that implicate changes in the regulation of the *Shh* pathway in the loss of the hindlimb in cetaceans and in the variation in digit number in lizards. In the dolphin embryo hindlimb development is initiated and an AER forms but this limb bud degenerates early in development (Thewissen *et al.* 2006). Thewissen *et al.* (2006) show that while *Shh* is turned on and

maintained in the developing dolphin forelimb, this signal is never present in the hindlimb bud. The *Shh* signal is required to maintain *Fgf* expression in the AER and limb outgrowth, thus in its absence limb development is terminated (Thewissen *et al.* 2006). The duration of *Shh* expression, rather than its absence or presence, has been implicated in the diversity of digit number in the lizard genus *Hemiergis* (Shapiro *et al.* 2003). A short *Shh* expression period leads to the development of only two digits in *H. quadrilineata*, while a longer duration of expression leads to the growth of five digits in *H. initialis* and is associated with an increase in cell proliferation (Shapiro *et al.* 2003).

Cretekos *et al.* (2001) propose that similar alterations in the spatial and temporal regulation of key limb development genes are responsible for the evolution of the unique bat limbs. Recent studies of the molecular mechanisms of limb development in both the mouse (Bandyopadhyay *et al.* 2006) and the bat (Chen *et al.* 2005; Sears *et al.* 2006; Weatherbee *et al.* 2006; Cretekos *et al.* 2007) reveal that the *Shh* pathway is a suitable candidate for such changes during bat limb development.

In their analysis of the role of *Bmps* in mouse limb development Bandyopadhyay *et al.* (2006) show that in the absence of both *Bmp2* and *Bmp4* the limb bud is expanded posteriorly and the interdigital mesenchyme is retained. This phenotype is reminiscent of the posteriorly expanded, webbed bat wing. In the *Bmp* mutants, the survival of the interdigital tissue is due to a lack of an apoptotic signal, usually provided by *Bmps* (Zou *et al.* 1996), while the posterior expansion can be explained in terms of the *Shh-Ffg* feedback loop. Bandyopadhyay *et al.* (2006) show that this expansion is correlated with the enlargement of both the *Shh* and *Fgf8* expression domains in the ZPA and AER respectively. In addition, both *Shh* and *Fgf8* expression persist longer in the *Bmp* mutants than in wildtype embryos (*Shh*: E12.5, *Fgf8*: E15.5; Bandyopadhyay *et al.* 2006). *Bmp* antagonism usually suppresses *Fgf* expression in the AER (Zuniga *et al.* 1999). Thus in the absence of this antagonism, *Fgf* expression is expanded in time and space. Due to the positive effect of *Fgf's* on the *Shh* signal (Niswander *et al.* 1994) the *Shh* domain also experiences this expansion. This enhancement of the *Shh-Fgf* feedback loop leads to an increase in the number of cells in the limb bud, especially in the posterior where the ZPA is located.

In their study of wing development in *C. perspicillata*, Cretekos *et al.* (2007) and Weatherbee *et al.* (2006) also report changes in the expression patterns of key players in the *Shh-Fgf* feedback loop: the cell survival signal, *Fgf8*, and the *Bmp* inhibitor, *Gremlin.* Cretekos *et al.* (2007) show that *Fgf8* expression is first detected in the AER of stage 12 and 13 *C. perspicillata* forelimbs and hindlimbs respectively and persists until stage 15. Throughout this expression period, the width of *Fgf8* expression in the forelimb AER is 2.7 times greater in the bat than in equivalently staged mouse forelimbs (Cretekos *et al.* 2007).

Later in development, stage 16 and 17, Weatherbee *et al.* (2006) report novel domains for both *Fgf8* and *Gremlin* expression in the bat forelimb. *Gremlin* expression in developing limb buds is usually down-regulated at the time of interdigital apoptosis and *Ffg8* expression remains confined to the AER (Scherz *et al.* 2004). However, during *C. perspicillata* development, Weatherbee *et al.* (2006) show that both *Gremlin* and *Fgf8* are present in the interdigital tissue of the forelimb (Weatherbee *et al.* 2006). Weatherbee *et al.* (2006) suggest that *Gremlin* and *Fgf8* serve to block the cell death signal in the interdigital tissue of the forelimb.

In light of the results reported by Bandyopadhyay *et al.* (2006), it is possible that the expanded *Fgf8* and *Gremlin* expression patterns reported by Cretekos *et al.* (2007) and Weatherbee *et al.* (2006) are the result of an enhancement of the *Shh-Fgf* feedback loop. As in Bandyopadhyay *et al.* (2006), an enhancement of this signal relay may be responsible for the posterior expansion of the bat forelimb bud, as well as allowing the survival of the interdigital tissue. If this is so, one would expect to find alterations in the expression domains of *Shh* and its downstream targets especially in the posterior of the bat forelimb at the stages at which this expansion begins (stages 14-16).

Chen *et al.* (2005) report such changes in the expression patterns of the *Shh* target gene, *Hoxd13*, in the developing limbs of *C. perspicillata* when compared to the mouse. While in the forelimbs of both animals, the early (stage 13) posterior restricted expression patterns of *Hoxd13* are very similar, later (Stage 14-15) *Hoxd13* expression is shifted towards the posterior in the developing hand of the bat when compared to that of the mouse (Chen *et al.* 2005). As *Shh* signalling is thought to be

upstream of this second phase of *Hoxd13* expression (Spitz *et al.* 2003), it is possible that this posterior shift in *Hoxd13* expression is the result of change in *Shh* expression.

While changes in the expression patterns of the genes involved in the *Shh-Fgf* feedback loop implies a role for early patterning in the development of the unique bat limb anatomy, Sears *et al.* (2006) suggest that changes in the regulation of cartilage growth, rather than early patterning, are responsible for the extension on the bat forelimb digits. Sears *et al.* (2006) suggest that elongation of the bat forelimb digits relative to developing mouse digits begins at stage 20 of bat development and that prior to this stage the early digit primordia of the mouse and bat forelimb are similar in size. They show that at stage 20 of development the mRNA expression and protein levels of the growth factor *Bmp2* are higher in the bat metacarpals than in the bat hindlimb or mouse forelimb (Sears *et al.* 2006). In addition, Sears *et al.* (2006) show a distinct increase in the size of the hypertrophic zone and an increase in cell proliferation in the growth plate of the bat metacarpals at stage 20, when compared to that of the mouse metacarpals. This study suggests that a change in *Bmp2* expression at stage 20 of bat development, possibly through changes in the cis-regulation of the bat *Bmp* gene, stimulates the faster growth rate of the bat forelimb digits relative to the mouse, and thus is responsible for the elongation of the bat digits.

Sears *et al.* (2006), however, ignore the fact that the developing bat forelimb bud is clearly posteriorly expanded relative to the mouse forelimb as early as stage 15 (Chen *et al.* 2005). It is possible that the higher levels of *Bmp2* in the bat forelimb bud relative to the mouse forelimb and bat hindlimb bud at stage 20 are due to the larger relative size of the bat forelimb bud, rather than due to a change in the regulation of *Bmp2*. An early increase in the number of cells of the forelimb bud, as a result of an enhancement of the *Shh-Fgf* feedback loop, could lead to higher concentrations of *Bmp2* later in development as there would be more cells to produce this growth factor.

While an enhancement of the *Shh-Fgf* feedback loop may explain the posterior expansion of the bat forelimb and subsequent lengthening and webbing of the digits, an alternative hypothesis is needed to explain the lack of these features and the loss of anterior-posterior patterning in the bat hindlimb. An expansion of the *Shh* expression domain in the hindlimb bud and subsequent uniform expression of the SHH protein

across the limb bud may lead to the loss of anterior-posterior polarity in the expression pattern of downstream genes and thus the loss of asymmetrical patterning along this axis. The resulting digits would be identical in length.

The expression pattern of *Hoxd13* in the bat hindlimb is evidence that such a change may have occurred. Chen *et al.* (2005) showed that the early posterior restricted *Hoxd13* expression was absent (stage 13-14), while the second phase of *Hoxd13* expression, in which the protein is expressed along the anterior-posterior axis, was present (stage 15-16). This late *Hoxd13* expression, however, was detected uniformly along the anterior-posterior axis of the hindlimb bud, rather than in a gradient from posterior to anterior as in the mouse (Chen *et al.* 2005). This lack of polarity in the *Hoxd13* expression pattern may be due to a change in *Shh* expression, and may be responsible for the lack of differential identity of the hindlimb digits.

The hypothesised changes in *Shh* expression in both the forelimb and the hindlimb of the developing bat limb could be achieved through alterations in the limb specific *cis*-regulatory region for *Shh*, without affecting the SHH protein structure. Different changes occurring in separate forelimb and hindlimb specific regulatory regions could have resulted in the distinct skeletal patterns evident in the bat forelimb and hindlimb.

1.7. Study aims

The aim of this study was to test the hypothesis that the *Shh* expression pattern is altered during bat limb development. The expression patterns of *Shh* and its downstream target, *Ptc1*, were characterised in the developing limbs of the Natal clinging bat, *Miniopterus natalensis* (previously *Miniopterus schreibersii natalensis*: Simmons 2005, Miller-Butterworth *et al.* 2005) and the short-tailed fruit bat *Carollia perspicillata*. *M. natalensis* is a member of the chiropteran sub-order Verspertilioniformes and is found within the super-family Vespertilionoidea (Eick *et al.* 2005) and the family Miniopteridae (Miller-Butterworth *et al.* 2007). *C. perspicillata* belongs to the same sub-order and is part of the super-family Noctilionoidea and the family Phyllostomidae (Eick *et al.* 2005). The Noctilionoidea and the Vespertilionoidea are proposed to have shared a common ancestor 61 to 50

million years ago (Miller-Butterworth *et al.* 2007). The dual analysis of these two super-families will expose whether the programme for limb development is constant within the Verspertilioniformes and, if so, would support the monophyly of Verspertilioniformes (Teeling *et al.* 2005, Eick *et al.* 2005).

The embryonic development of *M. natalensis* has not been previously described. In this study, the detailed staging system developed for *C. perspicillata* (Cretekos *et al.* 2005) was used to characterise embryonic development in *M. natalensis*. The progression of limb growth in *M. natalensis* was then compared to that in the mouse to reveal when critical differences in limb bud shape and size become apparent. *Shh* and *Ptc1* expression patterns were then analysed at these stages of development.

Regions of *Shh* and *Ptc1* were amplified from cDNA by PCR, cloned and used as templates for RNA probes. The probes were used in the whole mount *in situ* hybridisation procedure to reveal *Shh* and *Ptc1* expression patterns in *M. natalensis*, *C. perspicillata* and the mouse. Expression patterns in the limbs of the two bat species were compared to one another and to those in equivalently staged mouse embryos to determine if bat-specific changes in gene expression are evident both between the bat forelimb and hindlimb and between the bat and mouse limbs.

Chapter 2

A comparison of embryonic development in *Miniopterus natalensis* with that in *Carollia perspicillata* and the mouse

---

2.1. Introduction

The progression of limb development during embryonic growth is very well described for the mouse (Martin 1990; Kaufman 1992) and, recently, Cretekos *et al.* (2005) provided a detailed description of embryonic development and limb growth for the short tailed fruit bat, *Carollia perspicillata*. However, embryonic development in *Miniopterus natalensis*, during the stages of limb bud initiation and growth, has never been described in detail. An embryonic staging system similar to that developed for *C. perspicillata* through the timed mating of captive-bred bats (Cretekos *et al.* 2005), could not be done for *M. natalensis* because this species does not survive in captivity. Thus, *M. natalensis* embryos were obtained from the wild and staged using the *C. perspicillata* staging system, which is based on the classic Carnegie system for human development (Cretekos *et al.* 2005). Progesterone levels were recorded for the pregnant *M. natalensis* females at the time of capture to determine if a correlation exists between maternal progesterone levels and the stage of embryonic development. If so, these recordings may provide a less invasive indicator of embryonic stage for future studies.

The progress of embryonic development in *M. natalensis* was compared to that described for *C. perspicillata* (Cretekos *et al* 2005) and *Pipistrellus abramus* (Tokita 2006) to determine when species-specific differences in adult morphology, such as differences in tail length and body size, become evident during embryonic development. In addition, the pattern of limb growth in *M. natalensis* was compared to equivalently staged mouse embryos to establish when in development limb bud shape and size begin to differ between bats and mice. Mouse and *C. perspicillata* embryos at these critical stages of limb development were collected to be used alongside *M. natalensis* embryos in subsequent gene expression analyses.

2.2. Background information on *M. natalensis* and *C. perspicillata*

2.2.1 Ecology of *M. natalensis* and *C. perspicillata*

M. natalensis is an insectivorous species with a wide distribution in Africa, extending from South Africa to Sudan and south-western Arabia (Simmons 2005). *C. perspicillata* is primarily a fruit eating species and is distributed throughout the neotropics from northern Argentina to Southern Mexico (Cloutier & Thomas 1992) where it is probably the most abundant mammal (Cretekos *et al.* 2005). Both species are generalists in their choice of foraging habitats, feeding both within the under-story of forests and at the forest edge or in the open (Fleming 1988; Jacobs 1999). They possess wings with moderate to low wing loading (weight/wing area), allowing for increased manoeuvrability within the cluttered forest under-story (7.4 N/m^2 for *M. natalensis* (Miller-Butterworth *et al.* 2005); 11.4 N/m^2 for *C. perspicillata* (Norberg & Rayner 1987)). The aspect ratio ($wingspan^2$/ area) measurements for both species are also moderate to low, allowing for increased aerodynamic efficiency when flying in both cluttered and open habitats (6.6 for *M. natalensis* (Jacobs 1999); 6.1 for *C. perspicillata* (Norberg & Rayner 1987)).

2.2.2. Reproductive cycle of *M. natalensis in* relation to seasonal migratory patterns

Little information exists on the reproductive cycle of the *M. natalensis* population at De Hoop Nature Reserve, Western Cape, which was the focus of this study. However, the reproductive cycle of the *M. natalensis* populations in the Limpopo and Gauteng provinces (the old Transvaal province) and Kwazulu Natal have been studied in detail. Links between reproductive cycle and migratory patterns have been established for the Transvaal population (van der Merwe & van Aarde 1989). The information provided for these populations was combined with field observations of the De Hoop population to estimate when pregnancy and early limb bud stages of embryonic development may occur in the De Hoop population.

M. natalensis breeds once a year. Copulation in the Transvaal population occurs from mid-February to the beginning of May after migration to winter hibernacula (van der Merwe 1986). Fertilisation is followed by a period of delayed implantation during which the bilaminar blastocyst floats freely within the lumen of the uterus in an inactive state (Bernard 1980; Bernard *et al.* 1996). Implantation of the embryo occurs from the beginning of July to mid-August (van der Merwe 1979). At the end of July the Transvaal populations migrate to northern maternity caves where pregnancy progresses and parturition occurs (van der Merwe 1975). Early limb-bud stage embryos were recorded in the middle of September for the Transvaal (van der Merwe & van Aarde 1989) and Kwazulu Natal populations (Bernard 1980). The overall gestation period for *M. natalensis* is about eight months, with birth occurring in December (Taylor 2000).

Observations of the De Hoop population suggest that this community follows similar seasonal migratory patterns to the Transvaal population. *M. natalensis* migrates seasonally between unknown winter hibernacula and summer maternity roosts, using De Hoop primarily as a summer roost (McDonald *et al.* 1990; Mills & Hess 1997; Miller-Butterworth *et al.* 2003) where maternity colonies of up to 100 000 pregnant females are found (Taylor 2000). In early April, both females and males are present at De Hoop (personal observation) however by May the majority of *M. natalensis* females have left (M.H. Walker, personal communication). In mid-August, very few females are present at the De Hoop cave suggesting that pregnant females have not yet returned from winter hibernacula (personal observation). By the end of August, however, the numbers of *M. natalensis* at De Hoop increase greatly (M.H. Walker, personal communication). Using these field observations and the observations for the Transvaal and Kwazulu Natal populations, it was assumed that the pregnant females would return to De Hoop by mid-September and would be carrying early limb bud stage embryos.

van der Merwe & van Aarde (1989) note that for the Transvaal population implantation of the embryo coincides with a peak in maternal plasma progesterone concentrations. This peak is followed by a drop in progesterone levels and another peak was recorded after the limb bud stages of development (van der Merwe & van Aarde 1989). In *Miniopterus schreibersii*, from the Eastern Cape, progesterone does

not peak at implantation but rather rises steadily from implantation to just before parturition (Bernard *et al.* 1991). In this study, maternal plasma progesterone levels were determined for both pregnant and non-pregnant females at De Hoop during September and November respectively. These measurements would give a fine resolution of the changes in progesterone levels over the period of limb development and reveal if any correlation exists between progesterone levels and stage of embryonic development.

2.2.3. Reproductive cycle of *C. perspicillata*

C. perspicillata breeds twice a year in the wild (Cloutier & Thomas 1992), with a gestation period of 113 to 120 days (Rasweiler & Badwaik 1997). On the island of Trinidad, where samples were collected for this study, the first pregnancy begins around September and parturition occurs in March or April after a period of developmental delay at the primitive streak stage (Rasweiler & Badwaik 1997). Females then conceive again during a post-partum oestrus (Chen *et al.* 2005). This second pregnancy does not include a developmental delay (Chen *et al.* 2005).

2.3. Materials and Methods

2.3.1. Field collection of *M. natalensis* and *C. Perspicillata* embryos

M. natalensis specimens for this study were collected from the 8th to the 24th September 2006 from De Hoop Nature Reserve, Western Cape Province, South Africa (Western Cape Nature Conservation Board permit number: AAA004-00030-0035; UCT Faculty of Science Animal Experimentation Committee application number: 2006/V4/DJ). Pregnant females were caught by placing a harptrap (Austbat & Faunatech, Victoria, Australia) just below the main entrance to the De Hoop Guano cave (34°26'S; 20°25'E) during the evening emergence. The harptrap was placed far enough from the cave entrance to ensure that emergence was not hindered. Reproductive females were identified by the presence of well-developed, naked nipples. Later stage pregnancies were distinguished from earlier stages by gently

palpating the abdomen of the specimen to assess the size of the swollen uterus (Racey 1969).

Prior to euthanasia, hind foot and total body length measurements were taken to ensure that each specimen was *M. natalensis* and not *M. fraterculus*, a morphologically similar species known to share roosts with *M. natalensis* (Taylor 2000). The measurements were inserted into the field identification equation provided by Stoffberg *et al.* (2004). Each specimen was then weighed, anaesthetised by halothane inhalation and subsequently killed by decapitation.

The uterus was removed and both length (longest diameter) and width (greatest diameter perpendicular to the length) measurements were taken. The uterus was dissected in diethyl pyrocarbonate (DEPC)-treated 1x phosphate buffered saline (PBS) to expose the embryo encased within the foetal membranes. The crown-rump length of the embryo was taken prior to removing the foetal membranes. The embryo was staged using the staging system provided by Cretekos *et al.* (2005). The progress of limb development was used as the key feature for determining the stage of development.

The majority of the embryos and the extra embryonic membranes (EEM), including the uterus, were placed in 4% paraformaldehyde (PFA, Sigma) in DEPC PBS for fixation overnight at 4°C. Following fixation, the embryos and EEM were dehydrated through a methanol series for storage at -20°C in 100% methanol. These embryos and EEM would be used for gene expression analysis by whole mount *in situ* hybridisation (Chapter 3). A selection of embryos from late stage 13 (13L) to stage 17, and all the embryos from stage 18 to stage 20 were placed in RNAlater (Qiagen) overnight at 4°C and subsequently moved to -20°C and later to -80°C, upon return from the field. These embryos were used as sources of RNA for both this study and a concurrent microarray study. PFA fixed embryos were photographed using a Nikon SMZ1500 stereoscopic zoom microscope fitted with a Nikon DS-U2 camera control unit and a Nikon DS-5Mc camera head (Nikon Instruments Inc., New York, U.S.A.). Photographs were formatted using NIS-Elements image capture software (Nikon Imaging Software, version 2.10) and Photoshop (Adobe, version 7.0).

Carollia perspicillata embryos used in this study were supplied by Dr. Behringer (University of Texas M.D. Anderson Cancer Centre, Houston, Texas). These embryos were collected on the island of Trinidad in either February or May of 2003 to 2006. The samples were collected and exported with the permission of the Wildlife Section, Forestry Division of the Ministry of Agriculture, Land and Marine Resources of the Republic of Trinidad and Tobago. Pregnant females were collected using hand-nets from colonies found roosting in caves, abandoned houses and water towers in the area of St. Augustine (10° 39' N, 61° 24' W). Specimens were killed by cervical dislocation and the reproductive tracts were dissected and fixed as described above for *M. natalensis* to be used for gene expression analysis by whole mount *in situ* hybridisation (Chapter 3).

2.3.2. *M. natalensis* maternal plasma progesterone analysis

In September 2006 blood was collected from the neck of the pregnant *M. natalensis* specimens after decapitation for use in progesterone analysis. In November 2006 additional blood samples were taken from non-pregnant females assumed to be suckling young due to the presence of large naked nipples and from non-reproductive females that lacked obvious nipples. During this additional sampling session blood was collected from the vein running parallel to the leading edge of the propatagium after warming the specimen on a heated blanket. The vein was punctured with a sterile needle and blood was collected using heparinised capillary tubes. All blood samples were centrifuged at high speed for seven minutes to obtain plasma, which was stored at -20°C for progesterone analysis by the National Health Laboratory Services at Groote Schuur Hospital, Cape Town. Plasma Progesterone was measured on the MODULAR E170 automated electrochemiluminescent immunoasssay system (Roche).

The means and standard error of the means for the progesterone readings for each stage of limb development and for the non-pregnant females were plotted using STATISTICA (Satsoft, version 7) to determine if a trend was visible in the change of progesterone levels during and after pregnancy.

2.3.3. Acquisition of mouse embryos

Mouse embryos were obtained from the Animal Unit at the University of Cape Town Medical School (Animal Ethics Committee application number: 006/040). Mature female mice (ICR strain) were placed in cages with males and checked for vaginal plugs the following day. Midnight of the day prior to the appearance of a vaginal plug was defined as time zero of development (E0). Pregnant mice were sacrificed at midnight to obtain embryos aged E10.0, E11.0, E12.0 and E13.0 while embryos aged E10.5, E11.5, E12.5 and E13.5 were obtained from pregnant females sacrificed at midday. Pregnant mice were anesthetised by halothane inhalation and subsequently killed by cervical dislocation. The reproductive tract was dissected and the embryos were fixed, stored and photographed as described above. The stage of embryonic development was confirmed by comparing the progress of limb growth to the staging systems provided by Martin (1990) and Kaufman (1992).

2.4. Results

2.4.1. Staging and measurements of *M. natalensis* embryos and analysis of maternal plasma progesterone levels

All of the bats captured and examined were *M. natalensis* specimens according to the field identification system provided by Stoffberg *et al.* (2004). A total of 60 *M. natalensis* specimens were sacrificed and 53 embryos were obtained. Most of the *M. natalensis* embryos could easily be assigned to a distinct stage using the *C. perspicillata* staging system (Cretekos *et al.* 2005). Some of the embryos were placed in early or late stage categories (e.g. 12E: early; 13L: late; 15VE: very early) based on the progression of limb development (Table 2.1).

Table 2.1 Staging and measurements for *M. natalensis* embryos including the date that each stage was first obtained in the field in September 2006, the key limb features used to determine the stage based on Cretekos *et al.* (2005) and the number of specimens obtained for each stage. The average uterus and crown-rump measurements are shown in bold (±standard deviation) with the range of measurements given below.

Stage	Date	Key limb bud features	No. embryos	Uterus width (mm)	Uterus length (mm)	Crown-rump length (mm)
11	09/09	No limb buds present.	1	**3.00** -	-	-
12E	09/09	Forelimb bud (Flb) protrudes slightly.	2	**4.00 (+/- 0.71)** 3.5-4.0	-	**1.81 (+/- 0.20)***
12	09/08	Flb forms a distinct bulge in body wall.	1	**4.50** -	-	**2.79***
13	09/10	Flb extends along proximal-distal axis forming a semi-circular bulge; AER is present; hindlimb bud (Hlb) present.	1	**6.00** -	- -	**5.50** -
13L	09/09	Anterior side of Flb lengthens; Hlb forms a semi-circular bulge.	8	**5.50 (+/- 0.41)** 5.0 - 6.0	- -	**5.25 (+/- 0.27)** 5.0 - 5.5
14E	09/08	Flb is longer than it is wide; a flexure in the forelimb bud divides the proximal from the distal limb bud; Hlb AER present.	2	**5.50** -	- -	**6.00** -
14	09/08	Flb lengthens further along proximal-distal axis; propatagium primordium present as bulge on Flb proximal-anterior edge; anterior side of Hlb lengthens.	3	**6.33 (+/- 0.58)** 6.0 - 7.0	**10.50** -	**5.75 (+/- 0.35)** 5.5 - 6.0
14L	09/15	Plagiopatagium primordium (Plp) present as bulge on Flb proximal-posterior edge; distal Flb widens along anterior-posterior axis; anterior side of Hlb lengthens further forming an asymmetrical bud.	4	**6.5 (+/- 0.71)** 5.5 - 7.0	**10.50** -	**6.75 (+/- 1.19)** 5.5 - 8.0
15VE	09/16	Symmetrical hand plate forms; distal Hlb widens along anterior-posterior axis.	3	**7.00** -	**10.25 (+/- 1.06)** 9.5 - 11.0	**6.67 (+/- 0.29)** 6.5 - 7.0
15E	09/15	Thumb primordium protrudes from anterior hand plate, posterior hand plate expands; symmetrical foot plate forms.	2	**8.25 (+/- 0.35)** 8.0 - 8.5	**11.00** -	**7.75 (+/- 0.35)** 7.5 - 8.0
15	09/15	Further expansion of posterior hand plate; Plp bulges further outwards; further anterior- posterior expansion of foot plate.	5	**8.10 (+/- 0.22)** 8.0 - 8.5	**11.17 (+/- 0.76)** 10.5 - 12.0	**8.06 (+/- 0.56)** 7.5 - 9.0
16VE & E	09/10	Digit condensations visible in hand plate; edge of interdigital tissue between digits 4 and 5 takes on slight convex shape; further anterior- posterior expansion of foot plate.	3	**8.00 (+/-1.32)** 7.0 - 9.5	**11.00** -	**8.50 (+/- 0.50)** 8.0 - 9.0
16	09/18	Digit primordia extend slightly beyond hand plate edge resulting in a wavy appearance; foot plate digit condensations visible.	5	**8.70 (+/- 0.45)** 8.0 - 9.0	**12.30 (+/- 0.76)** 12.0 - 13.0	**9.5 (+/- 0.35)** 9.0 - 10.0
16L	09/17	Plp extends over the edge of the hand plate; interdigital tissue of foot plate begins to recede resulting in a "scalloped" appearance.	4	**9.13 (+/- 0.63)** 8.5 - 10.0	**12.50 (+/- 1.00)** 11.0 - 13.0	**9.75 (+/- 0.29)** 9.5 - 10.0
17E	09/17	Interdigital tissue between the thumb and digit 2 begins to recede; apoptosis of foot plate interdigital tissue advances.	2	**9.00** -	**12.75 (+/- 1.06)** 12.0 - 13.5	**9.5 (+/- 0.71)** 9.0 - 10.0
17	09/17	Interdigital tissue between the thumb and digit 2 recedes further; tips of foot plate digits are free.	5	**8.8 (+/- 0.57)** 8.0 - 9.5	**12.38 (+/- 1.18)** 11.5 - 14.0	**10.6 (+/- 0.42)** 10.0 - 11.0
18E	09/23	Thumb completely free; foot plate interdigital tissue receded a quarter of the way along the digits.	1	**9.00** -	**14.00** -	**11.00** -
18L	09/17	Third digit of hand lengthens; foot plate interdigital tissue receded half way along the digits.	1	**10.50** -	**16.00** -	**12.00** -
20	09/24	Digits of the hand lengthen and curve inwards; digits of the foot are completely free.	1	**10.00** -	**14.00** -	**15.00** -

* Measurement made using the Measure Tool in Adobe Photoshop 7.0 after the embryo was photographed.

The embryos ranged from stage 11 to stage 20 of development, with the youngest obtained early in September and the oldest in late September (Table 2.1). Both the uterus dimensions and embryo crown-rump length increased at a constant rate with increasing embryonic age (Table 2.1; Fig. 2.1). Maternal plasma progesterone levels increased steadily during development, peaking at stage 17 and dropping after parturition (Fig. 2.2).

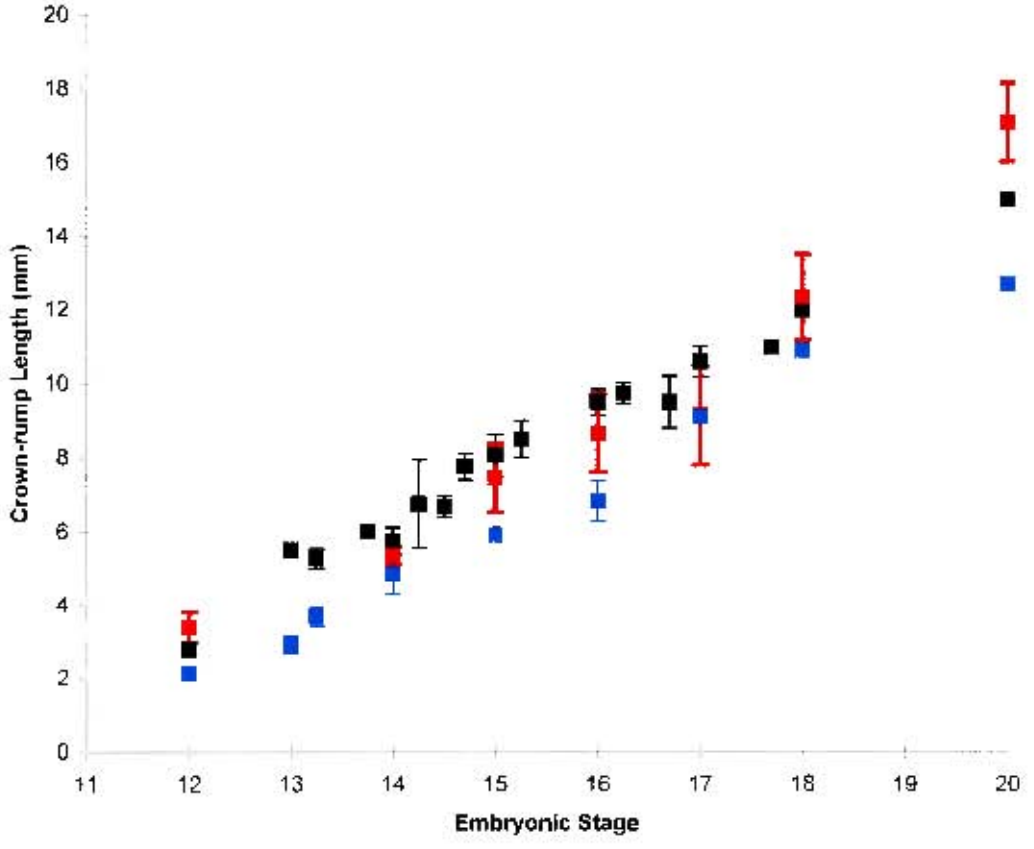

Fig. 2.1 Changes in the mean embryonic crown-rump length during development for *M. natalensis* (black), *C. perspicillata* (red; after Cretekos *et al.* 2005) and *P. abramus* (blue; after Tokita 2006). Error bars indicate standard deviations from the mean when more than one measurement was available.

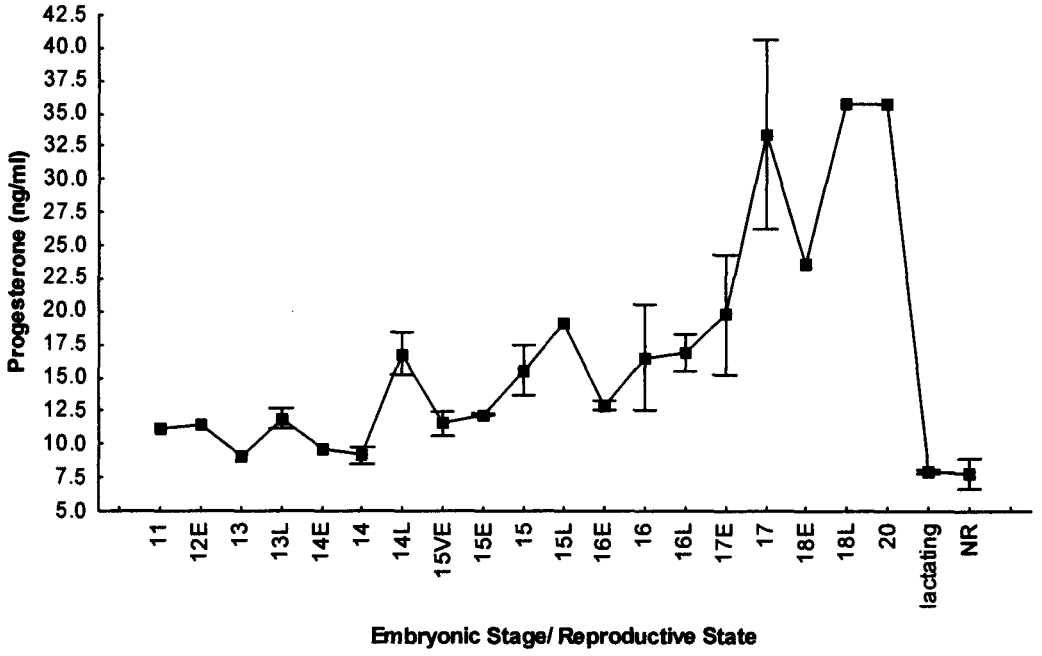

Fig. 2.2 Mean maternal plasma progesterone levels for *M. natalensis* during the early stages of embryonic development and while lactating. NR indicates samples taken from non-reproductive females, identified by the lack of conspicuous nipples. Error bars indicate the standard error of the mean when more than one measurement was available.

2.4.2. Detailed description of staged *M. natalensis* specimens

The appearance of the *M. natalensis* embryos at each stage of development was described in detail to compare the progression of limb development to that in the mouse and to determine when differences in limb bud size and shape become apparent between bats and mice. Although one stage 11 embryo was identified by visual inspection, this sample was not available for analysis as it was damaged during dissection. Embryos older than stage 17 were placed in RNAlater (Qiagen) for a concurrent microarray project and became deformed before a photograph was taken. Thus the detailed descriptions of *M. natalensis* development below include only stages 12 to 17.

2.4.2.1. Stage 12

Early in this stage the embryo is curved into a tight corkscrew-like curl, and the forelimb buds are visible as very slight projections from the flank (data not shown). As the stage progresses the curl of the embryo relaxes slightly and the forelimb buds are present as distinct semi-circular protrusions from the flank at the point of curvature of the embryo (Fig. 2.3A). The tail bud is present as a caudal projection and is bordered at its base by expanding flank on either side, which will form the hindlimb buds in the following stage (Fig. 2.3B; Fig. 2.4B). Three pharyngeal arches (mandibular, hyoid and glossopharyngeal) are present on either side of the developing cranial region, with the distal end of the glossopharyngeal arch hidden beneath that of the hyoid arch (Fig. 2.3A). The otic vesicles are visible as a tear-drop shaped 'sacs' just dorsal of the pharyngeal arches (Fig. 2.3A and C) and optic evaginations (Fig. 2.3A-B) are present on the sides of the forebrain.

2.4.2.2. Stage 13

The forelimb buds extend distally, increasing the radius of their semi-circular shape (Fig. 2.3E; Fig. 2.4D). Later in this stage the forelimb buds become distinctly longer than they are wide (Fig. 2.4H). The apical ectodermal ridge (AER) is visible along the distal edge of the forelimb buds (Fig. 2.3H; Fig. 2.4H). Hindlimb buds appear on the posterior flank of the embryo, caudal to the tail bud (Fig. 2.3F; Fig. 2.4F), and begin to resemble the early semi-circular forelimb buds by the end of the stage (Fig. 2.4J). The mandibular arch expands distally and a distinct oral groove is formed (Fig 2.3E). The glossopharyngeal arch is almost completely hidden beneath the hyoid arch (Fig 2.3E). The optic cups form and a projection, the endolymphatic appendage, extends dorsally from the otic vesicle (Fig 2.3E).

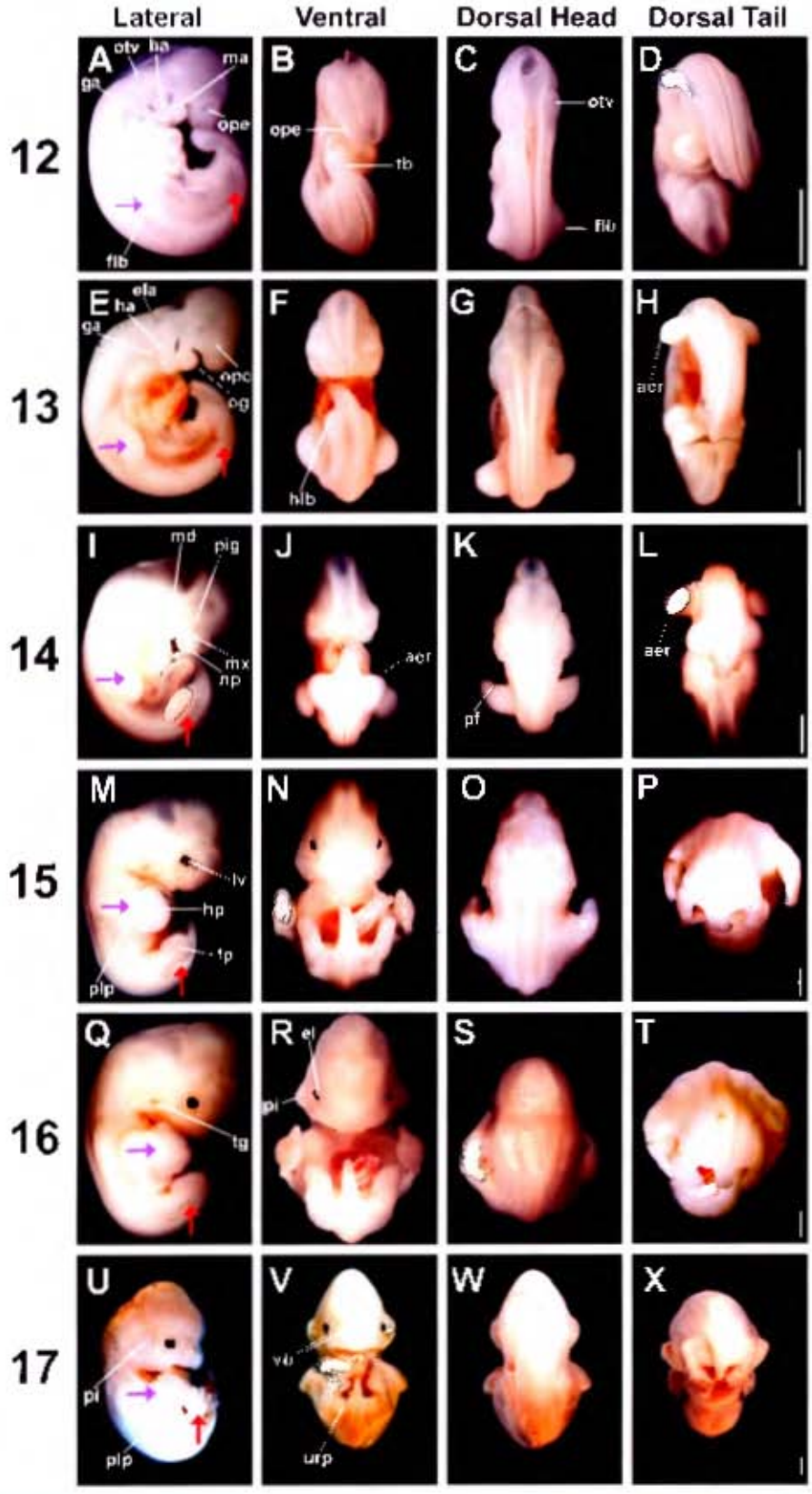

Fig. 2.3 Embryos from stages 12 to 17 of *M. natalensis* development. The first column (A,E,I,M,Q,U) shows lateral views with dorsal to the left, the second column (B,F,J,N,R,V) shows ventral views, the third column (C,G, K,O,S,W) shows dorsal views of the head and trunk and the fourth column (D,H,L,P,T,X) shows dorsal views of the trunk and tail. In the first column, purple arrows indicate the position of the forelimb and red arrows indicate the position of the hindlimb. aer, apical ectodermal ridge; el, eyelid; ela, endolymphatic appendage; flb, forelimb bud; fp, foot plate; ga, glossopharyngeal arch; ha, hyoid arch; hlb, hindlimb bud; hp, hand plate, lv, lens vesicle; ma, mandibular arch; md, mandible; mx, maxilla; np, nasal pit; og, oral groove; opc, optic cup; ope, optic evagination; otv, otic vesicle; pf, point of flexure; pi, pinna; pig, pigment; plp, plagiopatagium; tb, tail bud; tg, tragus; urp, uropatagium; vb, vibrissae. Scale bars = 1 mm in D (applies to A-D), in H (applies to E-H), in L (applies to I-L), in P (applies to M-P), in T (applies to Q-T) and in X (applies to U-X).

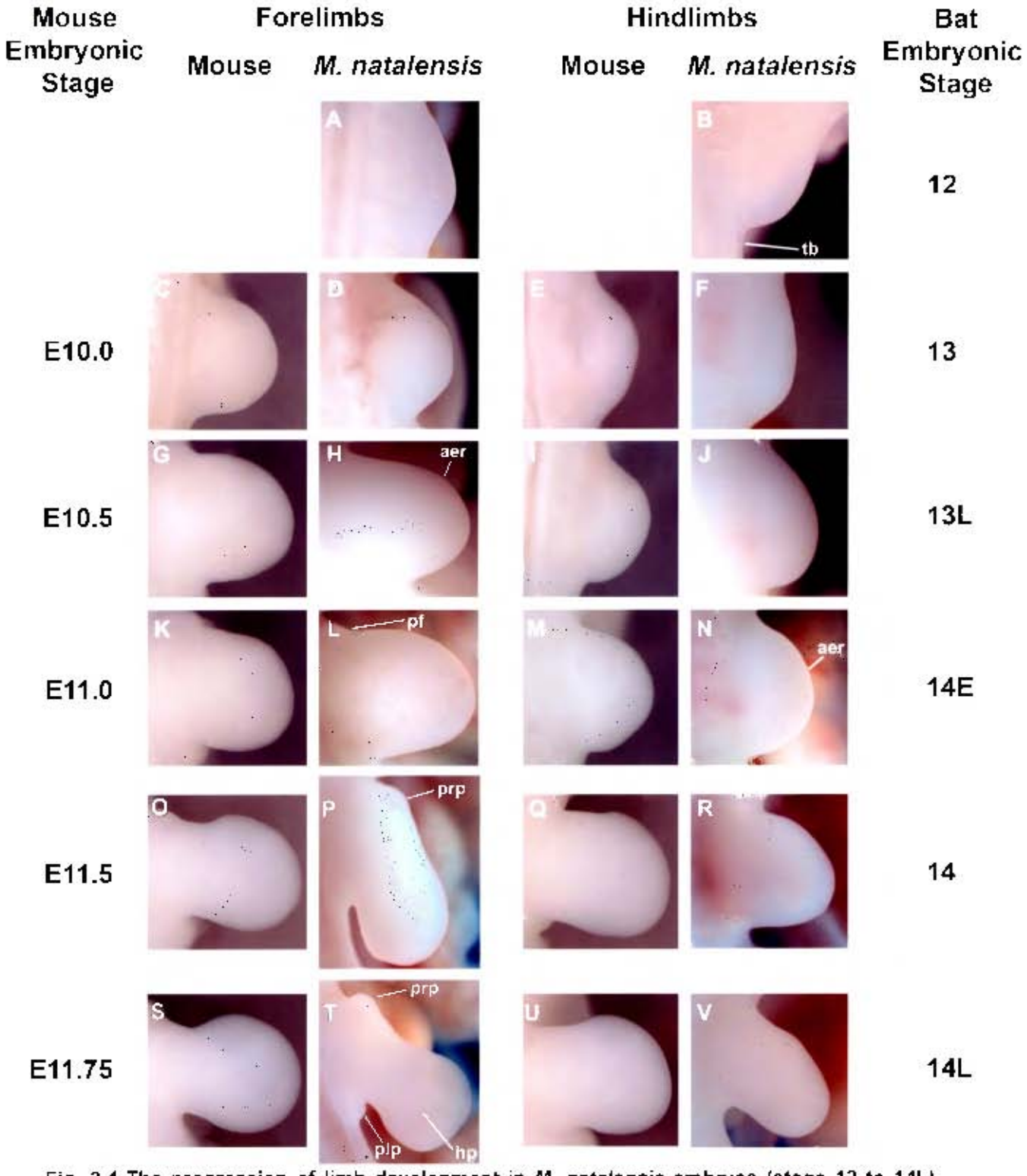

Fig. 2.4 The progression of limb development in *M. natalensis* embryos (stage 12 to 14L) compared to equivalently staged mouse embryos (E10.0 to E11.75). *M. natalensis* forelimbs: A, D, H, L, P and T *M. natalensis* hindlimbs: B, F, J, N, R and V. Mouse forelimbs: C, G, K, O, and S. Mouse hindlimbs: E, I, M, Q and U. The embryonic day (E) of mouse development is indicated down the left side, while the stage of bat development based on Cretekos *et al.* (2005) is indicated down the right side. aer, apical ectodermal ridge; hp, hand plate; pf, point of flexure; plp, plagiopatagium primordium; prp, propatagium primordium; tb, tail bud. All panels show the dorsal surface of the limb with anterior towards the top and proximal at left. Views are not to scale.

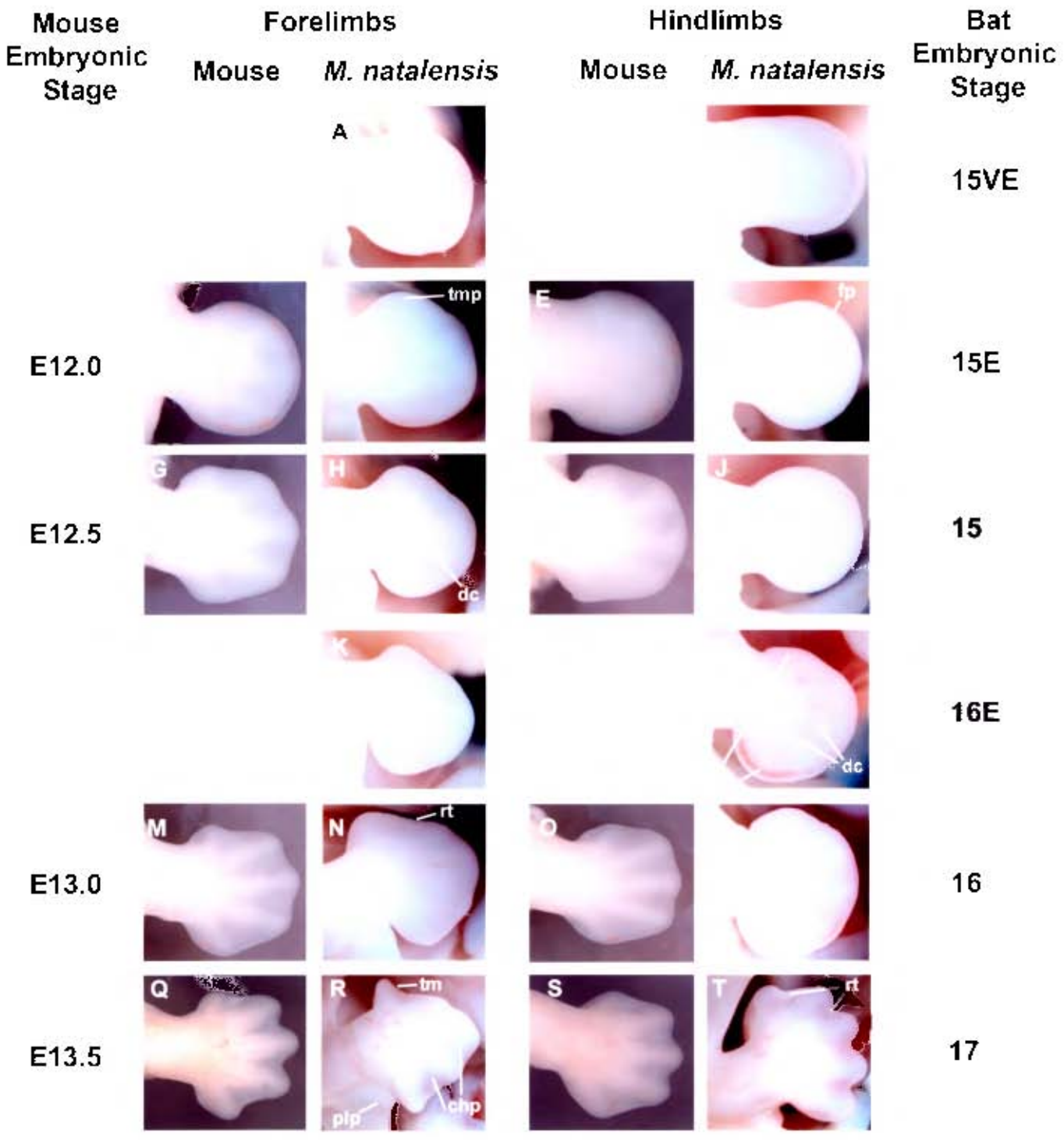

Fig. 2.5. The progression of limb development in *M. natalensis* embryos (stage 15VE to 17) compared to equivalently staged mouse embryos (E12.0 to E13.5). *M. natalensis* forelimbs: A, D, H, K, N and R. *M. natalensis* hindlimbs: B, F, J, L, P and T. Mouse forelimbs: C, G, M, and Q. Mouse hindlimbs: E, I, O, and S. The embryonic day (E) of mouse development is indicated down the left side, while the stage of bat development based on Cretekos *et al.* (2005) is indicated down the right side. chp, chiropatagium; dc, digit condensation; fp, foot plate; pe, proximal expansion; plp, plagiopatagium; rt, receding tissue; tm, thumb; tmp, thumb primordium. All panels show the dorsal surface of the limb with anterior towards the top and the proximal at left. Views are not to scale.

2.4.2.3. Stage 14

Early in this stage, a point of flexure appears in the forelimb buds, dividing the proximal limb bud from the distal limb bud (Fig. 2.3K; Fig. 2.4L). An AER is present along the distal edge of the hindlimb buds (Fig. 2.3J; Fig. 2.4N). As the stage progresses the forelimb buds extend greatly along their proximal-distal axes, and lie against the flank of the embryo (Fig. 2.3I). The primordia of the propatagia (the membrane at the leading edge of the wing) appear as a bulge at the proximal-anterior edge of the forelimb buds (Fig. 2.4P). The hindlimb buds lengthen distally, resembling the late stage 13 forelimb buds (Fig 2.4R). Later in this stage, the distal forelimb buds expand along their anterior-posterior axis to form the beginnings of hand-plates (Fig. 2.4T). The propatagium primordia extend further and the plagiopatagium primordia (the wing membrane between the forelimb and hindlimb) become visible at the proximal-posterior edge of the forelimb buds (Fig. 2.4T). The hindlimb buds lengthen along their anterior sides, taking on an asymmetrical shape curving towards the base of the tail (Fig. 2.4V). The head of the embryo takes on a "podgy" form as the mandibular arch expands, dividing into maxillary and mandibular components and nasal pits form (Fig. 2.3I & J). A circle of pigment is visible in the developing retina (Fig. 2.3I).

2.4.2.4. Stage 15

Very early in this stage the forelimb buds expand further along the anterior-posterior axis and flatten dorso-ventrally to form 'paddle-like', symmetrical hand plates (Fig. 2.3M, Fig. 2.5A). The limb buds no longer lie alongside the body, but rather project outwards at right angles to the body axis (Fig. 2.3M). The anterior edges of the hindlimb buds expand slightly, however the hindlimbs retain their asymmetrical shape (Fig. 2.5B). As the stage progresses, the hand plates become asymmetrically shaped (Fig. 2.5D). Thumb primordia protrude from the anterior edge of the hand plates, while the posterior edges retain a rounded paddle shape (Fig. 2.5D). The hindlimb buds continue their anterior expansion, resulting in symmetrical foot plates (Fig. 2.5F). At the pinnacle of this stage the hand plates are distinctly asymmetrical due to the protrusion of the thumb primordia on their anterior edges and the expansion of

their posterior borders (Fig. 2.5H). Digit condensations become visible in the mesenchyme of the hand plates (Fig. 2.5H). The foot plates continue to expand symmetrically along their anterior-posterior axes (Fig. 2.5J). Throughout this stage the plagiopatagium primordia expand along the posterior edges of the forelimb bud, reaching the wrist, and begin to expand caudally forming membranous flaps along the flanks of the embryo (Fig. 2.5A, D & H). The retina becomes fully pigmented and the lens vesicle is present (Fig. 2.3M & N).

2.4.2.5. Stage 16

Early in this stage the thumb is easily distinguished from the rest of the hand plate as the tissue between the developing thumb and the primordium of digit 2 begins to recede, taking on a concave appearance (Fig. 2.3Q, Fig. 2.5K). The posterior-distal edges of the hand plates expand further accentuating the extreme asymmetry of the hand plates (Fig. 2.5K). The foot plates also continue to expand along the anterior-posterior axis. This expansion is concentrated at the most proximal edges of the foot plates (Fig. 2.5L). Digit condensations form in the foot plates and the tissue between these condensations begins to recede resulting in a disruption of the smooth edge of the foot plates seen at stage 15 (Fig. 2.5L & P). As the stage progresses the digital rays of the hand plates begin to extend distally. This extension, in combination with inter-digital tissue cell death at the border of the hand plates, results in a wavy appearance in the border of the hand plates (Fig. 2.5N). The interdigital tissue between the thumb and the primordium of digit 2 becomes corrugated as the tissue dies (Fig. 2.5N). Eyelid primordia are present as swellings around the eyes (Fig. 2.3R). Both the pinnae and tragii of the developing ears are clearly visible (Fig. 2.3Q & R).

2.4.2.6. Stage 17

The limbs show pronounced flexures at the elbow and knee joints, and the wrists are flexed (Fig. 2.3U). As a result the hands are tucked beneath the chin (Fig. 2.3V). The interdigital tissue between the thumb and digit 2 is almost completely receded, while

the tissue between the remaining digits persists to form the primordia of the chiropatagia (the wing membrane) (Fig. 2.5R). The digits are clearly defined and their phalanges begin to curve inwards (Fig. 2.5R). The tips of the digits of the foot plates are free from interdigital tissue and appear to be equal in length (Fig. 2.5T). The plagiopatagia extend between the wrists and the ankles (Fig. 2.3U; Fig. 2.5R). The uropatagium (tail membrane) extends half way along the length of the tail and along the posterior edges of the hindlimbs (Fig. 2.3V). The pinnae of the ears are lengthened at their distal tips and fold inwards (Fig. 2.3U & V). The mouth is open and vibrissae follicles are visible on the snout and around the eyes (Fig. 2.3U & V).

2.5. Discussion

2.5.1. Staging of embryonic development in *M. natalensis*

In their embryonic staging paper for *C. perspicillata*, Cretekos *et al.* (2005) show that their staging system is very robust when used to stage embryonic specimens of species within the Phyllostomidae (*Phyllostomus hastatus* and *Desmodus rotundus*). In addition, the staging system developed by Cretekos *et al.* (2005) has been successfully applied to specimens from the Miniopteridae (this study) and the Vespertilionidae (Tokita 2006). *M. natalensis* embryos were easily placed in the stages defined by Cretekos *et al.* (2005) by comparing the progress of limb development and other features, such as eye and ear development, to that for *C. perspicillata*. While the progress of development of these features is very similar between species, it is unknown whether the same can be said for the timing of development. Early limb bud stage *M. natalensis* embryos are present by mid-September (Table 2.1), as has been reported for the populations in the Limpopo and Gauteng provinces (van der Merwe & van Aarde 1989) and Kwazulu Natal (Bernard 1980), however the date of implantation is not known for the De Hoop population, and thus the age of the *M. natalensis* specimens could not be determined.

As found for *C. perspicillata* (Cretekos *et al.* 2005), the uterus dimensions of *M. natalensis* are a good indicator of embryonic stage. It is possible to feel for this increase in uterus size by massaging the belly of the bat as described by Racey (1969)

for *Pipestrellus pipistrellus*. As pregnancy progresses the boundary between the uterus and the rib cage becomes less distinguishable. In this manner earlier stages (13-14) can be distinguished from later stages (16-18) prior to dissection.

Maternal plasma progesterone levels may be a further, more accurate indicator of embryonic stage. This study provides greater resolution of the changes in maternal plasma progesterone during limb development than those previously reported for *M. natalensis* from the Limpopo and Gauteng provinces (van der Merwe & van Aarde 1989) and for *M. schreibersii* (Bernard *et al.* 1991). Although these studies indicated a distinct rise in progesterone levels from early to late pregnancy, they provided only four readings during post-implantation pregnancy and the stages of embryonic development corresponding to these data points were not described in detail. In this study, progesterone levels are shown to increase steadily from stage 11 to stage 17 of development. Three distinct groups can be visualised within this trend: stages 11-14, 14L-17E and 17-20 representing early, middle and late stages of limb development respectively. These three groups are all visibly different from the lactating and non-reproductive females. However, due to the low number of samples at some stages, these groups could not be characterised as statistically diagnostic entities. Further sampling is needed to show if maternal progesterone levels can be used as a statistically robust non-invasive indicator of embryonic stage in *M. natalensis*.

2.5.2. Species-specific differences in development between bat species

Alongside the similarities in development between species, species-specific differences between adult *M. natalensis* and *C. perspicillata*, such as differences in tail length, become evident during embryonic development. The tail of the adult *C. perspicillata* is highly reduced, while that of *M. natalensis* is long and completely encased within the uropatagium. Until stage 15 of development the tail primordia of the two species are very similar, both extending far beyond the hindlimb buds. At stage 15 the tail bud of *C. perspicillata* begins to recede and by stage 17 it is barely visible within developing uropatagium (Cretekos *et al.* 2005). In *M. natalensis* the tail bud remains long at stage 15 and by stage 17 the uropatagium is only half way along its length. A similar pattern of tail development is evident in *Pipistrellus abramus*,

whose long tail is completely encased in the uropatagium by stage 20 (Tokita 2006). Thus, the pattern of tail development in these three species mirrors their phylogenetic relationship, with the closely related miniopterids and vespertilionids showing very similar development and adult features. The differences in the adult tail morphology between these species are most likely linked to differences in flight and feeding behaviour.

Tokita (2006) suggests that species-specific differences in adult size may also be evident during embryonic development. The crown-rump length (CRL) of *P. abramus* is always smaller than *C. perspicillata* at each stage of development (Tokita 2006), correlating with the smaller size of the adult bat (head and body length (HBL) *P. abramus*: 41-60 mm (Maeda 2005 in Tokita 2006); *C. perspicillata*: 48-65mm; (Nowak 1999)). The CRL of *M. natalensis* is larger than *P. abramus* throughout the observed stages of development while falling within the range of *C. perspicillata* measurements between stages 14 and 17 (Fig 2.1.). These observations support the trend suggested by Tokita (2006) as adult *M. natalensis* are larger than *P. abramus* and share much of their adult size range with *C. perspicillata* (HBL *M. natalensis*: 40-78mm; (Nowak 1999)). Measurements for *M. natalensis* embryos at later stages of development are needed to provide further support for this trend.

2.5.3. Comparing limb development between *M. natalensis* and the mouse

The progression of limb development in *M. natalensis* was compared to that of the mouse to determine when noticeable differences in limb bud shape and size become apparent. It is possible that these differences are caused by changes in the expression patterns of limb patterning genes. Thus, these stages of development would be the focus of subsequent comparative gene expression analyses.

During the early stages of development the growing limb buds of *M. natalensis* and the mouse are very similar in size and shape. In both organisms, the forelimb bud appears first, with the hindlimb bud lagging a stage behind. Forelimb development commences in the mouse at E9.5, appearing as a slight protrusion from the embryonic

flank (Martin 1990). This semi-circular protrusion is similar in shape to the forelimb bud of the *M. natalensis* embryo, which appears at stage 12 (Fig. 2.4A). The hindlimb bud appears in the mouse at E10.0 (Martin 1990; Fig. 2.4E) resembling the first sign of the hindlimb bud in the stage 13 *M. natalensis* embryo. Up to stage 14 of *M. natalensis* development, both fore- and hindlimb development progress in a similar manner to that of the mouse, with stages 13, 13L and 14E corresponding to E10.0, E10.5 and E11.0 of mouse development respectively (Fig. 2.4C-N). During these stages the limb buds of both organisms grow out to form protrusions that are distinctly longer than they are wide.

At stage 14 of *M. natalensis* development, the forelimb bud becomes distinct from the equivalently staged mouse limb bud at E11.5 (Fig. 2.4O & P). The primordia of the wing membranes, the propatagia and the plagiopatagia, become apparent at the distal-anterior and posterior edges of the limb bud respectively (Fig. 2.4P & T). As development progresses, symmetrical hand plates form in equivalently staged *M. natalensis* (14L-15VE; Fig. 2.4T & Fig.2.5A) and mouse embryos (E11.75; Fig. 2.4S). In the mouse, this hand plate flattens dorso-ventrally and expands equally at its anterior and posterior edges forming a paddle-like shape by E12.0 (Fig. 2.5C). In *M. natalensis* this expansion takes place between stages 15E and 16 (Fig 2.5D, H, K, N), with the posterior edge experiencing a far greater expansion than that seen in the mouse, resulting in a distinctly larger hand plate at stage 16 than that of an E13.0 mouse (Fig. 2.5M & N). By stage 17, this expanded tissue begins to condense into digits and the interdigital tissue is retained, forming the chiropatagium (Fig. 2.5R). At this stage the bat wing is clearly defined. In contrast, the interdigital tissue of the mouse forelimb begins to recede at E12.5 (Fig. 2.5G) and the digits of the paw are almost completely free by E13.5 (Fig. 2.5Q). Thus, between stage 14 and stage 16 of bat limb development, equivalent to E11.0 to E13.0 of mouse development, the pattern is laid down for wing development in the bat in contrast to paw development in the mouse.

In both *M. natalensis* and the mouse, the hindlimb lags a stage behind the forelimb in its progress of development. The hindlimb bud of the bat resembles that of the mouse up to stage 15E or E12.0 of development (Fig. 2.5E & F). At this stage, both organisms display symmetrically shaped foot plates with smooth edges, as interdigital

tissue death has not yet begun (Fig. 2.5E & F). At E12.5 in the mouse and stage 16E *M. natalensis* the foot plate begins to take on a "scalloped" appearance as interdigital tissue death proceeds (Fig. 2.5I & L). In addition, between stages 15 and 16 the *M. natalensis* footplate appears to experience further expansion along the anterior-posterior axis, especially at it most proximal boundaries (Fig. 2.5J, L & P). This results in a much wider foot plate in *M. natalensis* at stage 16 than that of the E13.0 mouse (Fig. 2.5O & P). This additional hindlimb expansion is also evident during *C. perspicillata* development (Cretekos *et al.* 2005). As a result of this expansion, it is possible that the pool of cells that will contribute to the most proximal digits of the bat foot (digits 1 and 5) is larger than the same pool of cells in the mouse foot. The availability of a larger pool of cells for digit formation may result in digits 1 and 5 growing longer than those of the mouse. As a result, the developing digits of the *M. natalensis* foot at stage 17 appear to be equal in length, while the digit 1 and 5 of the mouse foot are noticeably shorter than the remaining digits by E13.5 (Fig. 2.5S & T).

These differences in early limb development between *M. natalensis* and the mouse suggest that the early genetic signals for limb patterning have been altered in the bat, laying down the blueprint for the unique bat forelimb and hindlimb skeletal structure prior to digit formation. The experiments described in the following chapters test this hypothesis by investigating one such early limb patterning signal, the *Sonic Hedgehog* pathway, during bat limb development.

Chapter 3

Shh and *Ptc1* expression analysis in developing mouse and bat limbs by whole mount *in situ* hybridisation

---

3.1. Introduction

The developing bat forelimb begins to differ from that of the mouse as early as stage 14 of development with the appearance of the wing membrane primordia (Fig. 2.4). This difference is further enhanced by stage 15 when the posterior of the bat hand plate is expanded, leading to the elongated, webbed digits visible in the stage 17 forelimb (Fig. 2.5). The bat hindlimb begins to differ from that of the mouse between stages 15 and 16 of development. The bat foot plate undergoes a proximal expansion resulting in digit primordia of equal length at stage 17, while in the mouse hindlimb the primordia of digits 1 and 5 are shorter than digits 2 to 4 (Fig. 2.5). It is possible that changes in the expression pattern of the limb patterning signal, *Shh*, and its downstream target, *Ptc1,* account for both the morphological differences between the bat and mouse limbs and the skeletal differences between the bat forelimbs and hindlimbs.

Whole mount *in* situ hybridisation was used to visualise the expression patterns of *Ptc1* and *Shh* in stage 13L to 17 *Miniopterus natalensis* and *Carollia perspicillata* limbs and these expression patterns were compared to those in E10.0 to E13.5 mouse limbs. This procedure required the preparation of labelled RNA probes that are complimentary to the mRNA sequence of *Ptc1* and *Shh.* cDNA was prepared from both *M. natalensis* and mouse embryonic RNA in the hope of generating bat- and mouse-specific RNA probes. A short sequence of both *Ptc1* and *Shh* was isolated from the cDNA using the polymerase chain reaction (PCR) and cloned into a vector to be used in an *in vitro* transcription RNA probe synthesis reaction. This labelled probe was then used for whole mount *in situ* hybridisation.

3.2. Materials and Methods

3.2.1. Cloning of *Ptc1* and *Shh* orthologs

3.2.1.1. Extraction of RNA and first strand cDNA synthesis

Total RNA was extracted from whole stage 13L *M. natalensis* and E13.5 mouse embryos stored in RNAlater (Qiagen, see Chapter 2) using the RNeasy Lipid Tissue Mini Kit (Qiagen) according to the manufacturer's protocol. The concentration and quality of the extracted RNA was quantified by measuring the absorbance at 260 nm and 280 nm. RNA integrity was verified by denaturing 1 µg of RNA in 9 µl formamide at 70 °C for 10 min and snap-cooling for one min, followed by electrophoresis through a 1.0 % agarose gel.

A standard 20 µl reverse transcription reaction was prepared as follows. 5 µg of total RNA was mixed with 50 µM Oligo (dT) primer, 500 ng Random Primers (Promega) and 0.5 mM dNTPs (a mixture of dATP, dGTP, dCTP and dTTP at equal concentrations). This mixture was denatured at 65 °C for 5 min and snap-cooled on ice for 5 min. Following denaturation, 1x First-Strand Buffer (Invitrogen), 2.5 mM DTT, 40 U Protector RNase Inhibitor (Roche) and 200 U Superscript III Reverse Transcriptase (Invitrogen) were added and the mixture was incubated at 25 °C for 5 min. The mixture was then moved to 55 °C. After 2 hours an additional 200 U Superscript III Reverse Transcriptase (Invitrogen) was added to the mixture and incubated overnight at 55 °C.

3.2.1.2 PCR amplification *Ptc1* and *Shh* orthologs

PCR primers for the amplification of the *M. natalensis* and mouse orthologs of *Ptc1* and *Shh* were designed from regions of near identity in cDNA sequence alignments of human, mouse, rat and dog *Ptc1* and *Shh* respectively (Appendix A: Fig. A1 & A2), with Inosine (I) being used in the place of non-conserved base pairs (Note: bat cDNA sequences were not included in the alignments as the primers were designed prior to

the release of the *Myotis lucifugus* genome on Ensembl). *Ptc1* primers (Ptc1Fwd: 5'ACC TTT GGA CTG CTT CTG GGA A 3'; Ptc1Rev: 5'AAA IGG CAA AAC CTG AGT TG 3') were designed to amplify a region of 830 bp from exon 5 to 10 of the gene (Fig. 3.1A). *Shh* primers (Shhfwd: 5' AGC CAA GAA GGT CTT CTA CGT G 3'; ShhRev: 5' AIA TIT GGT AGA GCA GCT GCG A 3') were designed to amplify a region of 520 bp from exon 3 of the gene (Fig. 3.1B). The 5' terminal Adenosine (A) was added to the *Shh* primers to increase cloning efficiency (Peist *et al.* 2002).

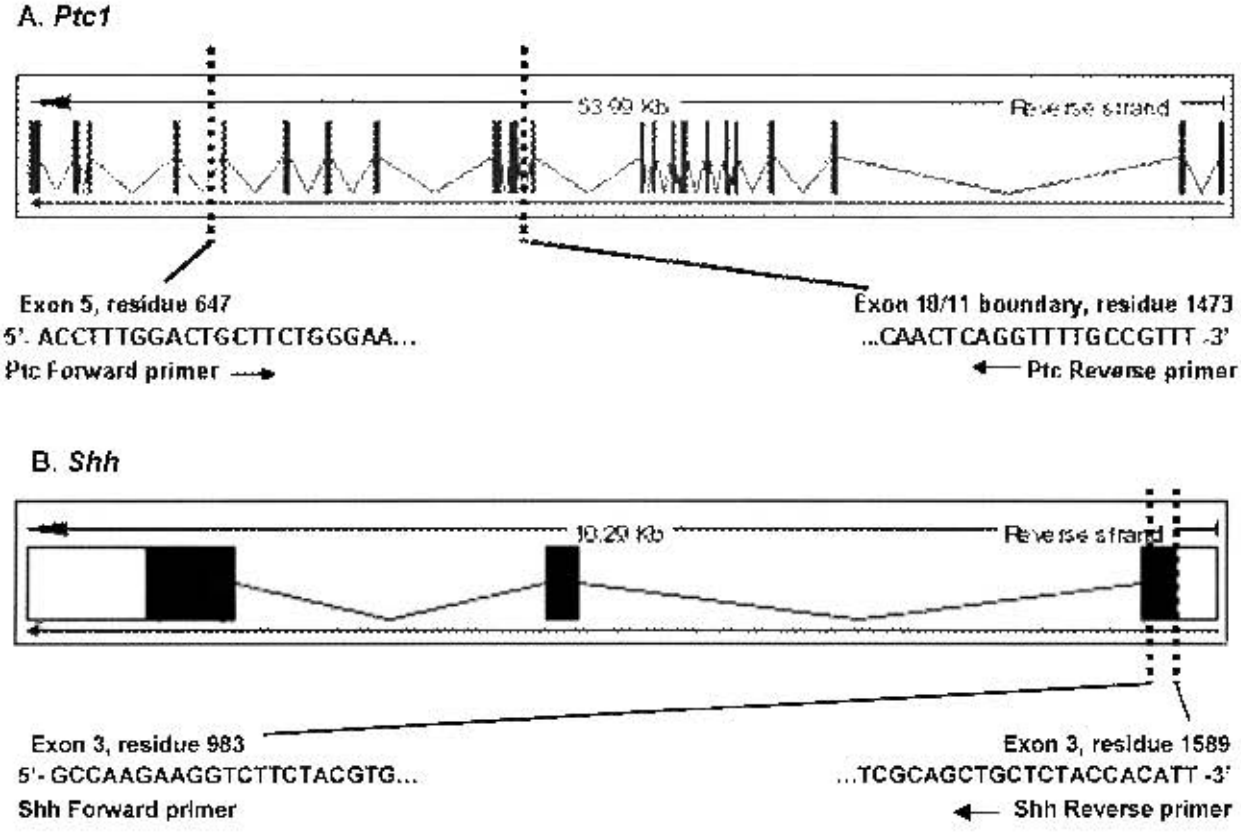

Fig 3.1 Primer design for the amplification of *Ptc1* and *Shh* orthologs by PCR. The Ensembl (release 46) transcript constructs for (A) mouse *Ptc1* (ENSMUST00000021921) and (B) mouse *Shh* (ENSMUST00000002708) showing the positions of the primers used to clone 830bp of *Ptc1* and 520bp of *Shh* from mouse and *M. natalensis* cDNA.

Either 2 µl of the *M. natalensis* first strand synthesis cDNA reaction or 1 µl of a 1 in ten dilution of the mouse first strand synthesis cDNA reaction was used as a template in the following standard 25 µl PCR reaction: 1x Reaction Buffer, 1.5 mM $MgCl_2$, 0.2 mM dNTPs, 0.4 µM of each primer and 1 U of Super-Therm Polymerase (Southern

Cross Biotechnology). The PCR cycling conditions for amplification of *Ptc1* from both *M. natalensis* and mouse cDNA were as follows: 94 °C for 2 min (1 cycle), 94 °C for 30 sec, 50 °C for 30 sec, 72 °C for 1 min (35 cycles) and 72 °C for 5 min (1 cycle).

The PCR cycling conditions for amplification of *Shh* from mouse cDNA were as follows: 94 °C for 1 min (1 cycle), 94 °C for 30 sec, 62 °C for 1 min, 72 °C for 1 min (35 cycles) and 72 °C for 5 min (1 cycle). Variations on these cycling conditions (annealing temperatures from 40 °C to 60 °C) and a series of primer pairs (Appendix A: Table A) were used in an attempt to amplify *Shh* from *M. natalensis* cDNA. PCR was performed using the GeneAmp PCR System 9700 DNA amplifier (Applied Biosystems).

3.2.1.3. Cloning and transformation of *Ptc1* and *Shh* orthologs into *E. coli*

PCR products were resolved on a 1 % low melting point agarose gel, excised and purified using the QIAquick Gel Extraction Kit (Qiagen) according to the manufacturer's protocol. The extracted DNA fragments were ligated into the pDrive Cloning Vector (Qiagen) according to the manufacturer's protocol. 5 µl of the ligation mix was transformed into 100 µl competent *E. coli* DH5α cells. Initial positive transformants (white colonies) were identified by β-galactosidase insertional inactivation and ampicillin resistance on Luria-Bertani agar plates supplemented with 0.5 mM IPTG, 80 µg/ml X-Gal and 100 µg/ml ampicillin.

3.2.1.4. Screening transformants for correct inserts and sequencing

White colonies were randomly picked and screened for inserts by colony PCR using SP6 and T7 primers in the following 20 µl PCR reaction: 1x Reaction Buffer, 1.5 mM $MgCl_2$, 0.2 mM dNTPs, 0.4 µM of each primer, and 1 U of Super-Therm Polymerase (Southern Cross Biotechnology). The PCR cycling conditions were as follows: 94 °C

for 5 min (1 cycle), 94 °C for 30 sec, 52 °C for 30 sec, 72 °C for 1 min (30 cycles) and 72 °C for 5 min (1 cycle). PCR products were resolved by gel electrophoresis through a 1 % agarose gel. Insert positive reactions were cleaned up using the QIAquick PCR Purification Kit (Qiagen) according to the manufacture's protocol and quantified by measuring absorbance at 260 nm. The purified PCR products were sequenced by Macrogen Inc. (Seoul, Korea) in both directions with SP6 and T7 primers using a Big Dye terminator v3.1 Cycle Sequencing kit (Applied Biosystems) according to the manufacturer's protocol.

3.2.1.5. Bioinformatics analysis of *Ptc1* and *Shh* orthologs

A consensus sequence for each insert was obtained by aligning the sequences obtained with the Sp6 and T7 primers in BioEdit Sequence Alignment Editor 7.0.2 (Hall 1999). Sequences were positively identified as *Ptc1* or *Shh* using the Basic Local Alignment Search Tool (BLAST) (Altschul *et al.* 1997) provided by the National Center for Biotechnology Information. The appearance of *Ptc1* or *Shh* cDNA sequences within the top five Blastn results indicated that the insert contained the correct sequence. The percent sequence identity between the isolated mouse and *M. natalensis Ptc1* sequences and between the isolated *M. natalensis Ptc1* sequence and the published *M. lucifugus Ptc1* sequence (ENSMLUT00000016253) was determined using the Two Sequence Alignment Tool provided by DNAMAN version 5.2.9 (Lynnon Biosoft).

3.2.2. *Ptc1* and *Shh* DIG-labelled RNA probe synthesis

Four DIG-labelled RNA probes were synthesised: two *Ptc1* probes using the isolated mouse (PtcProbeM) and *M. natalensis* (PtcProbeB) *Ptc1* sequences as templates and two *Shh* probes using the isolated mouse *Shh* sequence (ShhProbeM1) and an additional mouse *Shh* sequence (ShhProbeM2) provided by Dr. Behringer (University of Texas M.D. Anderson Cancer Centre, Houston, Texas) as templates. Overnight cultures of colonies containing *Ptc1* and *Shh* insert-positive plasmids were prepared in Luria-Bertani medium containing 100 µg/ml ampicillin. Plasmids were purified from

the overnight cultures using the QIAprep Spin Miniprep Kit (Qiagen) according to the manufacturer's protocol. Purified plasmids were checked for inserts in the following 20 µl restriction digest reaction at 37 °C, for one hour: 500 ng plasmid DNA, 1x Restriction Enzyme Buffer and 2 U EcoR1 restriction enzyme (Fermentas).

Insert positive plasmid DNA was linearised in the following 20 µl restriction digest reaction at 37 °C, left overnight: 10 µg plasmid DNA, 1x Restriction Enzyme Buffer and 2 U restriction enzyme. ShhProbeM1 and PtcProbeB plasmids were linearised with BamH1 (Fermentas), ShhProbeM2 plasmids were linearised with HindIII (Fermentas) and PtcProbeM plasmids were linearised with Sal1 (Fermentas). Plasmid linearisation reactions were cleaned up using the QIAquick PCR purification Kit (Qiagen) according to the manufacturer's protocol. The purified linearised plasmid was eluted in 30 µl Tris-EDTA Buffer (pH 8.0) and quantified by measuring absorbance at 260 nm.

2.5 µg of linearised plasmid was used in the following 50 µl *in vitro* transcription RNA labelling reaction at 37 °C for two hours: 1x DIG RNA labelling mix (Roche, contains digoxigenin labelled UTP), 1x Transcription Buffer and 2 U RNA polymerase. ShhProbeM1 and PtcProbeB DIG-labelled probes were transcribed with Sp6 RNA polymerase (Roche), ShhProbeM2 was transcribed using T3 RNA polymerase (Roche) and PtcProbeM DIG-labelled probe was transcribed using T7 RNA polymerase (Roche). The plasmid template was subsequently degraded with 5 U Rnase-free DNAse I (Ambion) at 37 °C for 15 min. This reaction was stopped by adding 0.8 µl 0.5M EDTA (pH 8.0). A Sigma-Spin Post Reaction Clean-up Column (Sigma) was used to clean up the DIG-labelled RNA probe solution according to the manufacturer's protocol. The concentration of the probe solution was determined by measuring absorbance at 260 nm. The integrity of the probe was checked by denaturing 1 µl of the probe solution in 9 µl formamide at 70 °C for 10 min, followed by electrophoresis through a 1 % agarose gel. 1 µl 0.5M EDTA (pH 8.0) and 9 µl RNAlater (Qiagen) was added to the probe solution and it was stored at -80 °C.

3.2.3 Whole mount *in situ* hybridisation on *M. natalensis*, *C. perspicillata* and mouse embryos

3.2.3.1. Pre-treatment of embryos

The whole mount *in situ* hybridisation protocol that was used is based on Hecksher-Sorenson *et al.* (1998) and Xu & Wilkinson (1999). PFA fixed embryos were rehydrated from 100 % methanol (see chapter 2) through a series of 75 %, 50 % and 25 % methanol in DEPC PBS for 10 min at each step. All steps were carried out on ice and the embryos were allowed to sink into each solution. The embryos were cut in half along their midlines while in DEPC PBS to allow for analysis of *Shh* expression on one side and *Ptc1* expression on the other. The embryos were rinsed several times in DEPC PBS containing 0.1 % Tween 20 (PBST) and treated with 10 µg/ml Proteinase K (Fermentas) in PBST at room temperature for the following time periods: Mouse Embryos: E10.0: 22 min, E11.0: 25 min, E11.5 & E11.75: 28 min, E12.0: 30 min, E12.5: 35 to 45 min, E13.0: 35 min and E13.5: 37 min; *M. natalensis* embryos: 13L: 20 min, 14E: 22 min, 14: 24 min, 14L: 25 min, 15VE and 15E: 27 min, 15: 29 min, 16VE and 16E: 32 min, 16: 37 min, 17: 43 min; *C. perspicillata* embryos: 14E: 23 min, 14: 25 min, 14L: 26 min, 15VE: 28 min, 15E: 29 min, 15: 31 min, 16E: 32 min, 16L: 43 min and 17: 65 min. Following Proteinase K treatment the embryos were rinsed several times in PBST and fixed in 4 % PFA (Sigma) in DEPC PBS for 55 min at room temperature.

3.2.3.2. Hybridisation of the DIG-labelled RNA probe

After fixation the embryos were washed twice in hybridization solution (50 % formamide, 5 x standard saline citrate (SSC), 2 % Blocking Reagent (Roche), 0.1 % Tween 20, 0.1 % CHAPS (Fluka), 5 mM EDTA, 0.05 µg/ml Heparin (Sigma) and 0.05 µg/ml yeast tRNA (Sigma)). The washes were carried out at room temperature and the embryos were allowed to sink into the solution. The embryos were incubated in pre-warmed hybridisation solution while rotating in a hybridisation oven. For *Shh* expression analysis the pre-hybridisation washes were performed at 57 to 60 °C for

mouse, *M. natalensis* and *C. perspicillata* embryos. For *Ptc1* expression analysis these washes were performed at 60 °C for mouse and *C. perspicillata* embryos and at 65 °C for *M. natalensis* embryos. After 1 hour the solution was changed and pre-hybridisation was continued for 4 hours. The DIG-labelled RNA probes were then added (0.5-1 µg/ml in hybridisation solution) and hybridisation was carried out overnight at the same temperature as the pre-hybridisation incubation.

The initial post-hybridisation washes were carried out at room temperature in decreasing concentrations of hybridisation solution in 5 x SSC (75 %, 50 % and 25 %) for 10 min each, while shaking. At each step, the embryos were first rinsed in a mixture of the previous solution and the new solution before the wash began. The washes were followed by two 30 min low stringency washes in 5 x SSC, 0.1 % CHAPS and two 30 min high stringency washes in 2 x SSC, 0.1 % CHAPS. These post-hybridisation washes were carried out at 65 °C for the mouse and *M. natalensis* embryos and at 60°C for the *C. perspicillata* embryos. The same post-hybridisation wash conditions were used for both *Shh* and *Ptc1* expression analysis.

3.2.3.3. Blocking of the embryos and the addition of the anti-DIG antibody

Following the post-hybridisation washes, the embryos were washed twice in DEPC PBS and once in PBST containing 0.1 % Triton X-100 before being rinsed twice in blocking solution (PBST, 0.1 % Triton X-100, 2 mg/ml bovine serum albumin (Sigma) and 15 % sheep serum (Sigma, heat-inactivated at 56 °C for 30 min)). The embryos were then pre-blocked for 4 hours in blocking solution at 4 °C, while shaking.

PFA fixed mouse or bat extra-embryonic membranes (EEM, see chapter 2) stored in 100 % Methanol were used to pre-absorb the Anti-DIG antibody. The EEM were equilibrated in PBST containing 0.1% Triton X-100 and incubated in blocking solution for 1 hour at room temperature, while shaking. The EEM were then incubated with 0.5 µl/ml Anti-Digoxigenin-Alkaline-Phosphatase (Roche) for three hours at 4

°C, while shaking. This pre-absorbed antibody solution was added to the pre-blocked embryos and left overnight at 4 °C, while shaking. Unbound antibody was removed by washing the embryos in PBST, 0.1 % Triton X-100 and 0.1 % BSA (Sigma) five times for one hour at room temperature. An additional wash was carried out overnight at 4 °C.

3.2.3.4. Signal visualisation by alkaline phosphatase colour reaction

The embryos were washed twice for 30 min in NMT buffer (100 mM NaCl, 50 mM $MgCl_2$, 100 mM Tris-Cl (pH 9.5)) containing 0.1 % Tween 20 and 0.1 % Triton X-100 at room temperature, while shaking. This was followed by three ten min washes in NMT buffer at room temperature, while shaking. The embryos were then transferred to glass bottles and the signal was visualised overnight in the dark in NMT buffer containing 3.8 µl/ml BCIP (50 mg/ml in 100 % dimethylformamide (Roche)).

Once the signal had developed to the desired extent, the colour reaction was stopped by washing the embryos several times in PBS. The embryos were then fixed in 4 % PFA in PBS and photographed using a Nikon SMZ1500 stereoscopic zoom microscope fitted with a Nikon DS-U2 camera control unit and Nikon DS-5Mc camera head (Nikon Instruments Inc., New York, U.S.A.). Photographs were formatted using NIS-Elements image capture software (Nikon Imaging Software, version 2.10) and Photoshop (Adobe, version 7.0).

3.3. Results

3.3.1. RNA integrity

RNA extraction yielded 752 ng/ µl and 335 ng/ µl of total RNA from E13.5 mouse and 13L *M. natalensis* embryos respectively. Gel electrophoresis showed that the RNA integrity was maintained. Clear 28S and 18S rRNA bands were visible with the former having twice the intensity of the latter (Fig. 3.2).

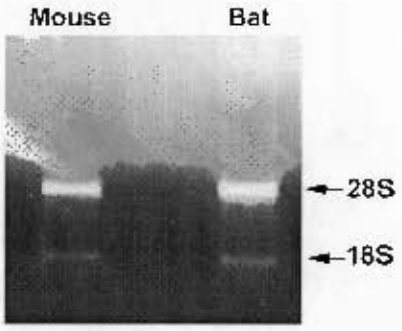

Fig 3.2 1µg of total RNA extracted from an E13.5 mouse embryo and a stage 13L *M. natalensis* (bat) embryo. Clear 28S and 18S rRNA bands are visible for both the mouse and *M. natalensis* RNA samples indicating intact RNA.

3.3.2. Cloning of *Ptc1* orthologs

PCR using primers based on highly conserved regions of mammalian *Ptc1* sequence yielded 800 bp products from both mouse and *M. natalensis* cDNA templates (Fig. 3.3). These products were extracted, cloned and sequenced. BLAST analysis and alignment of the cloned sequences with the corresponding Ensembl (version 46) *M. lucifugus* sequence confirmed that the sequences correspond to a region from exon 5 to 10 of the *Ptc1* gene (Fig. 3.4). The isolated *M. natalensis Ptc1* sequence contains a region that has not yet been published for *M. lucifugus Ptc1*, corresponding to exon 10 of the gene (Fig. 3.4). These cloned sequences were used as templates for mouse (PtcProbeM) and *M. natalensis* (PtcProbeB) specific *Ptc1* RNA probes.

Fig 3.3 Mouse and *M. natalensis* (bat) *Ptc1* orthologs amplified by PCR. 800 bp products were isolated for both mouse and *M. natalensis* using primers based on highly conserved regions of the *Ptc1* sequence. λDNA/*Pst1* molecular marker shown on the extreme left with applicable DNA fragment size (bp) indicated; –ve: negative PCR control using water as a template.

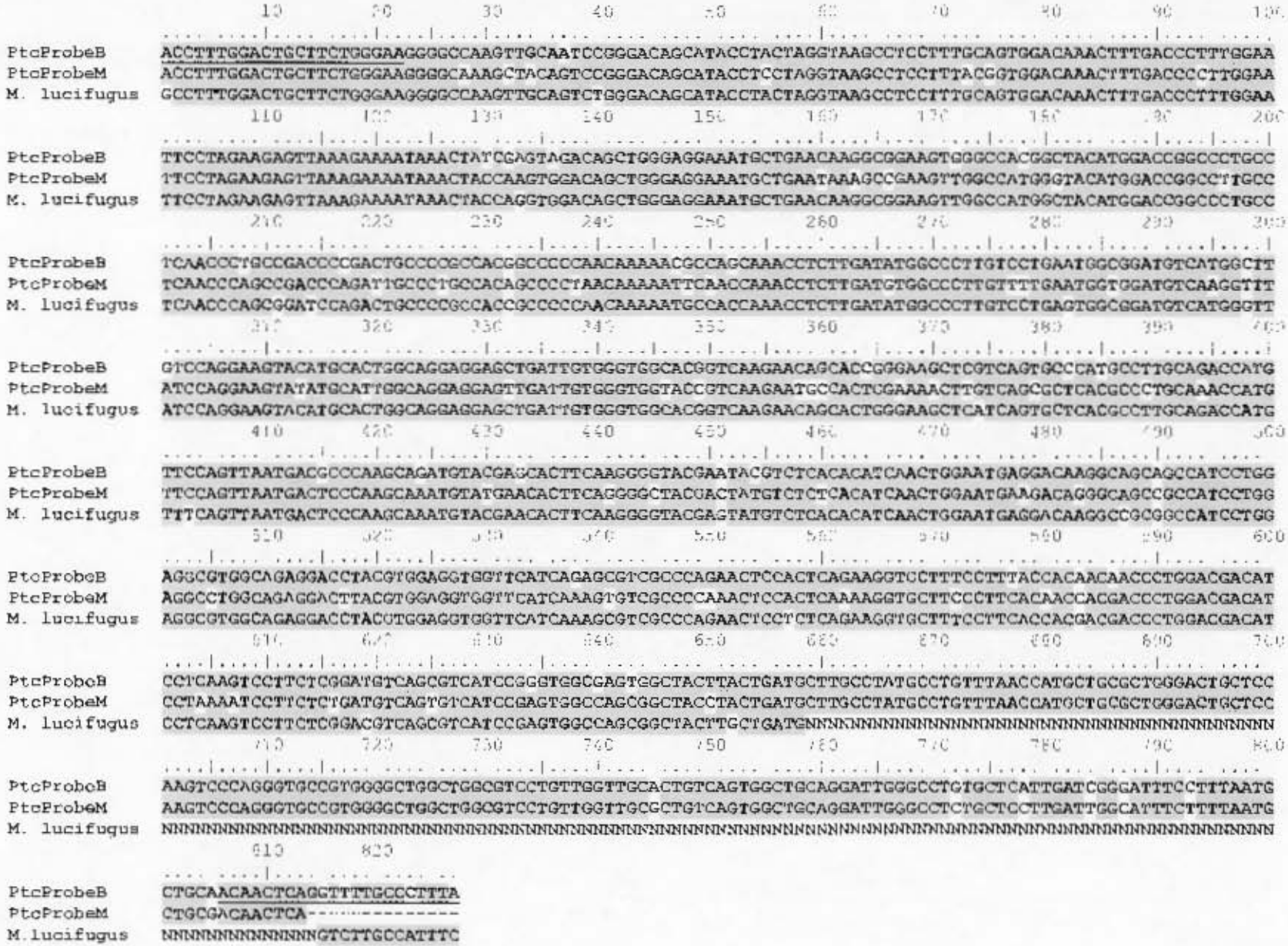

Fig. 3.4

Fig. 3.4 Isolated sequences of *Ptc1* from *M. natalensis* (PtcProbeB) and mouse (PtcProbeM) aligned with the corresponding Ensembl *M. lucifugus* sequence (ENSMLUT00000016253). The 827bp sequence corresponds to exons 5 to 10 of the *Ptc1* gene. Underlined regions indicate PCR primer sequences and shaded areas indicate regions of sequence similarity. The region that is shared by the isolated *M. natalensis* sequence and the *M. lucifugus* sequence shows 93.77 % similarity. The mouse and *M. natalensis* sequences show 88.81% similarity. 'NNN' in the *M. lucifugus* sequence corresponds exon 10, which has not yet been included in the Ensembl sequence (version 46). Both the *M. natalensis* and mouse sequences were used as templates for the synthesis of DIG-labeled RNA probes.

3.3.3. Cloning of *Shh* orthologs

PCR using primers based on highly conserved regions of mammalian *Shh* sequence yielded a 500bp product from the mouse cDNA template (Fig. 3.5). No products, however, were obtained from the *M. natalensis* cDNA template (data not shown). The mouse PCR product was extracted, cloned and sequenced. BLAST analysis and alignment of the cloned sequence with the Ensembl (version 46) mouse *Shh* sequence confirmed the sequence corresponded to a region from exon 3 of *Shh* (Fig. 3.6). An additional cloned region of mouse *Shh* was provided by Dr Behringer (M.D. Anderson Cancer Centre, Houston, Texas). This sequence corresponded to a 640 bp region spanning from exon 1 to 3 of the *Shh* gene (Fig. 3.6). Both these cloned *Shh* fragments were used as templates for the synthesis of two probes, ShhprobeM1 based on the sequence provided by Dr Behringer and ShhprobeM2 based on the *Shh* sequence isolated in this study.

Fig 3.5 Mouse (M) *Shh* amplified by PCR. A 500 bp product was obtained using primers based on exon 3 of the *Shh* sequence. λDNA/*Pst1* molecular marker shown on the extreme right with applicable DNA fragment size (bp) indicated; –ve: negative PCR control using water as a template

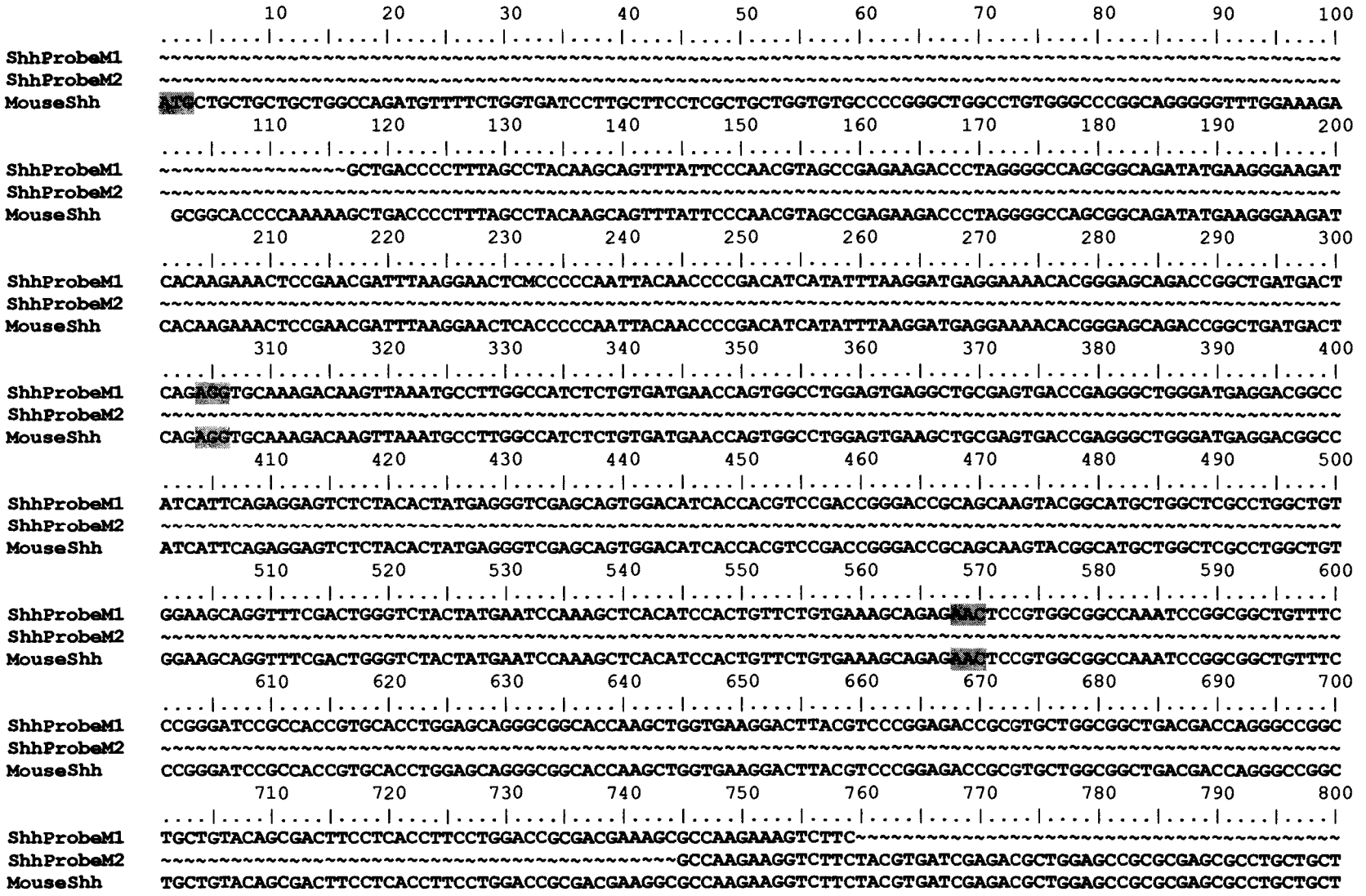
10 20 30 40 50 60 70 80 90 100
ShhProbeM1
ShhProbeM2
MouseShh ATGCTGCTGCTGCTGGCCAGATGTTTTCTGGTGATCCTTGCTTCCTCGCTGCTGGTGTGCCCCGGGCTGGCCTGTGGGCCCGGCAGGGGGTTTGGAAAGA
110 120 130 140 150 160 170 180 190 200
ShhProbeM1 ~~~~~~~~~~~~~~~~GCTGACCCCTTTAGCCTACAAGCAGTTTATTCCCAACGTAGCCGAGAAGACCCTAGGGGCCAGCGGCAGATATGAAGGGAAGAT
ShhProbeM2
MouseShh GCGGCACCCCAAAAAGCTGACCCCTTTAGCCTACAAGCAGTTTATTCCCAACGTAGCCGAGAAGACCCTAGGGGCCAGCGGCAGATATGAAGGGAAGAT
210 220 230 240 250 260 270 280 290 300
ShhProbeM1 CACAAGAAACTCCGAACGATTTAAGGAACTCMCCCCCAATTACAACCCCGACATCATATTTAAGGATGAGGAAAACACGGGAGCAGACCGGCTGATGACT
ShhProbeM2
MouseShh CACAAGAAACTCCGAACGATTTAAGGAACTCACCCCCAATTACAACCCCGACATCATATTTAAGGATGAGGAAAACACGGGAGCAGACCGGCTGATGACT
310 320 330 340 350 360 370 380 390 400
ShhProbeM1 CAGAGGTGCAAAGACAAGTTAAATGCCTTGGCCATCTCTGTGATGAACCAGTGGCCTGGAGTGAGGCTGCGAGTGACCGAGGGCTGGGATGAGGACGGCC
ShhProbeM2
MouseShh CAGAGGTGCAAAGACAAGTTAAATGCCTTGGCCATCTCTGTGATGAACCAGTGGCCTGGAGTGAAGCTGCGAGTGACCGAGGGCTGGGATGAGGACGGCC
410 420 430 440 450 460 470 480 490 500
ShhProbeM1 ATCATTCAGAGGAGTCTCTACACTATGAGGGTCGAGCAGTGGACATCACCACGTCCGACCGGGACCGCAGCAAGTACGGCATGCTGGCTCGCCTGGCTGT
ShhProbeM2
MouseShh ATCATTCAGAGGAGTCTCTACACTATGAGGGTCGAGCAGTGGACATCACCACGTCCGACCGGGACCGCAGCAAGTACGGCATGCTGGCTCGCCTGGCTGT
510 520 530 540 550 560 570 580 590 600
ShhProbeM1 GGAAGCAGGTTTCGACTGGGTCTACTATGAATCCAAAGCTCACATCCACTGTTCTGTGAAAGCAGAGAAGTCCGTGGCGGCCAAATCCGGCGGCTGTTTC
ShhProbeM2
MouseShh GGAAGCAGGTTTCGACTGGGTCTACTATGAATCCAAAGCTCACATCCACTGTTCTGTGAAAGCAGAGAAGTCCGTGGCGGCCAAATCCGGCGGCTGTTTC
610 620 630 640 650 660 670 680 690 700
ShhProbeM1 CCGGGATCCGCCACCGTGCACCTGGAGCAGGGCGGCACCAAGCTGGTGAAGGACTTACGTCCCGGAGACCGCGTGCTGGCGGCTGACGACCAGGGCCGGC
ShhProbeM2
MouseShh CCGGGATCCGCCACCGTGCACCTGGAGCAGGGCGGCACCAAGCTGGTGAAGGACTTACGTCCCGGAGACCGCGTGCTGGCGGCTGACGACCAGGGCCGGC
710 720 730 740 750 760 770 780 790 800
ShhProbeM1 TGCTGTACAGCGACTTCCTCACCTTCCTGGACCGCGACGAAAGCGCCAAGAAAGTCTTC~~~~~~
ShhProbeM2 ~~~~~~GCCAAGAAGGTCTTCTACGTGATCGAGACGCTGGAGCCGCGCGAGCGCCTGCTGCT
MouseShh TGCTGTACAGCGACTTCCTCACCTTCCTGGACCGCGACGAAGGCGCCAAGAAGGTCTTCTACGTGATCGAGACGCTGGAGCCGCGCGAGCGCCTGCTGCT

Fig. 3.6

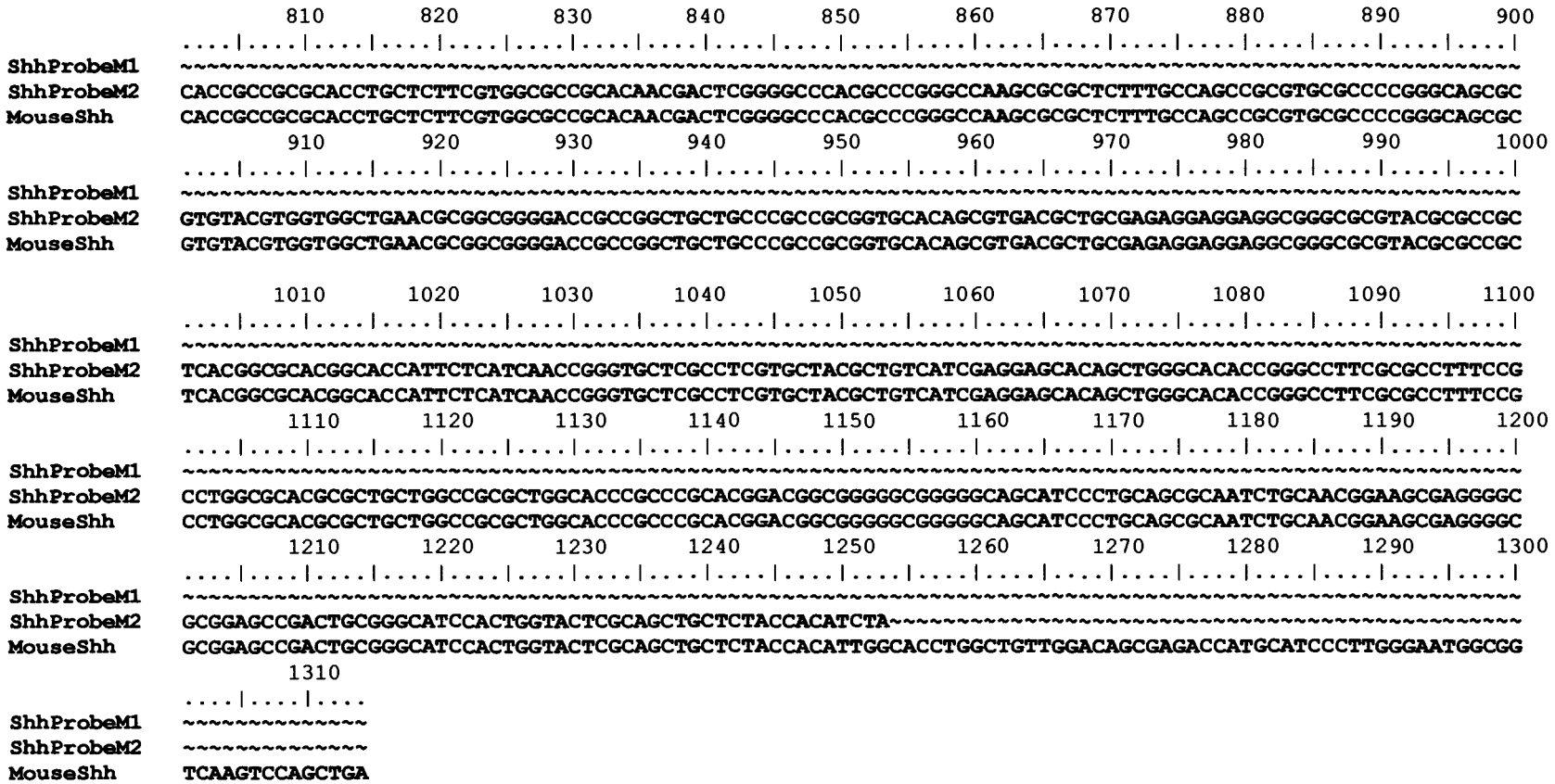

Fig. 3.6 continued. The mouse *Shh* sequence obtained from Dr Behringer (ShhProbeM1) and the mouse *Shh* sequence isolated by PCR in this study (ShhProbeM2) aligned with the entire Ensembl mouse *Shh* cDNA sequence (ENSMUST00000002708). ShhProbeM1 corresponds to a 640 bp region from exon 1 to 3 of the Ensembl sequence, while the sequence isolated by PCR in this study, ShhProbeM2, corresponds to a 500 bp region from exon 3 alone. ShhprobeM1 and ShhProbeM2 overlap by 15 bp at their 3' and 5' ends respectively. Shaded regions indicate the first codon of each exon.

3.3.4. Whole mount *in situ* hybridisation analysis of *Shh* and *Ptc1* expression in developing mouse, *M. natalensis* and *C. perspicillata* limbs

3.3.4.1. RNA Probes used for whole mount *in situ* hybridisation

PtcProbeB, PtcProbeM, ShhProbeM1 and ShhProbeM2 were tested on mouse and *M. natalensis* embryos to determine which probe produced the clearest signal with the lowest background (data not shown). ShhProbeM1 gave the best results and was used to visualise *Shh* expression in mouse, *M. natalensis* and *C. perspicillata* embryos. PtcProbeB was used to visualise *Ptc1* expression in *M. natalensis* embryos and stage 13L and 17 *C. perspicillata* embryos, while PtcprobeM was used on the mouse embryos and the remaining *C. perspicillata* stages.

3.3.4.2. *Shh* expression pattern in developing mouse limbs

Shh is first detected in both the forelimb and hindlimb at E10.0 in the mouse in a posteriorly restricted domain (Fig. 3.7Ai-ii). This signal is higher in forelimb than in the hindlimb. At E11.0 hindlimb expression is more obvious (Fig. 3.7Civ). Throughout the following stages of development, the hindlimb expression pattern always resembles the forelimb expression pattern from the previous stage of development.

Expression persists in both the forelimb and hindlimb from E11.0 to E11.75 (Fig. 3.7Ci, Civ, Di, Div, Ei & Eiv). The posteriorly restricted domain of expression expands distally with the growing limb buds. At 12.0 the *Shh* signal is no longer present in the forelimb (Fig. 3.7Gi) but persists in the hindlimb (Fig. 3.7Giv). Expression ceases in the hindlimb by E12.5 (Fig. 3.7Jiv). *Shh* remains off in both the forelimb and hindlimb through E13.0 and E13.5 (Fig. 3.7Ki, Kiv, Li & Liv).

3.3.4.3. *Shh* expression pattern in developing bat limbs

Shh is first detected at stage 13L in the *M. natalensis* forelimb in a posteriorly restricted domain (Fig. 3.7Bi). *Shh* is not detectable at this stage in the hindlimb (Fig. 3.7Bii).

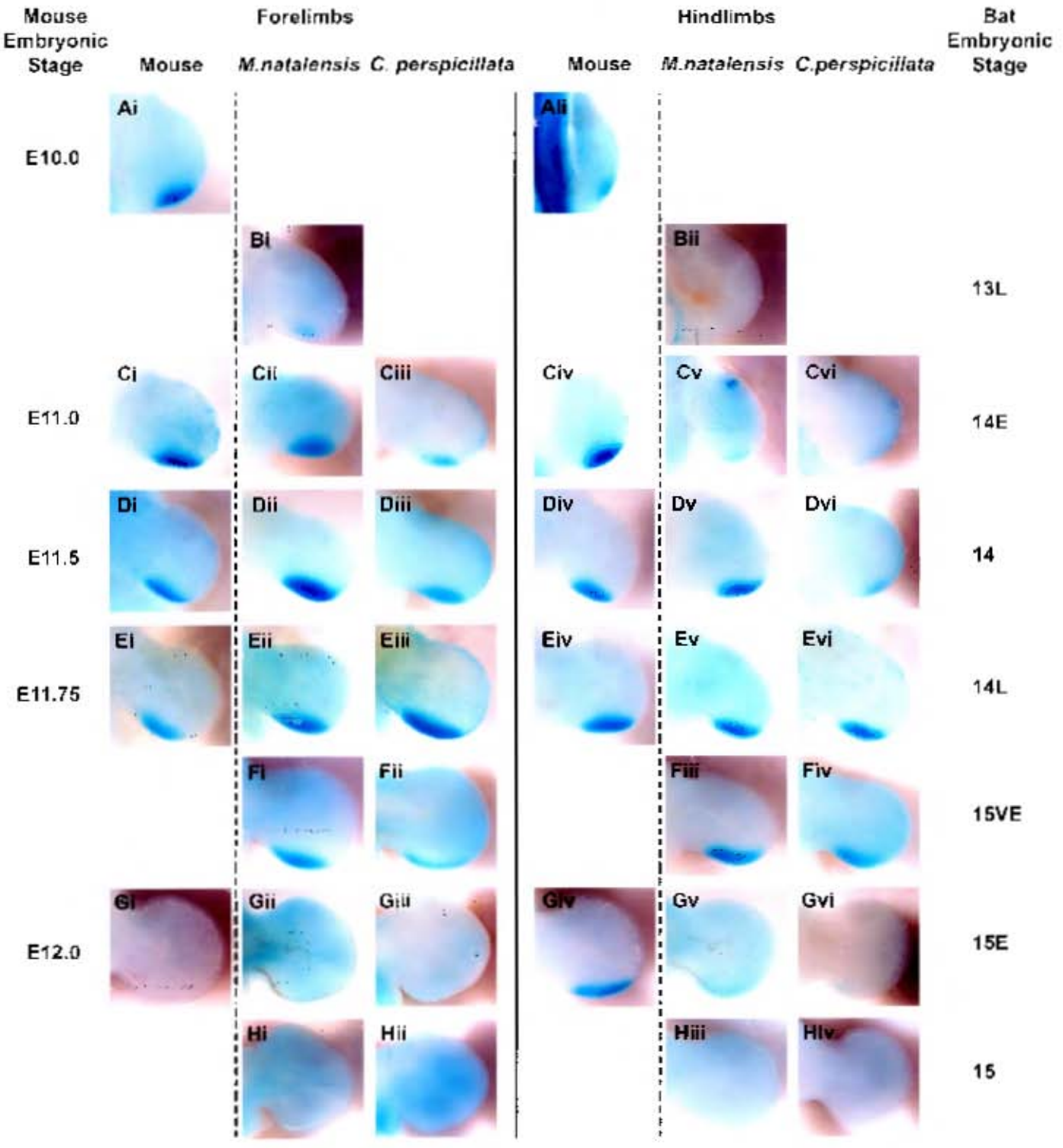

Fig. 3.7 Early phase *Shh* expression patterns in the forelimbs and hindlimbs of equivalently staged mouse, *M. natalensis* and *C. perspicillata* embryos.

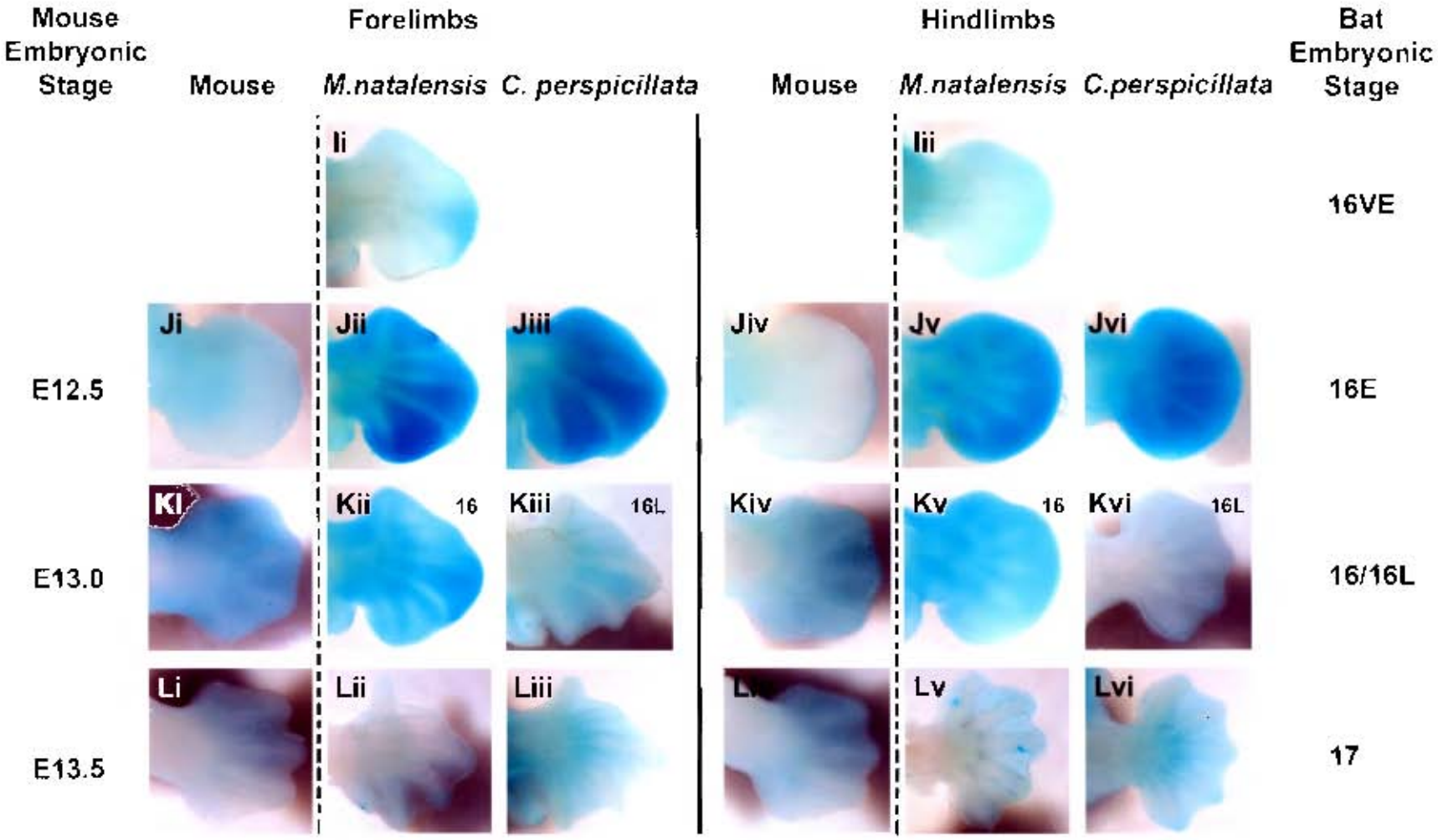

Fig 3.7 continued. Late phase *Shh* expression patterns in the forelimbs and hindlimbs of equivalently staged mouse, *M. natalensis* and *C. perspicillata* embryos. The embryonic day (E) of mouse development is indicated down the left side, while the stage of bat development based on Cretekos *et al.* (2005) and discussed in Chapter 2 is indicated down the right side. The dotted line divides the mouse limbs from the bat limbs, while the solid line divides the forelimbs from the hindlimbs.The anterior of each limb bud is towards the top and distal is towards the right.

During stage 14E and 14, the posteriorly restricted domain of expression in the forelimb of both *M. natalensis* and *C. perspicillata* expands both distally and anteriorly (Fig. 3.7Cii-iii & Dii-iii). This anterior expansion is especially prominent in *M. natalensis*, where a wide *Shh* expression domain is visible in the stage 14 forelimb (Fig. 3.7Dii). The first signs of *Shh* expression in the hindlimb appear weakly at stage 14E in *M. natalensis* (Fig. 3.7Cv) and become stronger and distally expanded by stage 14 (Fig. 3.7Dv). *Shh* is weakly visible in the *C. perspicillata* hindlimb at stage 14 (Fig. 3.7Dvi) and stronger at 14L (Fig. 3.7Evi).

Shh expression persists through stages 14L and 15VE in both the forelimb and the hindlimb of both species (Fig. 3.7Eii-iii, Ev-vi & Fi-iv). At stage 15E expression ceases in the forelimb (Fig. 3.7Gii-iii) and is very weak in the hindlimb of both species (Fig. 3.7Gv-vi). By stage 15, *Shh* is no longer detectable in either the forelimb or hindlimb of either species (Fig. 3.7Hi-iv).

At stage 16VE *Shh* expression returns to the *M. natalensis* forelimb in the tissue that will form the interdigital space between digits 3 and 4 (Fig. 3.7Ii). There is no expression in the hindlimb at this stage (Fig. 3.7Iii). By 16E expression is visible in both the forelimb and hindlimb of both *M. natalensis* and *C. perspicillata* embryos (Fig. 3.7Jii-iii & Jv-vi). In the forelimb, expression is localised to the interdigital tissue and is present in a gradient from posterior to anterior, with the highest expression found between digits 4 and 5 (Fig. 3.7Jii-iii). This gradient is more pronounced in *M. natalensis* (Fig. 3.7Jii) than in *C. perspicillata* (Fig. 3.7Jiii). In the hindlimb, *Shh* expression is also localised to the interdigital tissue, however this signal is uniform along the anterior-posterior axis and is not as strong as the forelimb expression (Fig. 3.7Jv-vi).

By stage 16 in *M. natalensis*, the interdigital *Shh* expression in both the forelimb and hindlimb is lower (Fig. 3.7Kii & Kv). Forelimb expression is highest in the tissue between digits 3 and 4 and along the borders of the condensations of all the digits (Fig. 3.7Kii). At stage 16L *Shh* expression is still present at very low levels in the interdigital tissue of *C. perspicillata* forelimb (Fig. 3.7Kiii) and is not detected in the hindlimb (Fig. 3.7Kvi).

By stage 17 in *M. natalensis* and *C. perspicillata*, *Shh* expression is absent from both the forelimb and hindlimb (Fig. 3.7Lii-iii & Lv-vi).

3.3.4.3. *Ptc1* expression pattern in developing mouse limbs

Ptc1 expression is visible in the forelimb and hindlimb of E10.0 mouse embryos in a gradient along the anterior-posterior axis, with highest levels in the posterior (Fig. 3.8Ai-ii). At E11.0 this gradient is more pronounced (Fig. 3.8Ci & Civ).

This graded expression pattern continues through to E11.5, however, a distinct down-regulation of the *Ptc1* signal is visible in a strip at the distal-posterior end of both the forelimb and hindlimb (Fig. 3.8Di & Div). By E11.75, this strip of low *Ptc1* expression extends further towards the proximal end of the forelimb and is bordered by very high levels of *Ptc1* signal (Fig. 3.8Ei). The hindlimb at E11.75 resembles the forelimb at E11.5, showing a small area of *Ptc1* down-regulation at the distal-posterior end (Fig. 3.8Eiv).

At E12.0 the strip of low *Ptc1* expression is no longer detectable in the forelimb (Fig. 3.8Gi). *Ptc1* is still expressed in a gradient from posterior to anterior with the highest signal at the most distal-posterior tip of the forelimb (Fig. 3.8Gi). The E12.0 hindlimb resembles the E11.5 forelimb in its expression pattern (Fig. 3.8Giv).

The pattern of *Ptc1* expression changes drastically in the E12.5 forelimb (Fig. 3.8Ji). *Ptc1* is visible in a region at the most proximal end of the forelimb, bordering the tissue condensations that will form the radius and ulna (Fig. 3.8Ji). *Ptc1* expression is also present at the bases of the tissue condensations that will form digits 2 to 4 (Fig. 3.8Ji). This area most likely corresponds to the metacarpals of the digits. The hindlimb expression pattern at this stage resembles the forelimb at E12.0 with the highest *Ptc1* signal at the most distal-posterior edge of the limb (Fig. 3.8Jiv).

At E13.0, *Ptc1* expression in the forelimb is present bordering the bases of the tissue condensations of digits 2 to 4 and weakly at the base of digit 5 (Fig. 3.8Ki). An additional area of lower *Ptc1* expression is visible at the distal tips of the condensations of digits 2 to 4, most likely corresponding to the area that will form the first phalange of the digits (Fig. 3.8Ki). In the hindlimb at E13.0 *Ptc1* is expressed strongly at the proximal edge of the limb, where the tibia and fibula will form, and along the length of the condensations forming digits 2 to 5 (Fig. 3.8Kiv). Distinct areas of expression in the base and at the tip of the digits, as in the forelimb, are not detected (Fig. 3.8Kiv).

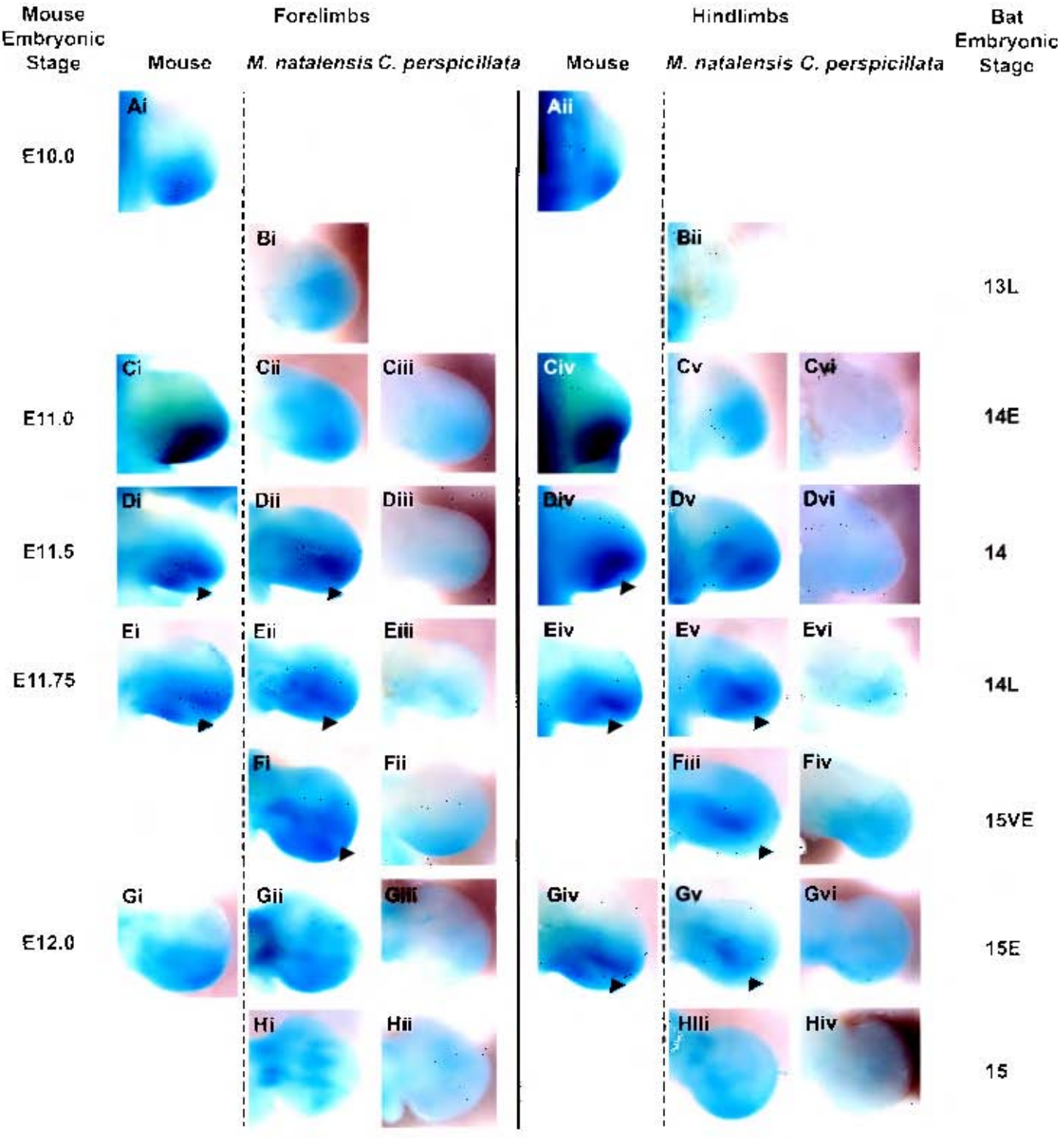

Fig 3.8 Early phase *Ptc1* expression patterns in the forelimbs and hindlimbs of equivalently staged mouse, *M. natalensis* and *C. perspicillata* embryos.

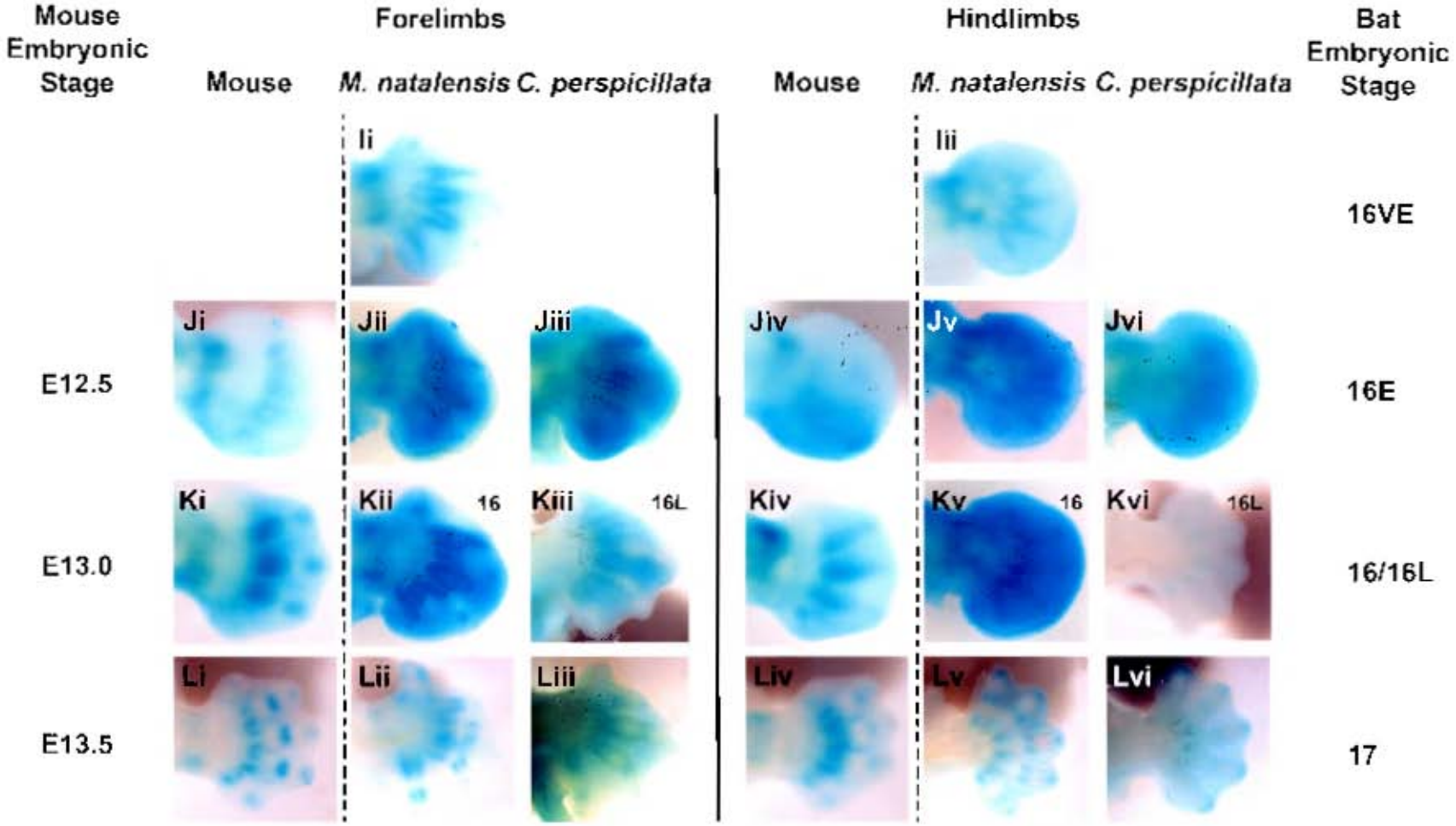

Fig 3.8 continued. Late phase *Ptc1* expression patterns in the forelimbs and hindlimbs of equivalently staged mouse, *M. natalensis* and *C. perspicillata* embryos. The embryonic day (E) of mouse development is indicated down the left side, while the stage of bat development based on Cretekos *et al.* (2005) is indicated down the right side. Arrow heads indicate regions of down-regulation of the *Ptc1* signal in the distal-posterior limb buds. The dotted line divides the mouse limbs from the bat limbs, while the solid line divides the forelimbs from the hindlimbs. The anterior of each limb bud is towards the top and distal is towards the right.

By E13.5 *Ptc1* expression in the forelimb is seen clearly bordering the bases of digital condensations 2 to 5 and weakly at the base of digit 1 (Fig. 3.8Li). Expression is also present bordering the area midway along digits 2 to 4 and low expression is visible at the tips of all the digits (Fig. 3.8Li). The expression pattern in the hindlimb is similar to the forelimb at E13.0, with the strongest *Ptc1* expression bordering the bases of all the digital condensations and an additional area of expression at the tip of each digit (Fig. 3.8Liv).

3.3.4.4. *Ptc1* expression pattern in developing bat limbs

Ptc1 expression is very low throughout *C. perspicillata* embryos from stage 14E to 15, including the developing neural tube where expression is expected to be high (data not shown). This could be due to low penetration of the probe during the *in situ* hybridisation procedure. Only the very highest areas of expression are visible in the limbs at these stages and thus are not comparable to the results obtained for *M. natalensis* and the mouse. Due to lack of samples, these experiments could not be repeated to optimise the results. *Ptc1* expression in stage 16E, 16L and 17 *C. perspicillata* embryos, however, is convincing throughout the embryos, including the developing neural tube (data not shown), and thus the *Ptc1* expression pattern in the limb buds at these stages is included in the description below.

At stage13L in *M. natalensis Ptc1* is expressed diffusely across the forelimb bud (Fig. 3.8Bi). A gradient is not clearly distinguishable, however, expression is lower at the most anterior end of the forelimb (Fig. 3.8Bi). *Ptc1* expression is not visible in the hindlimb at this stage (Fig. 3.8Bii).

In the stage 14E *M. natalensis* forelimb *Ptc1* is expressed in a gradient along the anterior-posterior axis, with highest expression in the posterior (Fig. 3.8Cii). The expression pattern in the hindlimb is diffuse as in the forelimb at stage 13L (Fig. 3.8Cv).

In the stage 14 and 14L forelimbs, *Ptc1* is still expressed in a gradient from posterior to anterior (Fig. 3.8Dii & Eii). However, as in the mouse limb, expression is down-

regulated in a small area at the most distal-posterior edge of the limb (Fig. 3.8Dii & Eii). The *Ptc1* signal is highest just anterior to this area of low expression (Fig. 3.8Dii & Eii). The stage 14 hindlimb expression pattern resembles the stage 13L forelimb, acquiring a graded pattern from posterior to anterior (Fig. 3.8Dv). The stage 14L hindlimb displays an area of down-regulated *Ptc1* expression at the most distal-posterior edge, as in the stage 14 forelimb (Fig. 3.8Ev).

At stage 15VE the area of down-regulated *Ptc1* expression in the posterior forelimb is restricted to a very small area at the distal edge of the forelimb (Fig. 3.8Fi). *Ptc1* is high surrounding this area and decreases towards the anterior (Fig. 3.8Fi). By 15E this area of down-regulation is absent from the forelimb and *Ptc1* is expressed in a gradient from the posterior edge to the anterior (Fig. 3.8Gii). *Ptc1* is highest at the most proximal region of the forelimb, where the radius and ulna condensations will form (Fig. 3.8Gii). The hindlimb at these stages continues to show a small area of down-regulation at the most distal-posterior edge, while *Ptc1* expression remains high just anterior to this region (Fig. 3.8Fiii & Gv).

At stage 15, high *Ptc1* expression persists in the proximal region of the forelimb and is present in the digital condensations of digits 2 to 4 (Fig. 3.8Hi). The hindlimb expression pattern at stage 15 resembles the stage 14L forelimb. Expression is highest at the most posterior edge of the foot plate where in previous stages expression was low (Fig. 3.8Hiii). *Ptc1* is present at the most proximal region of the hindlimb where the tibia and fibula will form (Fig. 3.8Hiii).

At stage 16VE, *Ptc1* is clearly visible in the forelimb bordering the digit condensations of digits 2 to 4 and within the condensations of digits 1 and 5 (Fig. 3.8Ii). In the hindlimb, *Ptc1* borders the digit condensations of digits 2 to 5 (Fig. 3.8Iii). In the stage 16E *M. natalensis* and *C. perspicillata* embryos, *Ptc1* is expressed throughout the interdigital tissue of both the forelimb and hindlimb and is highest at the borders of the digit condensations (Fig. 3.8Jii-iii & Jv-vi). In the forelimb, *Ptc1* is higher in the interdigital tissue between the posterior digits and is lower in the tissue between digits 1 and 2 (Fig. 3.8Jii-iii). This gradient is absent in the hindlimb (Fig. 3.8Jv-vi). *Ptc1* persists in the proximal region of the forelimbs and hindlimbs at these stages (Fig. 3.8Jii-iii & Jv-vi).

The stage 16 *M. natalensis* forelimb displays strong *Ptc1* expression bordering the bases of digits 1, 3, 4, and 5, while the entire length of digit 2 is bordered by *Ptc1* expression (Fig. 3.8Kii). Distinct areas of *Ptc1* expression are visible at the distal tips of digits 3 to 5 (Fig. 3.8Kii). Expression is also visible within the interdigital tissue between all the digits, except between digits 1 and 2 (Fig. 3.8Kii). In the hindlimb, *Ptc1* expression is highest bordering all the digital condensations and is expressed at a lower level throughout the interdigital tissue (Fig. 3.8Kv). *Ptc1* persists in the proximal region of the forelimbs and hindlimbs (Fig. 3.8Kv).

At stage 16L in *C. perspicillata*, *Ptc1* is expressed at a low level throughout the interdigital tissue of the forelimb (Fig. 3.8Kiii). The expression is highest at the borders of the digital condensations (Fig. 3.8Kiii). Expression is absent from the hindlimb (Fig. 3.8Kvi).

At stage 17 in *M. natalensis* forelimbs, *Ptc1* expression is visible bordering all the forelimb digits at their bases and midway along their lengths (Fig. 3.8Lii). Digits 3 to 5 of the forelimb display an additional weak area of *Ptc1* expression at their distal tips. A similar pattern is present in all the digits of the hindlimb (Fig. 3.8Lv). Comparable expression is seen in the limbs of *C. perspicillata*, however at lower levels (Fig. 3.8Liii & vi).

3.4. Discussion

3.4.1. Dig-labelled RNA probes used for whole mount *in situ* hybridisation

A region of the *Ptc1* sequence was successfully cloned from both *M. natalensis* and mouse cDNA to be used as a template for probe synthesis by *in vitro* transcription. The mouse and *M. natalensis* sequences showed very high sequence similarity and the probes based on these sequences produced similar expression patterns in the *in situ* hybridisation procedure. These results indicated that it was plausible to use the mouse *Shh* and *Ptc1* probes on bat embryos without encountering problems of non-specific binding and high background.

Shh was not successfully cloned from bat cDNA, however a region from exon 3 of *Shh* was cloned from the mouse. An additional sequence spanning the majority of the gene sequence was available for probe synthesis. The *Shh* probe based on the long *Shh* sequence (ShhProbeM1) gave the best signal with the lowest background when used on both the mouse and bat embryos. This longer sequence that spans several exons probably facilitated specific binding to more mature *Shh* mRNA transcripts.

3.4.2. Comparisons of gene expression patterns between mouse and bat limbs, and between bat forelimb and hindlimb.

3.4.2.1. *Shh and Ptc1* expression patterns in the mouse: Early and late phases of expression

The expression patterns that are observed for *Shh* and *Ptc1* in the developing mouse limbs correspond to previous descriptions (Echelard *et al.* 1993; Goodrich *et al.* 1996; Platt *et al.* 1997). The phases of *Shh* expression can be used to divide the examined stages of development into an early phase (E10.0 to E12.0) when *Shh* is present in a posteriorly restricted domain corresponding to the ZPA and a late phase (E12.5 to E13.5) when *Shh* is absent. The early phase of *Ptc1* expression is graded from posterior to anterior in direct response to the SHH morphogenic gradient across the anterior-posterior axis (Marigo *et al.* 1996a; Lewis *et al.* 2001). During the late phase, *Ptc1* is expressed in the perichondrium of the bone primordia in direct response to another hedgehog signalling molecule, *Indian Hedgehog* (*Ihh*) (Platt *et al.* 1997). *Ihh* is expressed by the proliferating cells of the developing cartilage elements (Vortkamp *et al.* 1996). Additional regions of *Ptc1* expression develop around the digital rays as each digital cartilage element begins to form, maturing sequentially along the proximal-distal axis (reviewed in Shimizu *et al.* 2007).

3.4.2.2. Early phase *Shh* and *Ptc1* expression patterns in the bat: Enhancement of the *Shh-Fgf8* feedback loop facilitates the expansion of the bat hand plate

During the early phase of *Shh* and *Ptc1* expression (13L to 15E), the patterns observed in *M. natalensis* and *C. perspicillata* limbs are very similar to that in the mouse. However, the timing of the initiation of expression differs slightly between mouse and bat. In *M. natalensis Shh* expression is only detected in the ZPA at stage 13L in the forelimb and 14E in the hindlimb. The corresponding *Ptc1* expression is very low and is not graded across the anterior-posterior axis. At these stages the limb buds are considerably larger than the E10.0 limb buds when *Shh* is first detected in the mouse. The apparent delay in the initiation of *Shh* expression in the bat could simply be an effect of using a cross-species RNA probe that is based on the mouse *Shh* sequence. It is possible that *Shh* is present in the stage 13 bat limb bud, which is equivalent in size to the E10.0 mouse limb, however at concentrations too low for a cross-species probe to detect.

The spatial extent of the *Shh* expression pattern at stage 14E and 14 in the bat forelimbs may, however, provide evidence that the delay in the initiation of the *Shh* signal is a true biological phenomenon. At these stages, the domain of *Shh* is anteriorly expanded in the *M. natalensis* forelimb and to a lesser extent in the *C. perspicillata* forelimb. At equivalent stages in the mouse *Shh* expression hugs the posterior edge of the limb bud. An expansion in the *Shh* signal has been implicated as part of the *Shh* auto-regulatory mechanism (Sanz-Ezquerro & Tickle 2000). Removal of ZPA cells by surgery or a reduction in *Shh* signal by the application of a signal-transduction inhibitor has been shown to lead to an expansion in the domain of *Shh* expression (Sanz-Ezquerro & Tickle 2000; Scherz *et al.* 2007). *Shh* is able to buffer its own expression, with more cells being induced to produce *Shh* if a loss of signal is detected (Sanz-Ezquerro & Tickle 2000). The apparent expansion in the *Shh* signal observed in the bat forelimbs could be due to an induction of this buffering mechanism. The initial lack of *Shh* may stimulate an expansion in the population of *Shh* producing cells at stage 14E and 14 when compared to equivalently staged mouse limbs.

This expansion in the *Shh* expression domain at stage 14 mirrors an expansion in the *Fgf8* expression domain in the AER (Cretekos *et al.* 2007). *Fgf8* in the AER of stage 14 *C. perspicillata* forelimbs is 2.7 to 3 times wider in the bat than in equivalently staged mouse forelimbs (Cretekos *et al.* 2007). This phenomenon has also been described in the limb buds of *Bmp* mutant mice, which display expanded *Fgf8* in the AER due to a lack of antagonism from BMP's (Bandyopadhyay *et al.* 2006). These mice also exhibit an expanded *Shh* expression domain (Bandyopadhyay *et al.* 2006). This phenomenon is explained by invoking an up regulation of both signals through the *Shh-Fgf* feedback loop in which these two signals reciprocally activate each-others expression in the ZPA and AER respectively (Bandyopadhyay *et al.* 2006). Interestingly, the *Bmp* mutant mice display posteriorly expanded limb buds, which is explained in terms of enhanced cell proliferation in response to the enhanced *Shh-Fgf* interaction (Bandyopadhyay *et al.* 2006). The expanded *Shh* and *Fgf8* domains in the stage 14 bat forelimb support the hypothesis that the same phenomenon may be occurring in the bat limb. *Shh* expression in the ZPA may be expanded by *Shh* autoregulation, leading to expansion of the *Fgf8* expression domain in the AER through the *Shh-Fgf* feedback loop. This phenomenon could lead to an increase in cell proliferation and cell survival, thus explaining the posterior expansion of the bat hand plate at stage 15E relative to the mouse E12.0 forelimb.

While the *Shh* expression domain is expanded in the bat forelimb, this does not occur in the hindlimb. Neither has an expansion in the *Fgf8* domain been reported for the hindlimb of *C. perspicillata* (Cretekos *et al.* 2007). The mechanisms that may allow the posterior expansion of the bat forelimb are absent from the hindlimb. As a consequence, the stage 15E bat hindlimb is equivalent in size and shape to the E12.0 mouse hindlimb.

This apparent expansion of the *Shh* domain in the stage 14 forelimb and the lack thereof in the hindlimb of the bat should be confirmed with additional samples. After *in situ* hybridisation the limb buds may be processed by cryostat sectioning and the spatial extent of the *Shh* expression domain may be measured and compared to that in the mouse. Due to time constraints and restricted sample size, this data was not available for this study.

3.4.2.3. Early phase *Ptc1* expression patterns: Posterior *Ptc1* is down-regulated in both mouse and bat limbs

In both mouse and bat limb buds, *Ptc1* is down-regulated in a distal-posterior domain soon after acquiring a graded expression pattern across the anterior-posterior axis. This region of down-regulation corresponds to the area of high *Shh* expression. High *Ptc1* signal returns to this region when *Shh* expression decreases (E12.0/stage 15E in the forelimb; E12.5/stage 15 in the hindlimb). Previous descriptions of *Ptc1* and *Gli1* (another target of *Shh* signalling) expression patterns in the developing mouse limb have also noted this area of down-regulation, indicating a loss of Shh-responsiveness in these posterior cells (Goodrich *et al.* 1996; Platt *et al.* 1997; Ahn & Joyner 2004).

Recently, Scherz *et al.* (2007) claimed that a down-regulation of *Ptc1* does not occur in these posterior cells. Scherz *et al.* (2007) aimed to provide support for the model that the most posterior digits are differentially patterned due to differences in the time of exposure to continued high-level SHH activity (Schertz *et al.* 2007). This model requires that the cells of the developing digits maintain continued SHH-responsiveness as long as the SHH signal is present. However, it is clear from this study of *Ptc1* expression in both the mouse and bat (and from Fig. 5K of Scherz *et al.* 2007 showing *Ptc1* in an E11.5 mouse forelimb) that the most posterior cells stop responding to SHH despite the high concentration of this signalling molecule in the ZPA. It is important that this factor of SHH signalling is incorporated into the model for anterior-posterior patterning of the limb. It is possible that a threshold response to the SHH signal is responsible for differentially patterning the most posterior digits 4 and 5, which both consist entirely of ZPA cells (Harfe *et al.* 2004). The cells that will form digit 5 may be differentiated from those that will form digit 4 by a temporal gradient in SHH-responsiveness after exposure to high SHH signal.

3.4.2.4. Late *Shh* and *Ptc1* expression patterns in the bat: Re-initiation of the *Shh-Fgf8* feedback loop facilitates the elongation of the forelimb digits and the survival of the interdigital webbing

Shh is absent by E12.0 and E12.5 from the mouse forelimb and hindlimb respectively. *Shh* is also absent from the bat limbs from stage 15E to 15. As in the mouse, *Ptc1* expression during these stages changes from being expressed in a gradient across the anterior-posterior axis to being confined to the perichondrium of the developing skeletal elements of the limb.

Surprisingly, during stage 16 *Shh* expression returns to both the forelimb and hindlimb of *M. natalensis* and *C. perspicillata* (Fig. 3.9). This novel expression begins at stage 16VE in the most distal region of the forelimb in the tissue between digits 3 and 4. By stage 16E, expression is visible throughout the interdigital tissue of the forelimb and hindlimb. Expression persists, though at lower levels, through to stage 16 and 16L in the hindlimb and forelimb respectively. During these stages, *Ptc1* is expressed in the interdigital tissue in response to the novel *Shh* expression, as well as being expressed at higher levels in the perichondrium of the developing digits, most likely in response to *Ihh* (Fig. 3.9).

Interestingly, *Gremlin* and *Fgf8* are also expressed in novel domains in the interdigital tissue of *C. perspicillata* at stages 16 and 17 (Weatherbee *et al.* 2006). *Shh, Fgf8* and *Gremlin* are all integral players in the *Shh-Fgf* feedback loop that promotes the outgrowth and expansion of the limb bud earlier in development (reviewed in Zeller & Zuniga 2007). The observed up-regulation of all three of these genes in the interdigital tissue supports the hypothesis that the *Shh-Fgf* feedback loop is initiated for a second time during bat limb development (summarised in Fig. 3.10.).

In the stage 16E forelimb, *Shh* is highest in the posterior two interdigital spaces and lower around the developing thumb. This *Shh* expression is complimentary to the expression pattern of *Gremlin,* which is higher in the anterior interdigital tissue than in the posterior (Weatherbee *et al.* 2006; Fig. 3.10). Earlier in development, *Shh* in the ZPA activates *Gremlin* expression in the limb mesenchyme, however, the *Shh* expressing cells themselves are not able to turn on *Gremlin* (Scherz *et al.* 2004;

Nissim *et al.* 2006). The complimentary novel domains of these genes suggest that the same is true when these genes are up-regulated later in development in the bat forelimb.

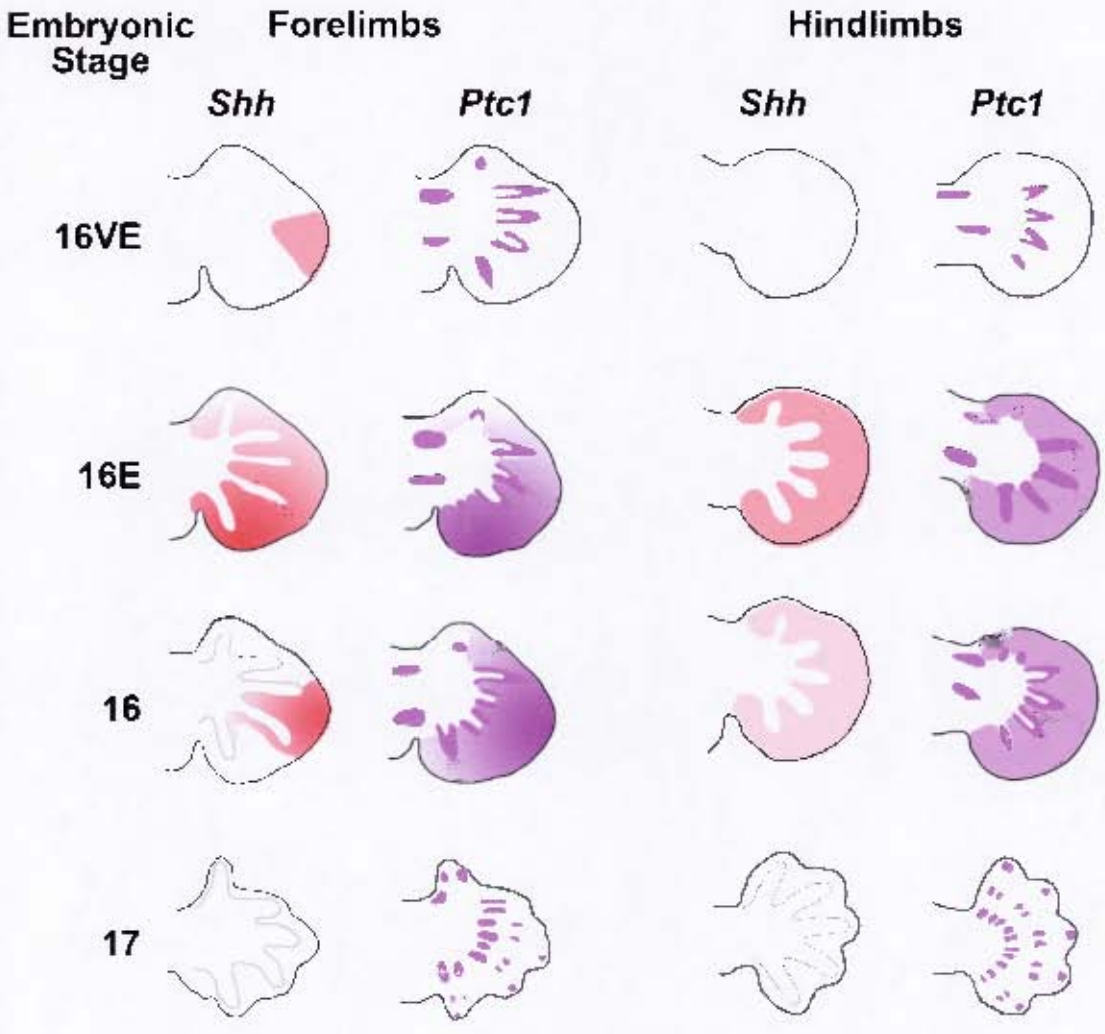

Fig 3.9 Summary of the late phase (stages 16VE to 17) of *Shh* and *Ptc1* expression in the forelimb and hindlimb of *M. natalensis*. *Shh* (red) expression is present at low levels in the interdigital tissue between digits 3 and 4 in the stage 16VE forelimb, but is absent from the hindlimb. At stage 16E *Shh* expression expands to the remaining interdigital spaces and is expressed in a gradient from posterior to anterior. By stage 16 *Shh* expression recedes to the interdigital space between digits 3 and 4, and is also present at lower levels at the borders of digits 4 and 5. In the hindlimb, *Shh* is expressed uniformly throughout the interdigital tissue at high and low levels at stages 16E and 16 respectively. At stage 17, *Shh* is absent from both the forelimb and hindlimb. From stages 16E to 17, *Ptc1* (purple) expression in the interdigital tissue corresponds to the *Shh* expression in this domain. *Ptc1* is also expressed in the perichondrium (dark purple) of the developing bones, most likely in response to *Ihh*.

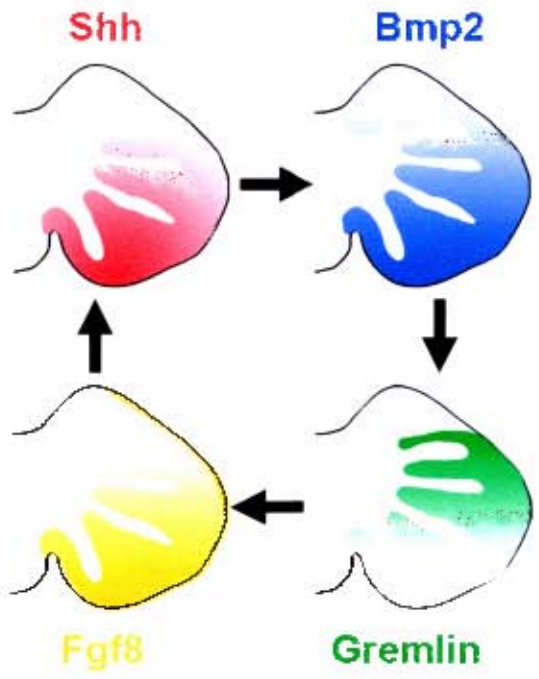

Fig. 3.10 A model for the re-initiation of the *Shh-Fgf* feedback loop in the interdigital tissue of the stage 16E bat forelimb. *Shh* (red) is expressed in the interdigital tissue of the stage 16E forelimb in a gradient from posterior to anterior. This novel expression leads to the subsequent activation of *Bmp2* (blue) expression in a corresponding fashion. *Bmp2* then activates *Gremlin* (green) in a complimentary domain (graded from anterior to posterior), with the highest expression located in the interdigital tissue between digits 2 and 3. *Gremlin* acts to suppress *Bmp's* in the interdigital tissue, allowing *Fgf8* (orange) to be expressed in the interdigital tissue in a gradient from posterior to anterior. *Fgf8* expression then feeds back to promote *Shh* expression in the interdigital tissue. *Fgf8* is also located within the AER bordering the hand plate. *Bmp, Gremlin* and *Fgf8* expression patterns based on Weatherbee *et al.* 2006.

Bmp2 is suggested to be the link between *Shh* and *Gremlin* expression in the *Shh-Fgf* feedback loop, activating the expression of its own antagonist (Nissim *et al.* 2006). In Weatherbee *et al.* (2006), *Bmp2* expression is detected in corresponding regions to *Shh* in this study (Fig. 3.10). Early in stage 16 both are highest in the posterior interdigital tissue, while later, both are highest between digits 3 and 4. Thus, it is possible that in the bat forelimb between stages 16 and 17, *Shh* is activating *Bmp2*, which in turn is activating *Gremlin* expression.

During limb bud outgrowth, the activation of *Gremlin* in the mesenchyme is suggested to promote *Fgf* expression in the AER, through the suppression of BMP's (Zuniga *et al.* 1999). *Fgf8* in the AER then activates *Shh* expression in the ZPA, completing the *Shh-Fgf* feedback loop (Vogel *et al.*1996). In the stage 16 bat

forelimb, *Shh* (this study) and *Fgf8* (Weatherbee *et al.* 2006) are both expressed at high levels in the posterior interdigital tissue (Fig. 3.10). Thus, it is possible that this re-inaction of the *Shh-Fgf* feedback loop differs from the earlier signalling loop in that *Shh* and *Fgf8* are able to promote each other's expression in the same domain rather than in the ZPA and AER respectively.

Weatherbee *et al.* (2006) suggest that the combination of *Fgf8* and *Gremlin* expression in the interdigital tissue of the bat forelimb leads to the webbing of the digits by activating cell survival and suppressing the apoptotic effect of BMPs. It is likely that *Shh* is responsible for the activation of these genes and the combined effect of all three genes in the interdigital tissue of the bat forelimb has facilitated not only survival of the interdigital tissue but also the lengthening of the posterior digits.

This model is supported by studies in the chicken where the application of SHH to the interdigital tissue of developing limbs leads to the lengthening of the digits and the survival of the interdigital tissue (Dahn & Fallon 2000; Sanz-Ezquerro & Tickle 2000; Sanz-Ezquerro & Tickle 2003). Ectopic SHH, provided in the form of SHH soaked beads, acts by prolonging the expression of *Fgf8* in the AER at the digit tips (Sanz-Ezquerro & Tickle 2003). This extended *Fgf8* signal could act as an anti-differentiation signal, promoting the proliferation of the mesenchyme cells in the digital rays while inhibiting their differentiation into cartilage (Cassanova & Sanz-Ezquerro 2007). The result is the elongation of the last phalange of the digit, and often the formation of an extra joint at the end of the digit, while the more proximal phalanges are not affected (Dahn & Fallon 2000; Sanz-Ezquerro & Tickle 2000; Sanz-Ezquerro & Tickle 2003).

In the posterior digits of the bat forelimb each bone is elongated and no extra phalanges are formed. This widespread elongation effect may be due to the activation of *Fgf8* by *Shh* throughout the posterior interdigital digit tissue rather than just in the AER, exposing the metacarpals and each phalanx to the *Fgf8* signal. The lack of extra phalanges in the bat forelimb digits could be due to the high levels of *Shh* surrounding the digits. Retroviral-induced misexpression of *Shh* at high concentrations within the digital rays of chicken limbs blocks the formation of joints (Merino *et al.* 1999). In addition, *Shh* misexpression in the chondrocytes of developing mouse digits under the

control of a procollagen gene promoter blocks joint formation and promotes cell proliferation (Tavella *et al.* 2006). Thus, the high *Shh* concentration surrounding the forelimb digits in the bat may have the same effect, allowing the cells of the digital rays to proliferate and suppressing the joint formation pathway until after *Shh* expression ceases. In contrast, the level of SHH provided by the beads in the ectopic expression studies in the chicken limbs (Dahn & Fallon 2000; Sanz-Ezquerro & Tickle 2000; Sanz-Ezquerro & Tickle 2003) may not have been strong enough to block joint formation, thus resulting in the development of extra phalanges.

While the posterior digits of the bat forelimb are elongated and webbed, digit 1 and all the digits of the hindlimb are not. In this study and in Weatherbee *et al.* (2006), all the players in the *Shh-Fgf* feedback loop are activated in the interdigital tissue of the hindlimb and in the interdigital tissue surrounding digit 1 of the forelimb. However, the expression levels of the *Shh-Fgf* loop genes in these locations seems to be lower than in the posterior forelimb and expression is present for a shorter duration. The brief up-regulation of the *Shh-Fgf* feedback loop in the hindlimb from stage 16E to 16 at a uniformly low concentration may be enough to promote cell proliferation in the proximal footplate. This would explain the proximal expansion of the bat footplate that occurs during these stages and the resulting uniform length of the bat hindlimb digits. However, the brief exposure to the cell survival and proliferation signals of the *Shh-Fgf* feedback loop may not be long or strong enough to suppress the apoptotic signal from the BMPs in the interdigital tissue. Thus, while the webbing persists in the posterior interdigital spaces of the forelimb, digit 1 of the forelimb and all the digits of the hindlimb are free of webbing.

Sears *et al.* (2006) suggest that the differential patterning of the bat forelimb and hindlimb does not begin during these early stages of limb development. They state that prior to stage 20, when cartilage development is underway in the digits, the bat forelimb digits do not display signs of elongation. Sears *et al.* (2006) suggest that at stage 20, an up-regulation of *Bmp2* expression in the digits of the bat forelimb promotes increased proliferation of the chondrocytes leading to the development of longer bones. In this study, it is clear that the molecular processes leading to differential skeletal structure of the bat forelimb and hindlimb are underway during early limb development. By stage 16, *Ptc1* expression is noticeably longer along the

proximal-distal axis of the developing digits in the bat forelimb than in the bat hindlimb and the mouse forelimb. This observation provides evidence that the primordia of the bat forelimb digits are longer than those of the mouse as early as stage 16. It is likely that the increased *Bmp2* expression in the forelimb digits relative to the hindlimb at stage 20 is not due to a change in *Bmp2* regulation, but is rather due to the larger population of cells in the digit primordia of the forelimb. The larger digit primordia are established by the cell proliferation and survival signals of the *Shh-Fgf* feedback loop prior to cartilage formation.

3.4.3. Comparisons of gene expression patterns between *M. natalensis* and *C. perspicillata*

There is little difference in the spatial and temporal expression patterns observed for both *Shh* and *Ptc1* in *M. natalensis* and *C. perspicillata*. This observation supports the hypothesis that the molecular mechanisms for forelimb and hindlimb development are constant within the Chiropteran super-family, Verspertilioniformes. Slight differences in the expression pattern of *Shh* may account for the differences in wing shape between the two bat species. Such differences include the extent of the anterior expansion in the early phase of *Shh* expression and the extent to which *Shh* expression is graded across the interdigital tissue during the late phase of expression. In the developing *M. natalensis* forelimb a very clear gradient in *Shh* expression is visible at stage 16, while this gradient is not as clear in *C. perspicillata*. This difference in *Shh* expression during limb development may contribute to the differences in digit length between the two species. Digit 3 of the adult *M. natalensis* forelimb is longer than that of *C. perspicillata*. As a result, *M. natalensis* have longer, narrower wings with a slightly higher aspect ratio ($wingspan^2/area$) than those of *C. perspicillata* (6.34 for *M. natalensis* at De Hoop Nature Reserve (Miller-Butterworth 2001), 6.1 for *C. perspicillata* (Norberg & Rayner 1987)). Interestingly, the aspect ratio for *M. natalensis* populations across South Africa ranges from 5.11 to 8.03 (Miller-Butterworth 2001). *Shh* expression analysis in embryonic specimens from a variety of *M. natalensis* populations may reveal whether this variation in adult wing shape can be accounted for by slight differences in gene expression during development.

3.4.4. Conclusion

Gene expression analysis has revealed that changes in the spatial and temporal expression patterns of the anterior-posterior patterning signal, *Shh*, and its downstream target, *Ptc1*, have contributed to the development of the unique bat limb. The expansion of the *Shh* expression domain during early limb development may be responsible for the reported expansion of *Fgf8* expression in the AER (Cretekos *et al.* 2007). The enhancement of this growth factor may contribute to the expansion of the forelimb hand plate by stage 15 of bat development. Later in development, a novel domain of *Shh* expression allows the re-initiation of the *Shh-Fgf* feedback loop within the interdigital tissue. The cell survival and proliferation signals involved in this signalling loop most likely contribute to the lengthening of the posterior forelimb digits and the survival of the webbing between the extended digits. The thumb and hindlimb digits experience these signals, however, for a shorter duration and at lower concentrations. Such exposure may be sufficient to ensure the equal length of the hindlimb digits, but does not lead to extensive elongation of the hindlimb digits or the thumb, and is not able to suppress the apoptotic signals within the interdigital tissue.

Chapter 4

Conclusions and suggestions for future research

The field of evolutionary developmental biology focuses on deciphering the molecular mechanisms behind the morphological diversity of the animal kingdom. A central hypothesis in this area of research is that evolutionary changes in anatomy are more likely to be brought about by alterations in the regulation of key developmental 'toolkit genes' rather than through changes in protein sequences (Carroll *et al.* 2005). Changes in the spatial and temporal regulation of these genes allow the 'old genes to perform new tricks' as their existing functions are recruited to devise novel phenotypes.

This study has shown that the recruitment of the early anterior-posterior patterning signal, *Shh*, to a novel time and space during limb development has contributed to the development of the unique limb morphology in the bat. Early in limb development, *Shh* in the ZPA interacts in a positive feedback loop with *Fgf's* in the AER to ensure the outgrowth of the limb bud (Niswander *et al.* 1994; Vogel *et al.* 1996). Preliminary evidence suggests that this early signaling loop has been enhanced in the bat forelimb, leading to an expansion in the *Shh* (this study) and *Fgf8* (Cretekos *et al.* 2007) expression domains. The enhancement of these signals may be the cause of the posterior expansion of the hand plate evident at stage 15 of bat development.

A few stages later, the *Shh-Fgf* feedback loop is activated for a second time in the developing bat limb and recruited to new domain within the interdigital tissue (*Shh*: this study; *Fgf8, Gremlin, Bmp2*: Weatherbee *et al.* 2006). Here, it is likely that the cell proliferation and survival signals provided by the *Shh-Fgf* signaling loop are co-opted to perform the novel dual functions of lengthening the posterior forelimb digits and promoting the survival of the interdigital tissue. The expression of the *Shh* target gene, *Ptc1* mirrors this novel expression pattern, indicating that the *Shh* signal is active in its new domain. While these signals are recruited to the same novel expression domain in the hindlimb and in the tissue around the developing thumb, the duration of expression is shorter and the level is lower. In addition, the *Shh* and *Ptc1*

signals are uniformly expressed across the hindlimb interdigital tissue, rather than in a gradient, as in the forelimb. It is possible the short exposure to these factors lengthens the primordia of digits 1 and 5 of the hindlimb, but is insufficient to extensively lengthen the remaining digits or suppress the apoptosis of the interdigital tissue. As a result the digits of the hindlimb and the thumb are free of webbing and the foot plate lacks differential patterning along its anterior-posterior axis.

In situ hybridization has allowed the characterisation of the spatial and temporal expression patterns of *Shh* during bat limb development. Additional experiments, such as quantitative RT-PCR analysis on equivalently staged bat and mouse limbs, will provide confirmation that the genes involved in the *Shh-Fgf* loop are up-regulated in the bat at stage 16 but not in the mouse. Such experiments may also reveal differences in the level of up-regulation of these genes between the bat forelimb and hindlimb. Further gene expression analysis is also required to expose the effect of the re-initiation of the *Shh-Fgf* loop on digit growth and differentiation. Analysis of the timing of expression of the joint specific marker, *Gdf5* (reviewed in Casanova and Sanz-Ezquerro 2007), may reveal that joint formation is delayed in the bat forelimb as a result of extended exposure to SHH. This delay would allow the digit primordia to increase in length, without the formation of extra phalanges.

The dual analysis of *Shh* and *Ptc1* expression in both *M. natalensis* and *C. perspicillata* has revealed that the novel expression domains of these genes are common within the chiropteran sub-order Verspertilioniformes. This observation suggests that the mode of wing development is constant within this taxon and supports the monophyly of the group (Teeling *et al.* 2005, Eick *et al.* 2005). Subtle differences in the spatial extent and timing of *Shh* expression in the forelimbs of the two species may allow for variation in the lengthening of the digits and lead to differences in adult wing shape. The analysis of *Shh* and *Ptc1* expression in the developing limbs of a species with a very different wing shape to *M. natalensis* and *C. perspicillata*, such the long narrow wings of the mollosid bats, may provide further support for this hypothesis. In addition, analysis of the expression patterns of these genes in a species from the Pteropodiformes, the second chiropteran sub-order, will reveal if the mechanism of wing development is constant within the Chiroptera and thus provide support for the hypothesis that wings evolved once within this order.

If this hypothesis is true, then the mode of regulation of *Shh* expression in the limb should be constant throughout the Chiroptera. Sequence analysis of the *Shh* limb specific cis-regulatory region, known as the ZPA regulatory sequence (ZRS), from diverse bat species and comparison with other mammalian species would reveal if any bat-specific sequence alterations are evident. The function of any bat-specific sequences alterations may then be tested by introducing these sequence changes into the mouse ZRS and observing if the altered regulatory region is able to direct novel *Shh* expression in the mouse and perhaps result in bat-like phenotypes in the mouse limb.

This study has provided further insight into the mechanisms behind the morphological diversity of the animal kingdom and may inform future studies of similar anatomical anomalies evident among the mammals. The aye-aye (a species of lemur: *Daubentonia madagascariensis*) and the long-fingered triok (a species of possum: *Dactylonax palpator*) are examples of mammals that have similarly elongated digits. While all the posterior digits of the bat forelimb are elongated, only digit 3 and digit 4 are elongated in the forelimb of the aye-aye and long-fingered triok respectively. It would be fascinating to reveal if the same 'toolkit genes' have been altered in these very distantly related organisms, allowing the convergent evolution of their unique limb morphology.

Chapter 5

References

ADAMS, R.A. 1992a. Stages of development and sequence of bone formation in the little brown bat, *Myotis lucifugus*. *Journal of Mammalogy* **73**: 160-167.

ADAMS, R.A. 1992b. Comparative skeletogenesis of the forearm of the little brown bat (*Myotis lucifugus*) and the Norway rat (*Rattus norvegicus*). *Journal of Morphology* **214**: 251-260.

ADAMS, R.A. 2000. Wing ontogeny, shifting niche dimensions, and adaptive landscapes. In: *Ontogeny, Functional Ecology, and Evolution of Bats,* (eds) R.A Adams & S.C. Pederson. 1st edn., Ch. 9. Cambridge University Press, Cambridge.

AHN, S. & JOYNER, A.L. 2004. Dynamic changes in the response of cells to positive Hedgehog signalling during mouse limb patterning. *Cell* **118**: 505-516.

ALTSCHUL, S.F., MADDEN, T.L., SCHÄFFER, A.A., ZHANG, J., ZHANG, Z., MILLER, W. & LIPMAN, D.J. 1997. Gapped BLAST and PSI-BLAST: a new generation of protein database search programs. *Nucleic Acids Research* **25**: 3389-3402.

AZA-BLANC, P., RAMIREZ-WEBER, F.A., LAGET, M.P., SCHWARTZ, C. & KORNBERG, T.B. 1997. Proteolysis that is inhibited by Hedgehog targets Cubitus interruptus protein to the nucleus and converts it to a repressor. *Cell* **89**: 1043-1053.

BANDYOPADHYAY, A., TSUJI, K., COX, K., HARFE, B.D., ROSEN, V. & TABIN, C.J. 2006. Genetic analysis of the roles of BMP2, BMP4, and BMP7 in limb patterning and skeletogenesis. *PloS Genetics* **2**(12): e216.

BERNARD, R.T.F. 1980. Reproductive cycles of *Miniopterus schreibersii natalensis* (Kuhl, 1819) and *Miniopterus fraterculus* (Thomas and Schwann, 1906). *Annals of the Transvaal Museum* **32**: 55-64.

BERNARD, R.T.F., BOJARSKI, C. & MILLER, R.P. 1991. Plasma progesterone and luteinizing hormone concentrations and the role of the corpus luteum and LH gonadotrophs in the control of delayed implantation in Schreibers' long-fingered bat (*Miniopterus schreibersii*). *Journal of Reproduction and Fertility* **93**: 31-42.

BERNARD, R.T.F., COTTERILL, F.P.D & FERGUSON, R.A. 1996. On the occurrence of a short period of delayed implantation in Schreibers' long fingered bat (*Miniopterus schreibersii*) from a tropical latitide in Zimbabwe. *Journal of Zoology London* **238**: 13-22.

CARROLL, S., GRENIER, J.K. & WEATHERBEE, S.D. 2005. *From DNA to Diversity: Molecular Genetics and the Evolution of Animal Design.* 2nd edn. Blackwell Publishing, Oxford.

CASSANOVA, J.C. & SANZ-EZQUERRO, J.J. 2007. Digit morphogenesis: Is the tip different? *Development, Growth and Differentiation* **49**: 479-491.

CHARITE, J., MCFADDEN, D.G. & OLSON, E.N. 2000. The bHLH transcription factor dHAND controls Sonic hedgehog expression and establishment of the zone of polarizing activity during limb development. *Development* **127**: 2461-2470.

CHEN, Y. & STRUHL, G. 1996. Dual roles for patched in sequestering and transducing Hedgehog. *Cell* **87:** 553-563.

CHEN, C., CRETEKOS, C.J., RASWEILER, J. & BEHRINGER, R.B. 2005. *Hox*d13 expression in the developing limbs of the short-tailed fruit bat, *Carollia perspicillata. Evolution and Development* **7**: 130-141.

CHIANG, C., LITINGTUNG, Y., HARRIS, M.P., SIMANDL, B.K., LI, Y., BEACHY, P.A. & FALLON, J.F. 2001. Manifestation of the limb prepattern: Limb development in the absence of Sonic hedgehog function. *Developmental Biology* **236:** 421-435.

CLOUTIER, D. & THOMAS, D.W. 1992. *Carollia perspicillata. Mammalian species* **419**: 1-9.

CRETEKOS, C.J., RASWEILER, J.J. & BEHRINGER, R.B. 2001. Comparative studies on limb development in mice and bats: a functional genetic approach towards a molecular understanding of diversity on organ formation. *Reproduction, Fertility and Development* **13**: 691-695.

CRETEKOS, C.J., WEATHERBEE, S.D., CHEN, C., BADWAIK, N.K., NISWANDER, L., BEHRINGER, R.B. & RASWEILER, J.J. 2005. Embryonic staging system for the short-tailed fruit bat, *Carollia perspicillata*, a model organism for the Mammalian Order *Chiroptera*, based upon timed pregnancies in captive-bred animals. *Developmental Dynamics* **233**: 721-738.

CRETEKOS, C.J., DENG, J., GREEN, E.D., NISC COMPARATIVE SEQUENCING PROGRAM, RASWEILER, J.J. & BEHRINGER, R.B. 2007. Isolation, genomic structure and developmental expression of Fgf8 in the short-tailed fruit bat, *Carollia perspicillata*. *International Journal of Developmental Biology* **51**: 333-338.

DAHN, R.D. & FALLON, J.F. 2000. Interdigital regulation of digit identity and homeotic transformation by modulated BMP signaling. *Science* **289**: 438-441.

ECHELARD, Y., EPSTEIN, D.J., ST-JACQUES, B., SHEN, L., MOHLER, J., MCMAHON, J.A. & MCMAHON, A.P. 1993. Sonic hedgehog, a member of a family of putative signaling molecules, is implicated in the regulation of CNS polarity. *Cell* **75**: 1417-1430.

EICK, G.N., JACOBS, D.S. & MATTHEE, C.A. 2005. A nuclear DNA phylogenetic perspective on the evolution of echolocation and historical biogeography of extant bats (Chiroptera). *Molecular Biology and Evolution* **22**: 1869-1886.

FERNANDEZ-TERAN, H., PIEDRA, M.E., KATHIRIYA, I.S., SRIVASTAVA, D., RODRIGUEZ-REY, J.C. & ROS, M.A. 2000. Role of dHAND in the anterior-posterior polarization of the limb bud: implications for the Sonic hedgehog pathway. *Development* **127**: 2133-2142.

FLEMING, T.H. 1988. *The short-tailed fruit bat*. The University of Chicago Press, Chicago.

GIANNINI, N., GOSWAMI, A. & SANCHEZ-VILLAGRA, M.R. 2006. Development of integumentary structures in *Rousettus amplexicaudatus* (Mammalia: Chiroptera: Pteropodidae) during late-embryonic and fetal stages. *Journal of Mammology* **87**: 993-1003.

GOODRICH, L.V., JOHNS, R.L., MILENKOVIC, L. MCMAHON, J.A. & SCOTT, P.M. 1996. Conservation of *hedgehog/patched* signalling pathway from flies to mice: induction of a mouse *patched* gene by Hedgehog. *Genes and Development* **10**: 301-312.

HALL, T.A. 1999. BioEdit: a user-friendly biological sequence alignment editor and analysis program for Windows 95/98/NT. *Nucleic Acids Symposium Series* **41**: 95-98.

HARFE, B.D., SCHERZ, P.J., NISSIM, S., TIAN, H., MCMAHON, A.P. & TABIN, C.J. 2004. Evidence for an expansion-based temporal Shh gradient in specifying vertebrate digit identities. *Cell* **118**: 517-528.

HECKSHER-SØRENSEN, J., HILL, R.E. & LETTICE, L. 1998. Double labelling for whole mount *in situ* hybridisation in the mouse. *Biotechniques* **24**: 914-918.

HILL, R.A. 2007. How to make a zone of polarizing activity: Insights into limb development via the abnormality preaxial polydactyly. *Development, Growth and Differentiation* **49**: 439-448.

INGHAM, P.W. & MCMAHON, A.P. 2001. Hedgehog signaling in animal development: paradigms and principles. *Genes and Development* **15**: 3059-3087.

JACOBS, D. S. 1999. Intraspecific variation in wingspan and echolocation call flexibility might explain the use of different habitats by the insectivorous bat, *Miniopterus schreibersii* (Vespertilionidae: Miniopteridae). *Acta Chiropterologica.* **1**: 93-103.

KAUFMAN, M.H. 1992. *The atlas of mouse development.* Academic Press limited, London.

KRAUS, P., FRAIDENRAICH, D. & LOOMIS, C.A. 2001. Some distal limb structures develop in mice lacking Sonic hedgehog signaling. *Mechanisms of Development* **100**: 45-58.

LAUFER, E., NELSON, C.E., JOHNSON, R.L., MORGAN, B.A. & TABIN, C.J. 1994. Sonic Hedgehog and Fgf-4 act through a signalling cascade and feedback loop to integrate growth and patterning of the developing limb bud. *Cell* **79**: 993-1003.

LAWRENCE, M. 1991. Biological Observations on a Collection of New Guinea *Syconycteris australis* (Chiroptera, Pteropodidae) in the American Museum of Natural History. *American Museum Novitates* **3024**: 1-27.

LEE, J.J., EKKER, S.C., VON KESSLER, D.P., PORTER, J.A., SUN, B.I. & BEACHY, P.A. 1994. Autoproteolysis in Hedgehog protein biogenesis. *Science* **266**: 1528-1537.

LETTICE, L.A., HORIKOSHI, T., HEANEY, S.J.H., VAN BAREN, M.J., VAN DER LINDE, H.C., BREEDEVELD, G.J., JOOSSE, M., AKARSU, N., OOSTRA, B.A., ENDO, N., SHIBATA, M., SUZUKI, M., TAKAHASHI, E., SHINKA, T., NAKAHORI, Y., AYUSAWA, D., NAKABAYASHI, K., SCHERER, S.W., HEUTINK, P., HILL, R.E. & NOJI, S. 2002. Disruption of a long-range cis-acting regulator for *Shh* causes preaxial polydactyly. *Proceedings of the National Academy of Sciences* **99**: 7548-7553.

LEWANDOSKI, M., SUN, X., & MARTIN, G.R. 2000. Fgf8 signaling from the AER is essential for normal limb development. *Nature Genetics* **26:** 460-463.

LEWIS, F.M., DUNN, M.P., MCMAHON, J.M., LOGAN, M., MARTIN, J.F., ST-JACQUES, B. & MCMAHON, A.P. 2001. Cholesterol modification of Sonic hedgehog is required for long-range signaling activity and effective modulation of signaling by Ptc1.*Cell* **105**: 599-612.

LI, Y., ZANG, H., LITINGTUNG, Y. & CHIANG, C. 2006. Cholesterol modification restricts the spread of Shh gradient in the limb bud. *Proceedings of the National Academy of Sciences* **103:** 6548–6553.

LITINGTUNG, Y., DAHN, R.D., LI, Y., FALLON, J.F. & CHIANG, C. 2002. *Shh* and *Gli3* are dispensable for limb skeleton formation but regulate digit number and identity. *Nature* **418**: 979-983.

LU, P., MINOWADA, G. & MARTIN, G.R. 2006. Increasing Fgf4 expression in the mouse limb bud causes polysyndactyly and rescues the skeletal defects that result from loss of Fgf8 function. *Development* **133**: 33-42.

MARIANI, F.V. & MARTIN, G.R. 2003. Deciphering skeletal patterning: clues from the limb. *Nature* **423**: 319-325.

MARIGO, V., SCOTT, M.P., JOHNSON, R.L., GOODRICH, L.V. & TABIN, C.J. 1996a. Conservation in hedgehog signaling: induction of a chicken patched homologue by Sonic hedgehog in the developing limb. *Development* **122**: 1225-1233.

MARIGO, V., DAVEY, R.A., ZUO, Y., CUNNINGHAM, J.M. & TABIN, C.J. 1996b. Biochemical evidence that Patched is the Hedgehog receptor. *Nature* **384**: 176-179.

MARTIN, P. 1990. Tissue patterning in the developing mouse limb. *International Journal of developmental Biology* **34:** 323-336.

MCDONALD, J.T., RAUTENBACH, I. L. & NEL, J.A.J. 1990. Foraging ecology of bats observed at De Hoop Provincial Nature Reserve, southern Cape Province. *South African Journal of Wildlife Research* **20**: 133-145.

MCGLINN, E & TABIN, C. J. 2006. Mechanistic insight into how Shh patterns the vertebrate limb. *Current Opinion in Genetics & Development* **16**:426-432.

MERINO, R., MACIAS, R.D., GANAN, Y., ECONOMIDES, A.N., WANG, X., WU, Q., STAHL, N., SAMPATH, K.T., VARONA, P. & HURLE, J.M. 1999.

Expression and function of *Gdf-5* during digit skeletogenesis in the embryonic chick leg bud. *Developmental Biology* **206**: 33-45.

MILLER-BUTTERWORTH, C.M. 2001. Population substructuring in Schreibers' long-fingered bat (Miniopterus schreibersii) in South Africa. PhD thesis, UCT.

MILLER-BUTTERWORTH, C.M., JACOBS, D.S. & HARLEY, E.H. 2003. Strong population substructure is correlated with morphology and ecology in a migratory bat. *Nature* **424**: 187-191.

MILLER-BUTTERWORTH, C.M., EICK, G.N., JACOBS, D.S., SCHOEMAN, M.C. & HARLEY, E.H. 2005. Genetic and phenotypic differences between South African long-fingered bats, with a global miniopterine phylogeny. *Journal of Mammalogy* **86**: 1121-1135.

MILLER-BUTTERWORTH, C.M., MURPHY, W.J., O'BREIN, S.J., JACOBS, D.S., SPRINGER, M.S. & TEELING, E.C. 2007. A Family Matter: Conclusive Resolution of the Taxonomic Position of the Long-Fingered Bats, *Miniopterus*. *Molecular Biology and Evolution* **24**: 1553-1561.

MILLS, G. & HESS, L. 1997. *The Complete Book of Southern African Mammals*. Struik Publishers, Cape Town.

MURONE, M., ROSENTHAL, A. & DE SAUVAGE, F.J. 1999. Sonic hedgehog signaling by the Patched–Smoothened receptor complex. *Current Biology* **9**: 76-84.

NELSON, C.E., MORGAN, B.A., BURKE, A.C., LAUFER, E., DIMAMBRO, E., MURTAUGH, L.C., GONZALES, E., TESSAROLLO, L., PARADA, L.F. & TABIN, C.J. 1996. Analysis of Hox gene expression in the chick limb bud. *Development* **122**: 1449-1466.

NEUWEILER, G. 2000. *The Biology of Bats*. Oxford University Press Inc., New York.

NISSIM, S., HASSO, S.M., FALLON, J.F. & TABIN, C.J. 2006. Regulation of Gremlin expression in the posterior limb bud. *Developmental Biology* **299**: 12-21.

NISWANDER, L., JEFFRY, S., MARTIN, G.R. & TICKLE, C. 1994. A positive feedback loop coordinates growth and patterning in the vertebrate limb. *Nature* **371**: 609-612.

NORBERG, U.M. & RAYNER, J.M.V. 1987. Ecological Morphology and Flight in Bats (Mammalia; Chiroptera): Wing Adaptations, Flight Performance, Foraging

Strategy and Echolocation. *Philosophical Transactions of the Royal Society of London. Series B, Biological Sciences* **316**: 335-427.

NOWAK, R.M. 1999. *Walker's Mammals of the World.* John Hopkins University Press, Baltimore.

PANMAN, L. & ZELLER, R. 2003. Patterning the limb before and after Shh signaling. *Journal of Anatomy* **202**: 3-12.

PEIST, R., HONSEL, D., RÜTJES, T. & LÖFFERT, D. 2002. Increasing efficiency of cloning PCR products. *Qiagen News* **3**: 5-7.

PEPINSKY, B., ZENG, C., WEN, D., RAYHORN, P., BAKER, D.P., WILLIAMS, K.P., BIXLER, S.A., AMBROSE, C.M., GARBER, E.A., MIATKOWSKI, K., TAYLOR, F.R., WANG, E.A. & GALDES, A. 1998. Identification of a palmitic acid-modified form of human Sonic hedgehog. *Journal of Biological Chemistry* **273**: 14037-14045.

PLATT, K.A., MICHAUD, J. & JOYNER, A.L. 1997. Expression of the mouse *Gli* and *Ptc* genes is adjacent to embryonic sources of hedgehog signals suggesting a conservation of pathways between flies and mouse. *Mechanisms of Development* **62**: 121-135.

PORTER, J.A., EKKER, S.C., PARK, W.J., VONKESSLER, D.P., YOUNG, K.E., CHEN, C.H., MA, Y., WOODS, A.S., COTTER, R.J., KOONIN, E.V. & BEACHY, P.A. 1996. Hedgehog patterning activity: Role of a lipophilic modification mediated by the carboxy-terminal autoprocessing domain. *Cell* **86:** 21-34.

RACEY, P. A. 1969. Diagnosis of pregnancy and the experimental extension of gestation in the pipestrelle bat, *Pipistrellus pipistrellus. Journal of Reproduction and Fertility* **19**: 465-474.

RASWEILER, J.J. & BADWAIK, N.K. 1997. Delayed development in the short-tailed fruit bat, *Carollia perspicillata. Journal of Reproduction and Fertility* **109**: 7-20.

RICHARDSON, M.K. & OELSCHLÄGER, H.H.A. 2002. Time, pattern, and heterochrony: a study of hyperphalangy in the dolphin embryo flipper. *Evolution & Development* **4**: 435-444.

RIDDLE, R.D., JOHNSON, R.L., LAUFER, E. & TABIN, C.J. 1993. Sonic hedgehog mediates the polarizing activity of the ZPA. *Cell* **75**: 1401-1416.

ROHATGI, R., MILENKOVIC, L. & SCOTT, M.P. 2007. Patched1 regulates Hedgehog signaling at the primary cilium. *Science* **317**: 372-376.

SANZ-EZQUERRO, J.J. & TICKLE, C. 2000. Autoregulation of *Shh* expression and Shh induction of cell death suggest a mechanism for modulating polarising activity during chick limb development. *Development* **127**: 4811-4823.

SANZ-EZQUERRO, J.J. & TICKLE, C. 2003. Fgf signaling controls the number of phalanges and tip formation in developing digits. *Current Biology* **13**: 1830-1836.

SCHERZ, P.J., HARFE, B.D., MCMAHON, A.P. & TABIN, C.J. 2004. The limb bud Shh-Fgf feedback loop is terminated by expansion of former ZPA cells. *Science* **305**: 396-399.

SCHERZ, P.J., MCGLINN, E., NISSIM, S. & TABIN, C.J. 2007. Extended exposure to Sonic hedgehog is required for patterning the posterior digits of the vertebrate limb. *Developmental Biology* **308**: 343-354.

SCHUMACHER, S. 1932. Die entwicklung der flerdermausflughaut. *Zeitschrift fur Anatomie und Entwicklungsgeschichte* **98**: 703-721.

SEARS, K.E., BEHRINGER, R., RASWEILER, J.J. & NISWANDER, L.A. 2006. Development of bat flight: Morphologic and molecular evolution of bat wing digits. *Proceedings of the National Academy of Sciences* **103**: 6581-6586.

SHAPIRO, M.D., HANKEN, J. & ROSENTHAL, N. 2003.Developmental basis of evolutionary digit loss in the Australian lizard *Hemiergis*. *Journal of Experimental Zoology*. **297B**: 48-56.

SHARPE, J., LETTICE, L., HECKSHER-SØRENSEN, J.H., FOX, M., HILL, R. & KRUMLAUF, R. 1999. Identification of *Sonic hedgehog* as a candidate gene responsible for the polydactylous mouse mutant *Sasquatch*. *Current Biology* **9**: 97-100.

SHIMIZU, H., YOKOYAMA, S. & ASAHARA, H. 2007. Growth and differentiation of the developing limb bud from the perspective of chondrogenesis. *Development, Growth and Differentiation* **49**: 449-454.

SIMMONS, N.B. 2001. Reassessing bat diversity: how many bat species are there in the world? *Bat Research news* **42**: 179-180.

SIMMONS, N.B. 2005. Order Chiroptera. In: *Mammal species of the world: a taxonomic and geographic reference Vol 1.* (eds) D. E. Wilson & D. M. Reeder. 3rd ed. Pp 312-529. Johns Hopkins University Press, Baltimore.

SPEAKMAN, J.R. 2001. The evolution of flight and echolocation in bats: another leap in the dark. *Mammal Review* **31**: 111-130.

SPILLMAN, F.R. 1925. Beitrage zur kenntnis des fluges der fledermause und der ontogenetischen entwicklung ihrer flugapparte. *Acta Zoologica* **6:** 217-224.

SPITZ, F., GONZALEZ, F. & DUBOULE, D. 2003. A global control region defines a chromosomal regulatory landscape containing the *HoxD* cluster. *Cell* **113**: 405-417.

STOFFBERG, S., JACOBS, D.S. & MILLER-BUTTERWORTH, C.M. 2004. Field identification of two morphologically similar bats, *Miniopterus schreibersii natalensis* and *Miniopterus fraterculus* (Chiroptera: Vespertilionidae). *African Zoology* **39**: 47-53.

STONE, D.M., HYNES, M., ARMANINI, M., SWANSON, T.A., GU, Q., JOHNSON, R.L., SCOTT, M.P., PENNICA, D., GODDARD, A., PHILLIPS, H., NOLL, M., HOOPER, J.E., DE SAUVAGE, F. & ROSENTHAL, A. 1996. The tumour suppressor gene patched encodes a candidate receptor for Sonic hedgehog. *Nature* **384**: 129- 134.

TAVELLA, S., BITICCHI, R., MORELLO, R., CASTAGNOLA, P., MUSANTE, V., COSTA, D., CANCEDDA, R. & GAROFALO, S. 2006. Forced chondrocyte expression of sonic hedgehog impairs joint formation affecting proliferation and apoptosis. *Matrix Biology* **25**: 389-397.

TAYLOR, P.J. 2000. *Bats of Southern Africa*. University of Natal Press, Pietermaritzburg.

TEELING, E.C., SPRINGER, M.S., MADSEN, O., BATES, P., O'BRIEN, S.J. & MURPHY, W.J. 2005. A molecular phylogeny for bats illuminates biogeography and the fossil record. *Science* **307**:580-584.

THEWISSEN, J.G.M., COHN, M.J., STEVENS, L.S., BAJPAI, S., HEYNING, J. & HORTON JR, W.E. 2006. Developmental basis for hind-limb loss in dolphins and origin of the cetacean bodyplan. *Proceedings of the National Academy of* Sciences. **103**: 8414-8418.

TICKLE, C. 2003. Patterning systems: from one end of the limb to the other. *Developmental Cell* **4**: 449-458.

TOKITA, M. 2006. Normal embryonic development of the Japanese pipistrelle, *Pipistrellus abramus*. *Zoology* **109**: 137-147.

VAN DER MERWE, M. 1975. Preliminary study on the annual movements of the Natal clinging bat. *The South African Journal of Science* **71**: 237- 241.

VAN DER MERWE, M. 1979. Foetal growth curves and seasonal breeding in the Natal clinging bat, *Miniopterus schreibersii natalensis*. *South African Journal of Zoology* **14**: 17- 21.

VAN DER MERWE, M. 1986. Reproductive strategies of *Miniopterus schreibersii natalensis*. *Cimbebasia (A)* **8**: 107-111.

VAN DER MERWE, M. & VAN AARDE, J. 1989. Plasma progesterone concentrations in the female natal clinging bat (*Miniopterus schreibersii natalensis*). *Journal of Reproduction and Fertility* **87**: 665-669.

VAUGHAN, T.A. 1970. The skeletal system. In: *Biology of Bats Volume I,* (ed) W.A. Wimsatt, 1st edn., Ch. 3. Academic Press Inc., London.

VOGEL, R., RODRIGUEZ, C. & IZPISUA-BELMONTE, J.C. 1996. Involvement of FGF-8 in initiation, outgrowth and patterning of the vertebrate limb. *Development* **122**: 1737-1750.

VORTKAMP, A., KAECHOONG, L., LANSKE, B., SEGRE, G.V., KRONENBERG, H.M. & TABIN, C.J. 1996. Regulation of the rate of cartilage differentiation by Indian Hedgehog and PTH-Related Protein. *Science* **273**: 613-622.

WANG, B., FALLON, J.F. & BEACHY, P.A. 2000. Hedgehog regulated processing of Gli3 produced an anterior/posterior repressor gradient in the developing vertebrate limb. *Cell* **100**: 423-434.

WEATHERBEE, S.D., BEHRINGER, R.R., RASWEILER, J.J. & NISWANDER, L.A. 2006. Interdigital webbing retention in bat wings illustrates genetic changes underlying amniote limb diversification. *Proceedings of the National Academy of Sciences*. **103**: 15103-15107.

WOLPERT, L.C. 1969. Positional information and the spatial pattern of cellular differentiation. *Journal of Theoretical Biology* **25**: 1-47.

XU, Q & WILKINSON, D.G. 1999. *In situ* hybridization of mRNA with hapten labelled probes. In: *In Situ Hybridization: A practical Approach*, (ed) D.G. Wilkinson. 3rd edn., Ch. 4. Oxford University Press, Oxford.

YANG, Y., DROSSOPOULOU, G., CHUANG, P.T., DUPREZ, D., MARTI, E., BUMCROT, E., VARGESSON, N., CLARKE, J., NISWANDER, L., MCMAHON, A. & TICKLE. C. 1997. Relationship between dose, distance and

time in Sonic Hedgehog-mediated regulation of anteroposterior polarity in the chick limb. *Development* **124**: 4393-4404.

ZAKANY, J., KMITA, M. & DUBOULE, D. 2004. A dual role for *Hox* genes in limb anterior-posterior asymmetry. *Science* **304**: 1669-1672.

ZELLER, R. 2004. It takes time to make a pinky: Unexpected insights into how SHH patterns vertebrate digits. *Science's STKE* **2004**: pe53.

ZELLER, R. & ZUNIGA, A. 2007. Shh and Gremlin1 chromosomal landscapes in development and disease. *Current Opinions in Genetics and Development* doi:10.1016/ j.gde.2007.07.006.

ZOU, H. & NISWANDER, L. 1996. Requirement for BMP signaling in interdigital apoptosis and scale formation. *Science* **272**: 738-741.

ZUNIGA, A., HARAMIS, A.P.G., MCMAHON, A.P. & ZELLER, R. 1999. Signal relay by BMP antagonism controls the SHH/FGF4 feedback loop in vertebrate limb buds. *Nature* **401**: 598-602.

Appendix A

Table A. Details of the primers used for *Shh* PCR's. Groups indicate combinations of forward and reverse primers that were used together. ShhFwd1b and ShhRev1a were used successfully to isolate a region of *Shh* from mouse cDNA. None of the primers worked successfully on *M. natalensis* cDNA. Letters in brackets indicate degenerate nucleotides. I – Inosine.

Primer name	Primer sequence (5'→3')
***Shh* PCR primers**	
Group A	
ShhFwd1a	AGA CGA IGG IGC CAA GAA GGT C
ShhFwd1b	AGC CAA GAA GGT CTT CTA CGT G
ShhRev1a	AIA TIT GGT AGA GCA GCT GCG A
ShhrRev1b	ACC AGG TGC CIA TIT GGT AGA G
Group B	
NewShhFwd	GTI ATG AA(TC) CA(AG) TGG C
NewShhRev1	CGA (GA)TA CCA (GA)TG (TGA)AT IC
NewShhRev2	TCG TA(GA) TAI ACC CA(GA) TC(GA)A A
Group C	
ShhPBFwd	AGA AAC TC(CG) GA(GA) CGA TTT AA(GA) GAA CT
ShhPBRev	AC(ATG)G A(CT)G TGG TGA TGT CCA C(TC)G
Group D	
NIShhF1	ACC AA(CT) GT(AG) GC(CG) GAG AAG ACC CT
NIShhF4	AGTG ATG AA(CT) CAG TGG CCI GG(ACG) GTG AA
NIShhR3	A TC AGC TGG ACT TGA C(TCG)G CCA T(TGC)C CCA
NIShhR4	ATT CAC (TGC)CC IGG CCA CTG (GA)TT CAT (CG)AC

Fig. A1 ClustalW alignment of highly conserved regions of the mouse (ENSMUST00000021921), rat (ENSRNOT00000008497), dog (ENSCAFT00000001978) and human (ENST00000331920) *Ptc1* cDNA sequences showing regions used to design the *Ptc1* PCR primers (shaded regions). Ptc1Fwd is located at position 642 of the mouse *Ptc1* cDNA sequence, while PtcRev is located at position 1455. Stars indicate conserved base pairs.

Fig. A2

Fig. A2 continued ClustalW alignment of highly conserved regions of the mouse (ENSMUST00000002708), rat (ENSRNOT00000026287), dog (ENSCAFT00000008207) and human (ENST00000297261) *Shh* cDNA sequences showing regions used to design the *Shh* PCR primers listed in Table A (shaded regions). Stars indicate conserved base pairs.